



โครงการ การพัฒนาสารกึ่งตัวนำอนินทรีย์ที่มีโฮลเป็นประจุ
พาหะและสามารถเตรียมได้จากกรรมวิธีที่ใช้สารละลาย เพื่อ
ใช้ประโยชน์ในอุปกรณ์ให้แสงสว่าง อุปกรณ์ผลิตพลังงาน
และอุปกรณ์ไมโครอิเล็กทรอนิกส์

โดย ดร.พิชญ พัฒนสัตยวงศ์ และคณะ

พฤษภาคม พ.ศ. 2561

รายงานวิจัยฉบับสมบูรณ์

โครงการ การพัฒนาสารกึ่งตัวนำอนินทรีย์ที่มีโฮลเป็นประจุ
พาหะและสามารถเตรียมได้จากกรรมวิธีที่ใช้สารละลาย เพื่อ
ใช้ประโยชน์ในอุปกรณ์ให้แสงสว่าง อุปกรณ์ผลิตพลังงาน
และอุปกรณ์ไมโครอิเล็กทรอนิกส์

ดร.พิชญ พัฒนสัตยวงศ์ ภาควิชาวัสดุศาสตร์และวิศวกรรมวัสดุ สำนักวิชาวิทยาการโมเลกุล สถาบันวิทยสิริเมธี

สนับสนุนโดยสำนักงานคณะกรรมการการอุดมศึกษา และ สำนักงานกองทุนสนับสนุนการวิจัย

(ความเห็นในรายงานนี้เป็นของผู้วิจัย สกอ. และ สกว. ไม่จำเป็นต้องเห็นด้วยเสมอไป)

Project Details

Project Code: MRG5980214

Project Title: Development of solution-processable hole-transporting inorganic semiconductors for lighting, energy generation, and plastic microelectronics การพัฒนาสารกึ่งตัวนำอนินทรีย์ที่มีโฮลเป็นประจุพาหะและสามารถเตรียมได้จาก กรรมวิธีที่ใช้สารละลาย เพื่อใช้ประโยชน์ในอุปกรณ์ให้แสงสว่าง อุปกรณ์ผลิตพลังงาน และอุปกรณ์ไมโครอิเล็กทรอนิกส์

Investigator :

Dr. Pichaya Pattanasattayavong

Department of Materials Science and Engineering

School of Molecular Science and Engineering

Vidyasirimedhi Institute of Science and Technology (VISTEC)

E-mail Address : pichaya.p@vistec.ac.th

Project Period : 2 May 2016 - 1 May 2018

Keywords: coordination polymer semiconductors, hole transport, wide band gap,

thin-film transistors, organic solar cells

1

Executive Summary

This project investigates the development of solution-processable inorganic semiconductors for thin-film opto/electronic devices. We have shown previously that copper(I) thiocyanate (CuSCN) is a promising transparent hole-transporting semiconductor. CuSCN is unique for its combination of optical and electrical properties, and its applications in a wide range of applications has been recently demonstrated, from thin-film transistors (TFTs), organic light-emitting diodes (OLEDs), to organic solar cells (OSCs). CuSCN is one of coordination polymers, a material group which has not been explored for electronic applications. In this work, our objectives are: (1) to develop a new transparent hole-transporting wide band gap inorganic semiconductor and (2) to improve the performance of CuSCN-based opto/electronic devices by tuning the processing.

We have successfully achieved both objectives correspondingly. We have synthesized and comprehensively characterized $Sn(NCS)_2$ to show that it is a new semiconductor with an electronic structure for a transparent hole-transporting material. $Sn(NCS)_2$ features a large band gap, yielding high optical transparency in the visible spectrum, as well as the Sn 5s electrons at the top of the valence band, resulting in hole-transporting states. We have also employed $Sn(NCS)_2$ as a hole transport layer (HTL) in OSCs. Preliminary results show promising power conversion efficiencies (PCEs) in the range of 4-6%. Further optimization of process and device structure is expected to increase the PCE.

In addition, we have employed the anti-solvent treatment to modify the thin film properties of CuSCN. Treating CuSCN films with tetrahydrofuran (THF) results in smooth films with low root-mean-square (RMS) roughness value around 1-2 nm. TFTs employing this CuSCN as the *p*-type semiconducting channel shows a significant increase in the hole field-effect mobility from 0.01 to 0.05 cm² V⁻¹ s⁻¹. Alternatively, treating CuSCN HTL on glass/ITO substrates with isopropyl alcohol (IPA) leads to the improve the PCEs of solar cells from 8.35% to 8.93%.

As for the output of this project, we have published two journal articles and submitted one which is currently under review. Three more publications are also in the pipeline based on the experimental results obtained from this work. As part of this project, we have been training three PhD students. They are now among a few people in Thailand who can fabricate TFTs and achieve high PCEs from OSCs. Our team have also participated in numerous conferences and discussions to promote the work and start new collaboration. Most importantly, we have opened up a new research direction of the development of 'coordination polymer semiconductors,' which is the main direction of our next proposed project.

Abstract

The unavailability of transparent hole-transporting inorganic semiconductors that can be solution-processed, has good stability, and shows excellent carrier transport characteristics remains one of the challenges in the field of organic electronics. This work aims to develop such semiconductors by focusing on coordination compounds based on the thiocyanate ligand. Our earlier investigations have shown that copper(I) thiocyanate (CuSCN) is a promising candidate as it shows hole mobility on average of 0.01 cm² V⁻¹ s⁻¹ and has a large optical band gap of 3.9 eV.

For the first part of the work, we expand the thiocyanate-based semiconductor library by showing that tin(II) thiocyanate [Sn(NCS)₂] is also a wide band gap semiconductor with promising electronic structure for hole transport. We synthesized the compound and comprehensively characterized it with a wide range of experimental techniques as well as studied theoretically with density functional theory (DFT). We can reveal the low-dimensional nature of the compound through in-depth analysis of the single crystal X-ray data. Sn(NCS)₂ is found to have a 1D polymeric chain that further form 1D ribbons and 2D sheets. The DFT calculations show that Sn(NCS)₂ has a wide band gap, a feature which is backed up by the experimental absorption spectrum that shows the optical band gap of 3.4 eV. The analysis of the density of states also shows that the Sn 5s electrons contribute to the states at the top of the valence band. These states are expected to favor good carrier transport. Furthermore, we explore the application of Sn(NCS)₂ as a hole transport layer in organic solar cells. Initial results of unoptimized systems are highly promising with solar cells showing efficiencies in the range of 4-6%. We expect that further optimizing of the structure and processing would enhance the efficiency further.

We also studied the effects of treating CuSCN thin films with anti-solvents on the film morphology and device applications. By treating CuSCN with tetrahydrofuran, *p*-type thin-film transistors based on CuSCN as the semiconducting channel show improved characteristics of higher on current and increased field-effect hole mobility from 0.01 to 0.05 cm² V⁻¹ s⁻¹. On the other hand, when CuSCN is deposited on glass/ITO substrates for organic solar cell device, treating CuSCN with isopropyl alcohol is found to increase the device power conversion efficiency from 8.35% to 8.93%. We have demonstrated that the simple anti-solvent treatment is a versatile and easily applicable method for improving the performance of CuSCN-based devices.

Through this project, we have shown that the 'coordination polymer semiconductors' are a novel family of compounds that have promising electronic properties. They can be solution-processed, and further modifications can be done based on coordination chemistry. Different metals and ligands await the exploration, and this the subject of our next project.

Project Output

1. Journal articles

Published

- Pattanasattayavong, P.*; Promarak, V.; Anthopoulos, T. D. Electronic Properties of Copper(I) Thiocyanate (CuSCN). Adv. Electron. Mater. 2017, 3 (3), 1600378. (IF2018 = 5.466)
- 1.2. Del Gobbo, S.; Mottram, A. D.; Ould-Chikh, S.; Chaopaknam, J.; Pattanasattayavong, P.; D'Elia, V. Physico-Chemical Investigation of ZnS Thin-Film Deposited from Ligand-Free Nanocrystals Synthesized by Non-Hydrolytic Thio-Sol–gel. Nanotechnology 2018, 29 (38), 385603. (IF2018 = 3.404)

Under review

1.3. Wechwithayakhlung, C.; Packwood, D. M.; Worakajit, P.; Ittisanronnachai, S.; Chanlek, N.; Promarak, V.; Kongpatpanich, K.; Harding, D. J.; Pattanasattayavong, P.* Tin(II) Thiocyanate Sn(NCS)₂ – a New Wide Band Gap Coordination Polymer Semiconductor with 2D Structure. Manuscript under review.

In preparation

- 1.4. Worakajit, P.; Pattanasattayavong, P.* Improved Hole Mobility in CuSCN Thin-Film Transistors by Anti-Solvent Treatment. Manuscript in preparation.
- 1.5. Worakajit, P.; Pattanasattayavong, P.* Enhanced Power Conversion Efficiency of Organic Solar Cells with CuSCN as Hole Transport Layer by Anti-Solvent Treatment. Manuscript in preparation.
- 1.6. Chaopaknam, J.; Pattanasattayavong, P.* Application of Sn(NCS)₂ as Hole Transport Layer in Organic Solar Cells. Manuscript in Preparation.

2. Research utilization

Academic aspect

- Training of three PhD students: Ms. Chayanit Wechwithayakhlung, Ms. Pimpisut Worakajit, and Ms. Jidapa Chaopaknam (expected to finish in 2020).
- Collaboration for further work on 'coordination polymer semiconductors' with
 - Assoc. Prof. Dr. David J. Harding, Walailak University, Thailand
 - Dr. Daniel M. Packwood, Kyoto University, Japan.

- Assoc. Prof. Dr. Akinori Saeki, Osaka University, Japan.
- Asst. Prof. Dr. Kittipong Chainok, Thammasat University, Thailand.

3. Others

Presentations at international conferences

- Chaopaknam, J.; Pattanasattayavong, P.* New Wide Band Gap Inorganic Semiconductor Tin(II) Thiocyanate [Sn(NCS)₂] and Its Application in Organic Solar Cells. *Nano Thailand 2018*; 2018 Dec 12-14; Bangkok, Thailand.
- Worakajit, P.; Pattanasattayavong, P.* Improving Charge Transport in CuSCN
 Hole Transport Layer by Anti-Solvent Treatment and Application in HighEfficiency Organic Solar Cells. Nano Thailand 2018; 2018 Dec 12-14; Bangkok,
 Thailand.
- Pattanasattayavong, P.*; Worakajit, P. Improving Hole Transport in CuSCN Thin-Film Transistors by Solvent Treatment. 11th International Symposium on Flexible Organic Electronics (ISFOE 2018); 2018 Jul 2-5; Thessaloniki, Greece.
- Pattanasattayavong, P.* Improving solution-processing of copper(I) thiocyanate hole transport material. 14th International Conference on Organic Electronics (ICOE 2018); 2018 Jun 18-22; Bordeaux, France.
- Pattanasattayavong, P.* Copper(I) Thiocyanate (CuSCN) as a Transparent P-type Semiconductor for Novel Organic Electronic Applications. 1st MRS Thailand International Conference; 2017 Oct 31 Nov 3; Chiang Mai, Thailand.
- Worakajit, P.; Pattanasattayavong, P.* Finding New Solvents for Processing Copper(I) Thiocyanate. 1st MRS Thailand International Conference; 2017 Oct 31
 Nov 3; Chiang Mai, Thailand.
- Pattanasattayavong, P.* Copper(I) Thiocyanate (CuSCN) for Plastic and Organic Electronics. 3rd International Congress on Advanced Materials (AM2016); 2016 Nov 27-30; Bangkok, Thailand.
- Pattanasattayavong, P.*; Mottram, A. D.; Yan, F.; Anthopoulos, T. D. Study of Hole Localized States and Transport Mechanisms of Copper(I) Thiocyanate Based on Field-Effect Measurements. *International Conference of Synthetic Metal 2016 (ICSM 2016)*; 2016 Jun 26-Jul 1; Guangzhou, China.

Table of Contents

Project Details	1
Executive Summary	2
Abstract	3
Project Output	4
Table of Contents	6
Chapter 1 Introduction	8
Objectives	10
Chapter 2 Tin(II) Thiocyanate – a New Wide Band Gap Coordination Polymer	
Semiconductor	11
2.1. Introduction	11
2.2. Methodology	11
Synthesis of Sn(NCS) ₂	11
Film deposition and device fabrication	12
Characterizations	12
Density functional theory calculations	12
2.3. Results and discussion	13
2.3.1. Physical properties of Sn(NCS) ₂	13
2.3.2. Electronic structure and density of states	17
2.3.3. Sn(NCS) ₂ thin films and applications in organic solar cells	20
2.4. Conclusions and outlook	22
Chapter 3 Improving Hole Transport in Thin-Film Transistors (TFTs) based on	
Copper(I) Thiocyanate (CuSCN) by Anti-Solvent Treatment	23
3.1. Introduction	23
3.2. Methodology	24
Solution and film preparation	24
Anti-solvent treatment	24
Device fabrication	24
Film and device characterizations	24
Synchrotron experiments	24
3.3. Results and discussion	
3.3.1. CuSCN thin-film transistors	25
3.3.2. Surface topography of CuSCN treated by anti-solvents	25

3.3.3. Microstructure and local atomic environment	27
3.4. Conclusions and outlook	28
Chapter 4 High-Efficiency Organic Solar Cells with Anti-Solvent-Treated Copper(I)	
Thiocyanate (CuSCN) as a Hole Transport Layer	29
4.1. Introduction	29
4.2. Methodology	29
Solution, film preparation, and anti-solvent treatment	29
Device fabrication and characterization	29
4.3. Results and Discussion	29
4.3.1. Performance of solar cells with HTL based on CuSCN treated by anti-	
solvents	29
4.3.2. Surface topography of CuSCN films on ITO after anti-solvent treatment	31
4.4. Conclusions and outlook	32
Chapter 5 Summary	33
Bibliography	34
Appendix	36

Chapter 1

Introduction

The field of organic electronics has grown tremendously in the past decade and has entered the stage of commercialization with the prime example being the flat or curved displays based on organic light-emitting diodes (OLEDs). The materials library has also expanded to include not only organic molecules or polymers but also a wider range of materials, such as inorganic semiconductors. The common trait or aim shared by the development of new materials is that they can be processed preferably by high-throughput methods onto large-area substrates. Solution-based processes, for example printing techniques, are always in the focus as they can satisfy the processing requirements. Also, basic solution-based techniques, such as spin-coating, are widely used and suitable for laboratory scale due to the cost-effectiveness and versatility.

For the development of inorganic materials for the so-called "large-area electronics," one of the key challenges is the lack of high-performance and stable hole-transporting (or p-type) inorganic semiconductors. Typically, inorganic semiconductors are based on metal oxides such as ZnO, SnO₂, and In₂O₃, which show excellent electron-transporting (or n-type) properties due to the metal ns character in the conduction bands (CBs) that leads to states with more dispersion. The spherical symmetry of the s states could also remain connected and result in delocalization even in the presence of structural disorder. These characteristics result in high electron mobility and consequently high-performance opto/electronic devices based on metal oxides. On the contrary, hole transport in these oxides is severely limited due to the presence of O 2p states in the valence bands (VBs) which create localizing states deep in energy. This means that their VBs are not accessible via injection or extraction by metal contacts and that the holes would have extremely low mobility.

The research community has been searching for alternative metal oxides with good hole-transporting characteristics. Many complex oxides have been proposed, but so far only Cu₂O, SnO, and NiO have been demonstrated to exhibit potential for practical applications.⁴ However, some important issues remain, in particular the phase stability problem as oxides of different oxidation states can co-exist, and the impurities of other phases are detrimental to charge transport. Moreover, these three oxides have small fundamental band gaps, resulting in the absorption in the visible spectrum that

restricts their applications as a hole transport layer in optoelectronic devices (that requires the optical transparency) such as organic solar cells (OSCs), perovskite solar cells (PSCs), or organic light-emitting diodes (OLEDs).

However, from the practicality point-of-view, we do not need to limit the materials scope to metal oxides. The required properties are hole-transport enabling, solution-processability (or more general, large-area compatibility), and, for use as the hole transport layer in optoelectronic devices, a wide band gap. We have shown previously that copper(I) thiocyanate (CuSCN), a metal pseudohalide, can satisfy all three criteria, and its applications in various thin-film devices have been demonstrated. The case of CuSCN, the copper is in +1 oxidation state similar to ${\rm Cu_2O}$, both of which show the same characteristic of ${\rm Cu}\ 3d$ states near the top of VB, leading to dispersed states for hole transport. However, SCN ligand is found to stabilize the Cu(I) state. For example, even for the preparation that starts from Cu(II) salts, the product exclusively contains CuSCN with Cu(I). Moreover, the SCN ligand widens the band gap due to the CB consisting of the antibonding π^* molecular orbital (MO) of the SCN which is high in energy.

In this work, to develop a new hole-transporting inorganic semiconductor, we extend the idea of SCN-based material to tin(II) thiocyanate $[Sn(NCS)_2]$. Comparing between Cu_2O and SnO, the latter consistently shows larger hole mobility, which could be due to the 5s electrons of Sn(II) contributing to hole-transporting states in the VB. This is similar to the case of the ns electrons in the CBs of the n-type oxides. Many reports have also predicted complex oxides based on Sn(II) that should have hole-transporting and transparent properties. $^{9-11}$ Taking a different and novel approach, we attempted to synthesize $Sn(NCS)_2$ with the expectation that the thiocyanate ligand can also stabilize Sn(II) state as well as widen the band gap. The compound was extensively studied both experimentally and theoretically. Initial device application was also investigated by employing $Sn(NCS)_2$ film as a hole transport layer in organic solar cells (OSCs). Also, this could be the starting point of a new family of materials – coordination polymer semiconductors.

As for further development of CuSCN, we aim to better understand its chemistry and processing to improve its performance. CuSCN can be processed from solution, but controlling the properties of the resulting thin films has been limited. Typically CuSCN is deposited from disulfide-based solvents and forms compact thin films with nanocrystalline grains.^{5,12} The film morphology has a strong impact on charge transport

and the overall device performance, and changing film morphology is another objective of this project. We employed the anti-solvent treatment, which has been used successfully in the fabrication of perovskite films to enlarge the grain size and significantly improve charge transport. An anti-solvent does not dissolve the material and can accelerate the nucleation of crystals during the film coating. In this case, different anti-solvents were added to CuSCN wet films after deposition, and the resulting films were characterized and applied in thin-film transistors (TFTs) and organic solar cells (OSCs).

Objectives

- 1. To synthesize and characterize a new coordination polymer semiconductor based on Sn(II) thiocyanate [Sn(NCS)₂] and explore its potential for opto/electronic applications.
- 2. To control the film physical properties of CuSCN prepared from solution-based methods and investigate its applications in opto/electronic devices.

Chapter 2

Tin(II) Thiocyanate – a New Wide Band Gap Coordination Polymer Semiconductor

2.1. Introduction

Tin in the +2 oxidation state is a high-potential candidate for an inorganic hole-transporting semiconductor due to its 5s electrons that can form the valence band (VB) as demonstrated by tin(II) oxide (SnO) and various articles reporting theoretical predictions of ternary oxides also based on Sn(II). SnO shows excellent hole mobility with several reports of values higher than 1 cm² V⁻¹ s⁻¹. However, SnO suffers from phase instability due to the co-existence of multiple oxidation states and the small fundamental band gap of 0.7 eV.

As seen in CuSCN, the thiocyanate SCN ligand can stabilize the reduced oxidation state due to its softer chemical properties compared to oxygen and also widen the band gap as its antibonding molecular orbital (MO) is high in energy. We were therefore interested in investigating the thiocyanate compound of Sn(II). There were a couple of historical reports on the synthesis and basic structural characterization of Sn(NCS)₂. In this work, we successfully synthesized Sn(NCS)₂ and comprehensively characterized the morphology and crystalline structure with modern analysis methods. Its electronic structure was also studied by the density functional theory (DFT) with the collaboration from Dr. Daniel M. Packwood, from the Institute for Integrated Cell-Material Sciences (iCeMS), Kyoto University. Finally, the film deposition and applications in thin-film electronic devices were also investigated. The latter is still an ongoing work and provides the foundation for further work.

2.2. Methodology

Synthesis of Sn(NCS),

 $Sn(NCS)_2$ was synthesized by simple mixing and crystallizing the aqueous solution containing thiocyanate and Sn(II) ions (from NaSCN and $SnSO_4$, respectively) in the presence of acid. NaSCN (12 g) was dissolved in de-ionized (DI) water (50 mL) while $SnSO_4$ (8 g) was separately dissolved in a solution made from DI water (42 mL) and H_2SO_4 (1 M, 8 mL). The $SnSO_4$ solution, appearing slightly cloudy, was filtered directly into the NaSCN solution. The mixture was left at room temperature for 5 h, during which

white powder precipitated out, and then transferred into a freezer and left at -20 °C for 18 h for further crystallization. The product was filtered, triple-washed with DI water, and dried in a vacuum oven (10 mbar) at 80 °C for 8 h. The average weight of the product was 3.8 g, a yield of 43.3% (based on Sn).

Film deposition and device fabrication

Solutions of $Sn(NCS)_2$ were prepared by dissolving the product from the synthesis in various solvents. Films were deposited from such solutions by spin-coating onto substrates. Devices were fabricated by stacking spin-coated layers of $Sn(NCS)_2$ and other components (depending on the device architecture) with metal contacts. The latter were prepared by thermal evaporation and patterned with shadow masks.

Characterizations

The sample was characterized by single-crystal X-ray diffraction (SC-XRD), powder X-ray diffraction (PXRD), scanning electron microscopy (SEM), and transmission electron microscopy (TEM) to study its structural and morphological properties. X-ray photoelectron spectroscopy (XPS) and attenuated total reflectance. Thermogravimetric analysis (TGA) was employed to study its thermal stability. The optical properties were investigated by the ultraviolet-visible-near infrared spectroscopy (UV-Vis-NIR).

The film thickness was measured by profilometry, and the film topography by the atomic force microscope (AFM). The transistor devices were measured by a probe station and a DC source-measure unit. The solar cells were characterized also by a DC source-measure unit under a sun simulator (AM1.5 and 100 mW cm⁻²).

Density functional theory calculations

The density functional theory (DFT) calculations were carried out using the Vienna Ab Initio Simulation Package (VASP) with plane wave basis sets and PAW-PBE pseudopotentials. The rev-vdW-DF2 exchange-correlation functional was also used to account for the dispersion forces. Band structure calculations were performed using a $8\times8\times8$ Γ -centered k-points mesh and a 640 eV basis set energy cut-off. Density of states and charge density calculations were performed using a $16\times16\times16$ Γ -centered k-points mesh and a 640 eV basis set energy cut-off. The Brillouin zone path follows that of a triclinic system as described by Setyawan and Curtarolo. The Brillouin zone path follows that

2.3. Results and discussion

2.3.1. Physical properties of Sn(NCS),

The synthesized product appears as white needles with some single-crystalline particles (Fig. 2.1), the latter of which were used for structural determination by SC-XRD. The results show the following parameters: M=234.85, triclinic, a=4.8792(4), b=5.6694(4), c=10.1845(8) Å, $\alpha=100.369(2)$, $\beta=97.316(2)$, $\gamma=93.225(2)^\circ$, V=273.96(4) Å³, T=143 K, space group $P\bar{1}$, Z=2, 1672 reflections measured, 1626 unique ($R_{\rm int}=0.0143$). The final w $R(F^2)$ was 0.0400. Structural data CCDC 1878409 is available from the Cambridge Crystallographic Data Centre.

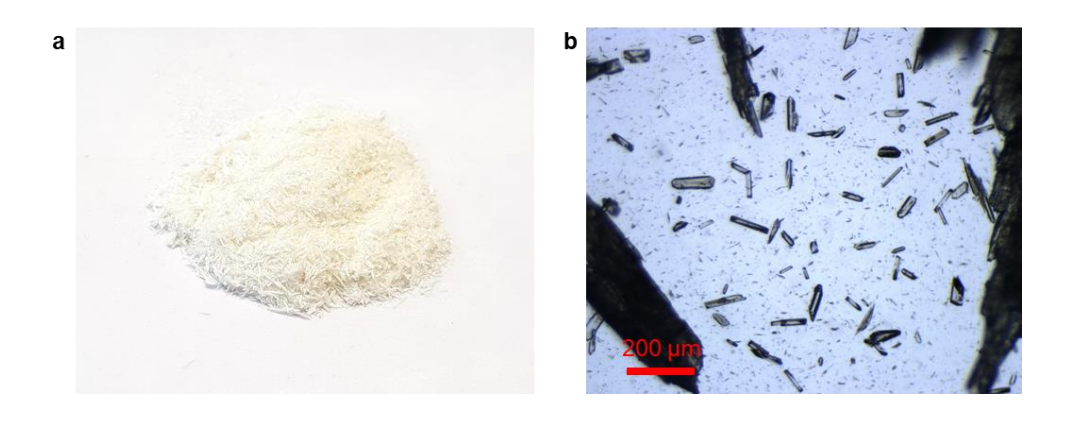


Figure 2.1. (a) Bulk sample of Sn(NCS)₂ obtained after synthesis. Lustrous white needles are visible. (b) Sn(NCS)₂ sample under optical microscope. Some particles are single crystals which were used for single crystal X-ray measurement and analysis. [Pattanasattayavong *et al.*, 2018, under review].

Fig. 2.2a shows the asymmetric unit which consists of a Sn center and two N-bonded thiocycnate units (and hence the NCS used in this case). N1-C1-S1 is in bridging mode ('bridging' NCS) and connects Sn along the b-axis forming a 1D chain whereas N2-C2-S2 is non-bridging ('terminal' NCS). The Sn center has monocapped octahedral geometry, being coordinated by 6 NCS units and capped with a lone pair (arising from $5s^2$ electrons) as shown in Fig. 2.2b. The Sn atom has three covalent bonds (two from the bridging NCS ligands and one from the terminal NCS) and three further non-covalent interactions with the sulfur ends of the NCS units (dashed lines in Fig. 2.2b). These significant interactions may be described based on the novel concept of sigma-hole interactions and could be categorized as the tetrel bonds. ^{19,20} Our close inspection reveals that these tetrel bonds connect the covalently-bonded 1D chains

together, forming the extended structures of the 1D ribbons (Fig. 2.2c and d) and the 2D sheets (Fig. 2.2e and f).

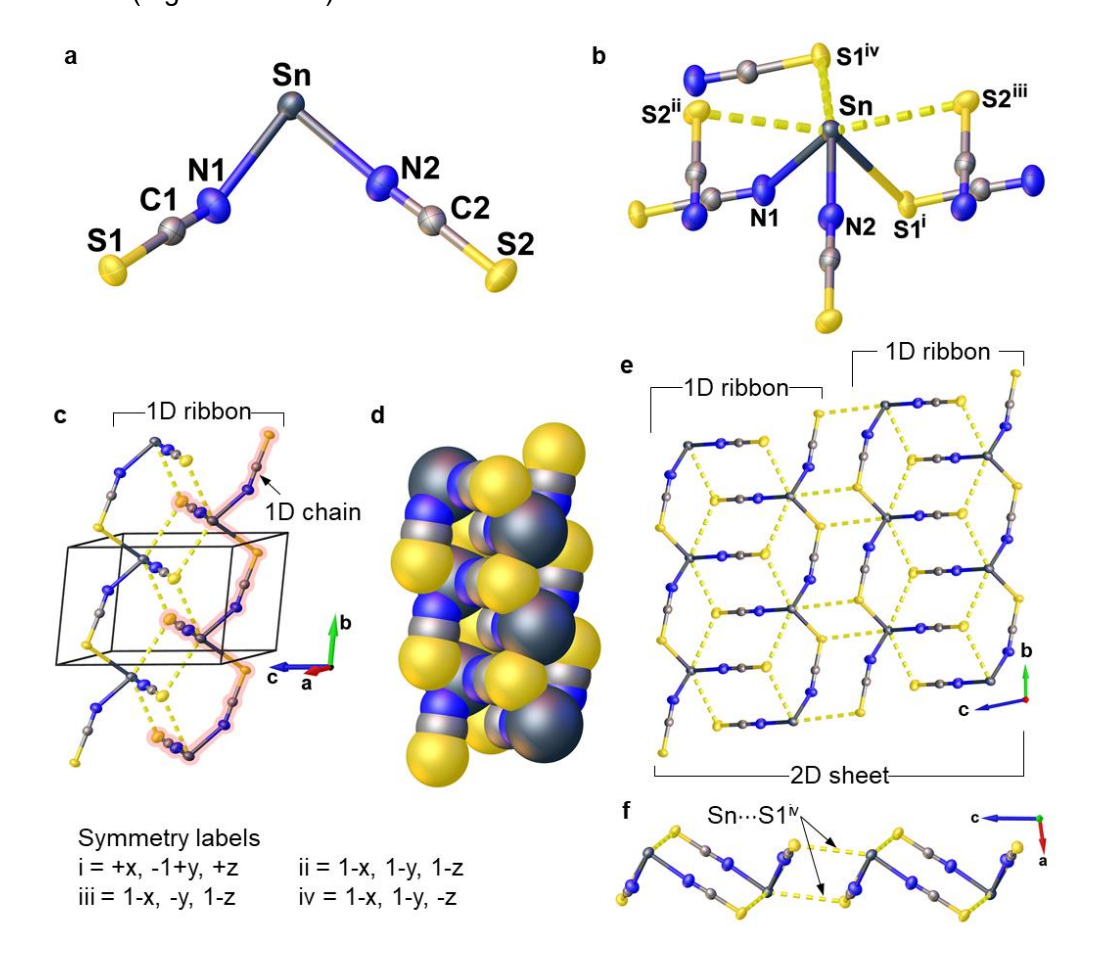


Figure 2.2. (a) Asymmetric unit of Sn(NCS)₂. (b) The full coordination of the Sn center with three covalent bonds and three tetrel bonds (Sn···S contacts), resulting in the monocapped octahedral geometry with the lone pair in the capping position. (c) 1D chains of covalently-bonded Sn(NCS)₂ propagating along the *b*-axis. One of the two centrosymmetric chains is highlighted. The two chains are linked together along the length via Sn····S2ⁱⁱⁱ and Sn····S2ⁱⁱⁱⁱ contacts to form the 1D ribbon. The unit cell is shown as a gray box. (d) Spacefill model showing the overlap of Sn and S2ⁱⁱⁱ/S2ⁱⁱⁱⁱ which confirms the significance of the non-covalent Sn···S contacts. (e) and (f) The 1D ribbons are linked into a 2D corrugated sheet via the Sn····S1^{iv} contact. [Pattanasattayavong *et al.*, 2018, under review].

The powder sample of $Sn(NCS)_2$ was also measured with PXRD as shown in Fig. 2.3a. The diffraction pattern of the as-synthesized sample matches with the simulated pattern based on the SC-XRD data. Also, remeasuring the sample after 6-month storage shows that the sample is stable. The SEM and TEM techniques were also employed to study the $Sn(NCS)_2$ powder sample. The SEM image in Fig. 2.3b reveals the layered structure that could substantiate the 2D structure explained from the

SC-XRD analysis. A closer inspection by TEM and high-resolution TEM (HRTEM) shows that the layered flakes are composed of small nanocrystalline domains (Fig. 2.3c to f). An example of the round nano-domains is shown in Fig. 2.3e (magnified image of region A1 marked in Fig. 2.3d). These round domains are randomly distributed and correspond to the broad ring in the selected-area electron diffraction (SAED) pattern in Fig. 2.3g. Another type of nanocrystalline domains is seen as elongated regions with clear lattice fringes, an example of which is shown in Fig. 2.3f (magnified image of region A2 marked in Fig. 2.3d). These fringes correspond to the (010) and higher-order diffractions observed in the SAED (Fig. 2.3g).

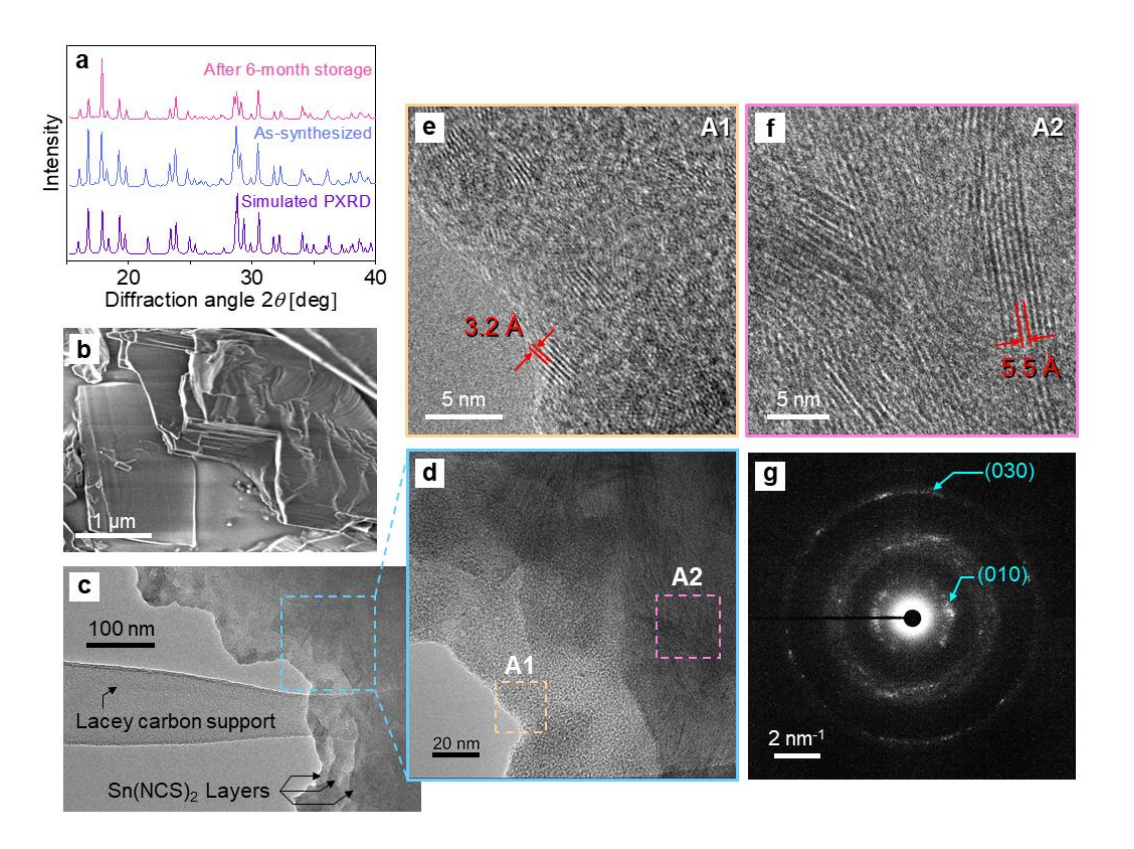


Figure 2.3. (a) PXRD patterns of as-synthesized and aged Sn(NCS)₂ samples. Simulated pattern from the single crystal data is also shown. (b) SEM image showing the layered structure of Sn(NCS)₂ flakes. (c) TEM image of an individual Sn(NCS)₂ flake. (d) HRTEM image of the region marked by the dashed blue square in (c). (e) Magnified image of an area marked as A1 in (d). (f) Magnified image of an area marked as A2 in (d). (g) Selected area electron diffraction pattern of (d). [Pattanasattayavong *et al.*, 2018, under review].

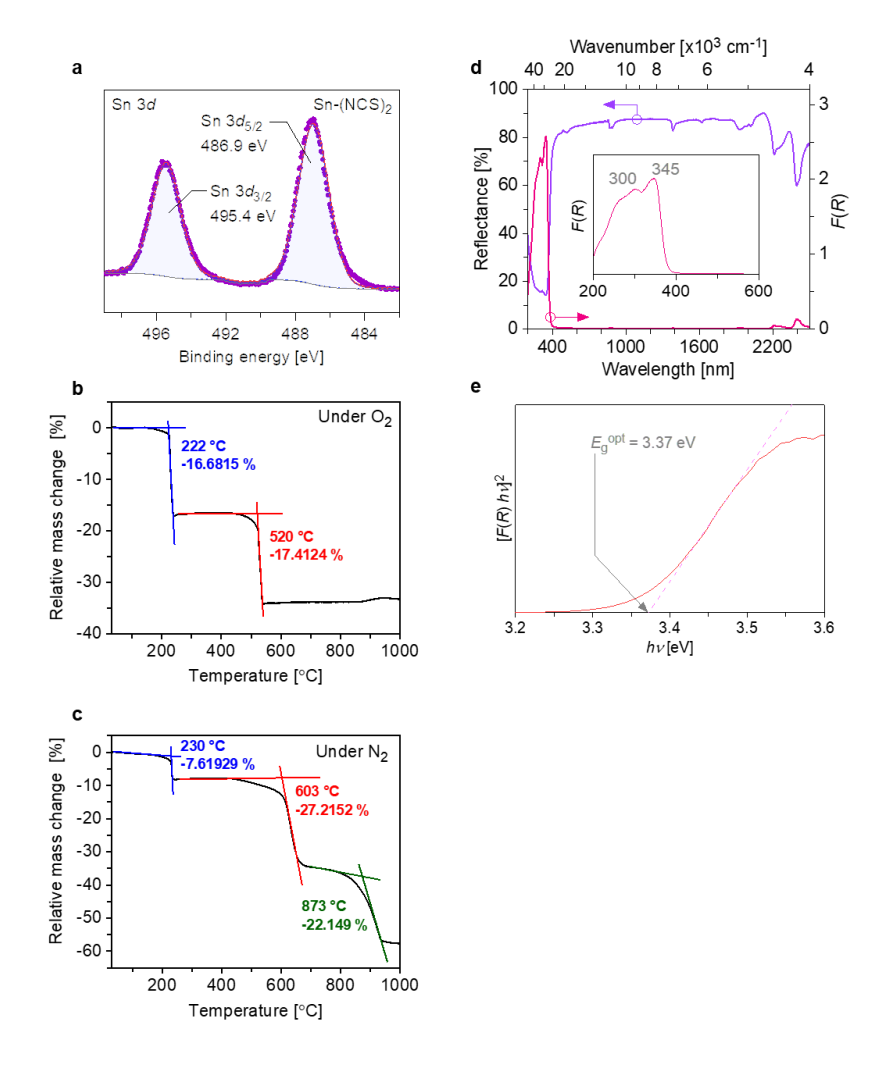


Figure 2.4. (a) Sn 3d core-level XPS spectrum of $Sn(NCS)_2$ sample. Scattered points are collected data. Solid gray line is the background. Dashed blue line and the corresponding blue-shaded region show the fitted peak. Solid red line is the reconstructed spectrum from the fitted peaks. The dashed blue line and the solid red line lie on top of each other in this case. Plots of relative mass changes of $Sn(NCS)_2$ powder samples from thermogravimetric measurements under (b) O_2 and (c) N_2 . (d) Optical reflectance spectrum and the Kubelka-Munk function [F(R)] of $Sn(NCS)_2$ powder sample. The short wavelength region of the latter is displayed in the inset. (e) Tauc plot showing the large optical band gap (E_g^{opt}) of 3.37 eV of $Sn(NCS)_2$ powder sample. [Pattanasattayavong *et al.*, 2018, under review].

The XPS scan of powder $Sn(NCS)_2$ sample shows that the Sn exists in one state (Fig. 2.4a), confirming our hypothesis that the NCS ligand can stabilize the Sn(II) state. The compound is also thermally stable up to 220 °C and 230 °C under O_2 and N_2 atmospheres, respectively (Fig. 2.4b and c). The optical absorption in the UV-Vis-NIR range is shown as the Kubelka-Munk function [F(R)], calculated from the reflectance spectrum of $Sn(NCS)_2$ powder sample (Fig. 2.4d). It shows excellent transparency

covering the whole visible spectrum as well as the NIR region. Some absorption features at longer wavelengths are ascribed to overtones of mid-IR absorptions. The absorption starts below 400 nm and peaks at 345 nm and 300 nm. The band gap as calculated form the Tauc plot (Fig. 2.4e) is found to be 3.37 eV. This further verifies our hypothesis that the NCS ligand can widen the band gap. As such, we have successfully obtained a stable thiocyanate compound of Sn(II) with a large band gap.

2.3.2. Electronic structure and density of states

The electronic band structure of Sn(NCS)₂ calculated from DFT is shown in Fig. 2.5. We can observe that the fundamental band gap of Sn(NCS)₂ is indirect and has a value of 2.35 eV. The smaller value compared to the experimental result is a known property of DFT. A direct gap with a slightly larger energy gap of 2.38 eV is also found. The experimental optical absorption, especially that of disordered sample, is expected to show the direct absorption feature.

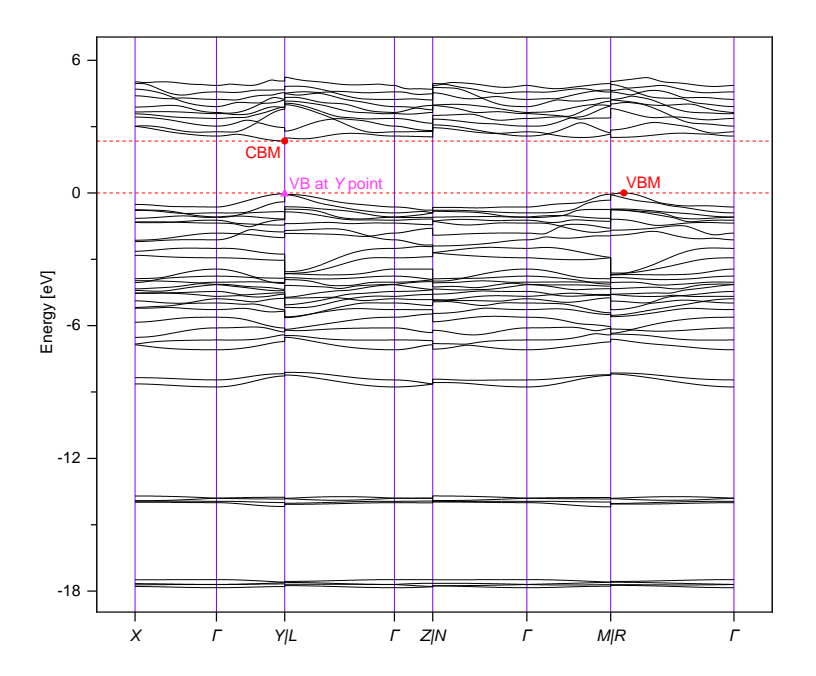


Figure 2.5. Electronic band structure of Sn(NCS)₂ calculated with DFT. The valence band maximum (VBM) and conduction band minimum (CBM) (solid red circles) occur at different *k*-points. Their energy difference, which in this case corresponds to the fundamental indirect band gap, is 2.35 eV. Also, the VB at Y point (solid pink triangle) is only 0.3 eV lower in energy than the VBM, resulting in a direct band gap of 2.38 eV. [Pattanasattayavong *et al.*, 2018, under review].

We also used DFT to calculate the density of states (DOS) and the orbital-projected partial density of states (PDOS) as displayed Fig. 2.6a and 2.6b. The DOS shows that the deep-energy states are bonding states with the NCS ligands, and the interactions between Sn and NCS are found between -10 eV and the top of the valence band (VB). Very interestingly, the Sn 5s electrons participate in the bonding with NCS ligands (Region I, Fig. 2.6b) and its antibonding states with strong character of S 3p contribute to the top of the VB where hole transport takes place. The general features of the VB can be compared to those of SnO as well. The conduction band (CB) is dominated by Sn 5p near the bottom and the antibonding MO on CN portion at higher energy (Fig. 2.6b). Overall, coordinating Sn(II) with NCS ligands indeed results in a compound with a stable Sn(II) state, wide band gap, and the Sn 5s electrons at the top of VB for hole transport. Also, the hole effective mass calculated form the curvature of the VB top is found to be $0.4m_0$, where m_0 is the electron rest mass. This value is close to that of CuSCN, and hence Sn(NCS) $_2$ is expected to show good hole mobility as well.

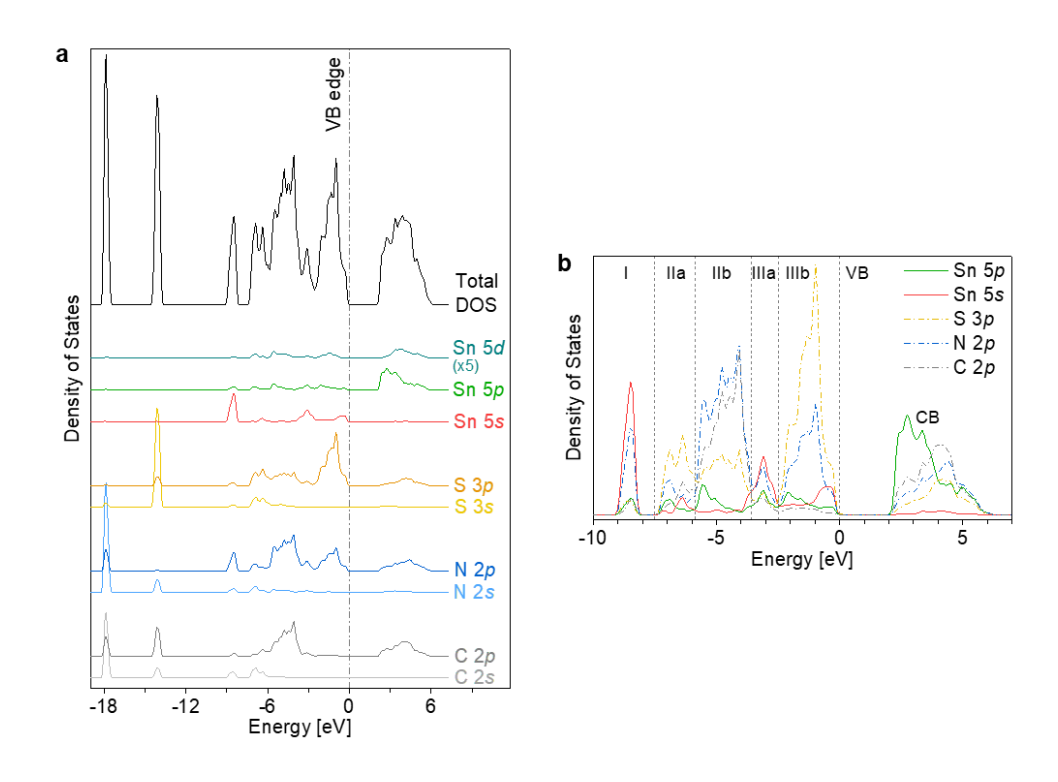


Figure 2.6. (a) Total DOS spectrum of Sn(NCS)₂ and valence orbital-projected PDOS spectra of the constituent atoms from DFT calculations. Valence band (VB) edge is set to zero energy. (b) PDOS spectra in the energy range -7 to 6 eV. Vertical dashed lines represent energy ranges of the VB subregions: I, IIa, IIb, IIIa, and IIIb. [Pattanasattayavong *et al.*, 2018, under review].

We also looked at the charge density distribution in Sn(NCS)₂ from the DFT calculations and have found that the lone pair indeed occupies the capping position (Fig. 2.7a), confirming our earlier structural analysis. By visualizing the electron density maps on the axial and basal planes (Fig. 2.7b), the bonding and antibonding character of the valence states (DOS and PDOS in the energy range of -10 eV to 0 eV in Fig. 2.6) can also be observed (Fig. 2.7c to n). Most importantly, the bonding (Region I; Fig. 2.7e and f) and antibonding states (Region IIIa and IIIb; Fig. 2.7k to n) formed by the Sn 5s electrons can also be seen.

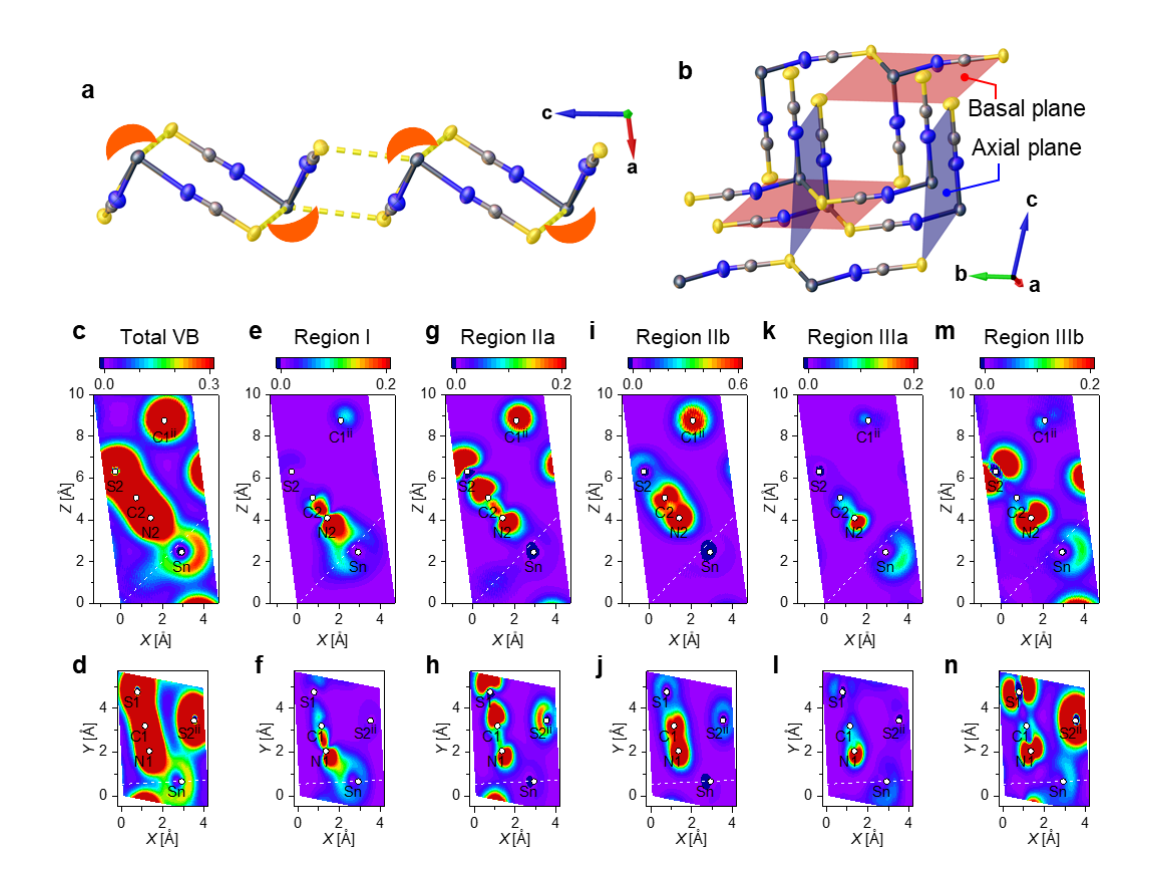


Figure 2.7. (a) Schematic of a $Sn(NCS)_2$ 2D sheet with the lone pair on Sn atoms. (b) Schematic showing the axial and basal planes used for the visualization of electron density. The contour maps of the electron density (number of electrons per Å³, represented by the color scale) of the whole VB (c, d) and VB sub-regions: Region I (e, f); Region IIa (g, h); Region IIb (i, j); Region IIIa (k, I); and Region IIIb (m, n). The electron density plots on the axial plane are plotted as projections on X-Z coordinates (c, e, g, i, k, and m) whereas those on the basal plane are plotted as projections on X-Y coordinates (d, f, h, j, I, and n). Positions of atoms which are located directly or approximately on the planes are labelled in the plots. Dashed white lines represent where the axial and basal planes intersect each other. [Pattanasattayavong *et al.*, 2018, under review].

2.3.3. Sn(NCS), thin films and applications in organic solar cells

Sn(NCS)₂ was found to dissolve well in many solvents, such as tetrahydrofuran, methanol, ethanol, isopropanol, dimethyl formamide, and dimethyl sulfoxide. We chose ethanol as the main solvent as due to the good solubility of Sn(NCS)₂ (up to 80 mg mL⁻¹) and appropriate boiling point (78 °C). Films of Sn(NCS)₂ were prepared by spin coating 20 mg mL⁻¹ of Sn(NCS)₂ in ethanol onto substrates at 2000 rpm and annealed at 80 °C. The films were first studied by XPS and UV-Vis-NIR, the results of which are shown in Fig. 2.8. The XPS results comparing between powder and film samples show that the Sn(II) state is retained (Fig. 2.8a). The films are also highly transparent with close to 100% optical transmission for wavelengths longer than 400 nm (Fig. 2.8b). The optical band gap extracted from the Tauc plot (Fig. 2.8c) is 3.98 eV, a value which is higher than the powder sample due to the very thin nature of the films.

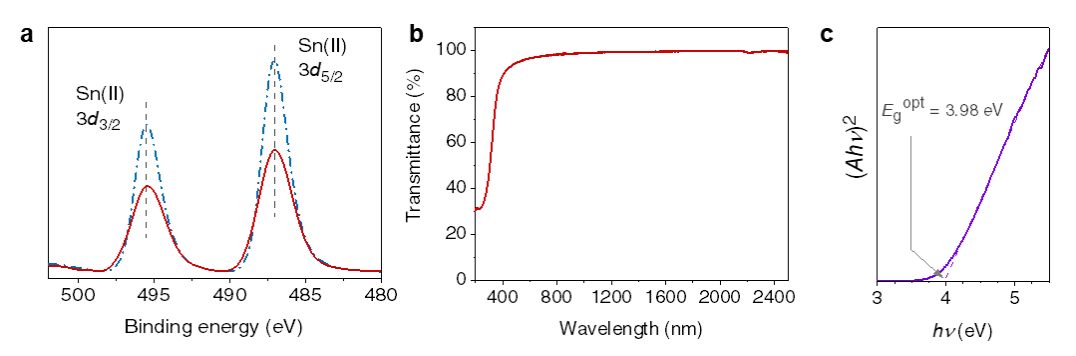


Figure 2.8. (a) Sn 3d core-level XPS spectra of $Sn(NCS)_2$ powder sample (blue dash-dot line) and film sample spin-coated from ethanol solution (red solid line). (b) Optical transmission spectrum of spin-coated $Sn(NCS)_2$ film sample. (c) Tauc plot calculated from the transmission spectrum. The optical band gap of the thin film is found to be 3.98 eV. [Pattanasattayavong *et al.*, Manuscript in Preparation].

The films of $Sn(NCS)_2$ were employed as the hole transport layer (HTL) in organic solar cells (OSCs), of which structure is shown in Fig. 2.9a. In this case, the active light-absorbing bulk-heterojunction (BHJ) layer was PTB7-Th:PC₇₀BM as the donor and acceptor (PTB7-Th = poly([2,6'-4,8-di(5-ethylhexylthienyl)benzo[1,2-b;3,3-b]dithiophene]{3-fluoro-2[(2-ethylhexyl)carbonyl]thieno[3,4-b]thiophenediyl}); and PC₇₀BM = [6,6]-Phenyl C₇₁ butyric acid methyl ester). The electron transport layer (ETL) was bathocuproine (BCP). The HTL was either $Sn(NCS)_2$ or PEDOT:PSS [or poly(3,4-ethylene dioxythiophene):poly(styrenesulfonate)] as a reference device. For device fabrication, the HTL and BHJ layers were deposited by spin-coating and the ETL and Al

layers by thermal evaporation. The active area of the solar cell device, as defined by the top Al contact patterned via a shadow mask, was 0.18 cm².

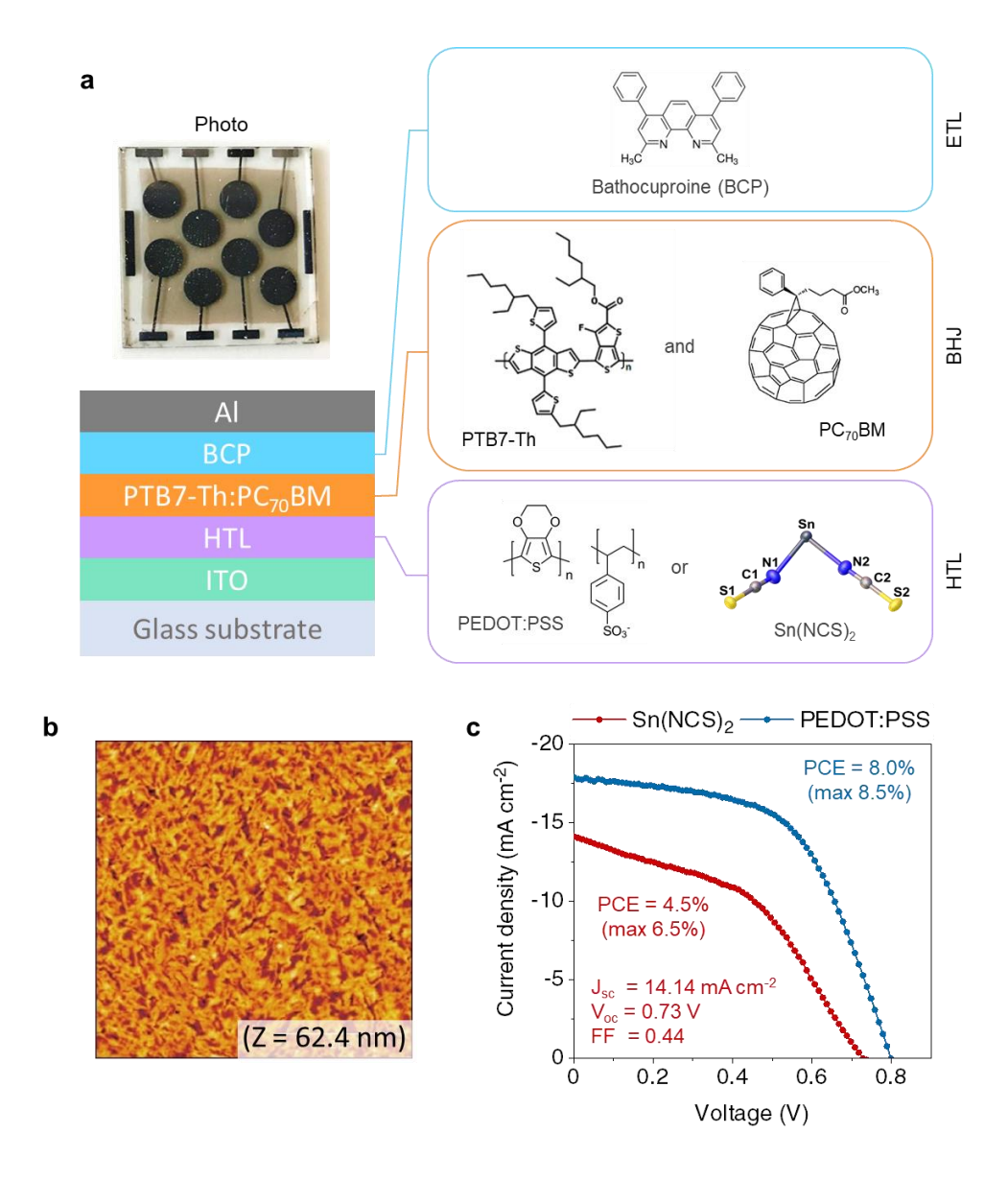


Figure 2.9. (a) Schematic diagram of the OSC structure and chemical structures of the components used. The hole transport layer (HTL) was either PEDOT:PSS (reference device) or $Sn(NCS)_2$. The bulk-heterojunction (BHJ) layer was PTB7-Th:PC₇₀BM as the donor-acceptor organic light-absorbing layer. The electron transport layer (ETL) was BCP. ITO and Al were used as the anode and cathode, respectively. A photo of the resulting device is also shown. The active device area was 0.18 cm². (b) Surface topography of the spin-coated $Sn(NCS)_2$ film from ethanol solution. Scan size = $5x5 \ \mu m^2$. Root-mean-square (RMS) roughness = $7.71 \ nm$. (c) Current density – voltage (J-V) characteristics of the OSC using $Sn(NCS)_2$ as the HTL (red filled circles) and the reference sample using PEDOT:PSS as the HTL (blue filled circle). The average cell parameters are also given with the maximum obtainable efficiency given in the brackets. [Pattanasattayavong *et al.*, Manuscript in Preparation].

The film topography measured by the AFM is shown in Fig. 2.9b. The film is relatively rough with a root-mean-square (RMS) roughness of 7.71 nm. The surface features resemble those of CuSCN film coated from sulfide-based solvents, i.e., a homogeneous distribution of elongated grains. The resulting solar cells with $Sn(NCS)_2$ HTL exhibit moderate power conversion efficiencies (PCEs) with an average value of 4.5% and maximum value of 6.5%. These are still inferior to the reference PEDOT:PSS samples which have PCEs higher than 8%, but the initial results are already highly encouraging. Other average cell parameters of $Sn(NCS)_2$ -based devices are: short-circuit current (J_{sc}) of 14.14 mA cm⁻², open-circuit voltage (V_{oc}) of 0.73 V, and fill-factor (FF) of 0.44. The lower FF indicates that the cells may suffer from poor film and interface qualities. Further optimization of film deposition and device fabrication process is expected to increase the PCE further.

2.4. Conclusions and outlook

We have identified Sn(NCS)₂ as a new wide band gap semiconductor with potential for use as a hole transport layer. This is a first report on a thiocyanate-based semiconductor with a different metal (other than Cu) and could provide a new research avenue on the field of 'coordination polymer semiconductor'. With the bridging NCS ligand, Sn(NCS)₂ forms a 1D chain via the covalent bonds and expands to 1D chains and 2D sheets via the non-covalent tetrel bonds. Compared to the *p*-type SnO, the NCS ligand is found to preserve the Sn 5s states near the top of VB and enlarge the band gap, resulting in the high transparency in the visible range of Sn(NCS)₂. This is similar to the case of CuSCN, which suggests that the thiocyanate ligand can potentially be used to engineer other transparent 'coordination polymer semiconductor'.

The application of Sn(NCS)₂ in opto/electronic devices is also demonstrated for the first time. Sn(NCS)₂ when used as the HTL in OSCs, albeit with moderate efficiency, shows promising characteristics for further investigation. Sn(NCS)2 is easily soluble in common alcohols and polar solvents, meaning that the deposition is simple and versatile. We have found that Sn(NCS)2 films are easily crystallized and form segregate islands that are detrimental to device operation. The current OSC fabrication also requires the treatment of the BHJ film with diiodooctane (DIO) to achieve high-efficiency. This step adversely affects the underlying Sn(NCS)₂ layer and is likely the cause of poor FF. Further optimization, for example, employing the inverted OSC architecture could mitigate the problem and is an ongoing investigation.

Chapter 3

Improving Hole Transport in Thin-Film Transistors (TFTs) based on Copper(I) Thiocyanate (CuSCN) by Anti-Solvent Treatment

3.1. Introduction

We have previously shown that copper(I) thiocyanate (CuSCN) can be used as the active semiconducting channel in thin-film transistors (TFTs). The hole-transporting ability and optical transparency in the visible spectrum of CuSCN results in the first demonstration of highly transparent p-type TFTs based on a solution-processed inorganic semiconductor.⁵ The field-effect hole mobility (μ_h^{FE}) was reported to be 0.01 cm² V¹ s⁻¹ on average.

Improving charge transport in CuSCN thin films is challenging as the control over the film properties is rather limited. CuSCN is not soluble in common solvents used in the film deposition in organic electronics; the common solvents used for CuSCN are sulfide-based, i.e., diethyl sulfide (DES) and dipropyl sulfide (DPS). A narrow window of deposition parameters is available, and the resulting thin films usually exhibit similar morphologies and yield the same average μ_h^{FE} of 0.01 cm² V⁻¹ s^{-1.5,7} Recently, Anthopoulos et al. have reported two methods that could increase the μ_h^{FE} of CuSCNbased TFTs by: (1) using aqueous ammonia as the solvent 12 and (2) doping CuSCN with $C_{60}F_{48}$. For the first method, they were able to obtain very smooth films of CuSCN that exhibit $\mu_h^{\rm FE}$ of 0.05 cm² V⁻¹ s⁻¹. When admixing $C_{60}F_{48}$ to CuSCN (process also based on DES solvent), the dopant was found to alter the morphology, increase hole concentration, and help reduce the trapping states at the dielectric/CuSCN interface; as a result, $\mu_h^{\rm FE}$ could be enhanced up to 0.1 cm² V⁻¹ s⁻¹. One drawback of the two methods is that the off-current also increases by more than one order of magnitude which is the common characteristic of doping. The current on-to-off ratio is inevitably reduced. Moreover, the aqueous ammonia solution is not easy to control due to the uncertainty in the ammonia concentration, the low boiling point, and the corrosive nature. Also, C₆₀F₄₈ is still an exotic compound which is not widely available.

In this work, we employed the anti-solvent treatment to adjust the film morphology and hole transport properties. ¹³ The anti-solvents are solvents that cannot dissolve CuSCN. In this case, we chose the common solvents, tetrahydrofuran (THF), acetone (Ace), methanol (MeOH), and isopropyl alcohol (IPA). These are widely available, making this method versatile and easily applicable.

3.2. Methodology

Solution and film preparation

CuSCN was dissolved in DES at a concentration of 10 mg mL⁻¹. The solution was spin-coated onto substrates at 2000 rpm under dry nitrogen atmosphere. The film was then annealed at 100 °C also under dry nitrogen atmosphere.

Anti-solvent treatment

While the film of CuSCN from DES solution was being spun, the anti-solvent was dropped directly onto the film prior to the annealing step. The anti-solvents used in this work were tetrahydrofuran (THF), acetone (Ace), methanol (MeOH), and isopropyl alcohol (IPA). The sample deposited from DES solution without treatment is designated as 'DES' whereas those treated are referred to as 'DES/THF', 'DES/Ace', 'DES/MeOH', and 'DES/IPA'.

Device fabrication

Top-gate bottom-contact (TG-BC) TFTs were fabricated by first preparing the bottom Cr/Au contacts on cleaned glass substrates by thermally evaporating Cr (5 nm) and Au (25 nm) through a shadow mask that defined the source/drain (S/D) contacts. The CuSCN layer was spin-coated on top using the procedure described above. The gate dielectric was prepared by spin-coating 25 mg mL⁻¹ of poly(vinylidene fluoride-trifluoroethylene-chlorofluoroethylene) [P(VDF-TrFE-CFE)] in 2-butanone onto the CuSCN layer at 3000 rpm. Finally, the gate contact was Al (40 nm) thermally evaporated through a shadow mask onto the dielectric layer.

Film and device characterizations

The surface morphology of CuSCN thin films was studied by the atomic force microscope. The CuSCN-based TFTs were characterized by a probe station and a DC source/measure unit under dry nitrogen atmosphere. The TFT parameters were calculated based on the gradual-channel approximation.

Synchrotron experiments

The sulfur K-edge X-ray absorption measurements were carried at Beamline 5.2XAS, Synchrotron Light Research Institute, Nakhon Ratchasima, Thailand. Powder samples of commercial CuSCN and crystallized $\{Cu(SCN)[(C_2H_5)_2S]\}_n$ [or Cu(SCN)(DES)] were

used as reference samples. CuSCN thin films with and without anti-solvent treatment were measured, and their spectra were processed by linear fitting of the CuSCN and Cu(SCN)(DES) spectra.

3.3. Results and discussion

3.3.1. CuSCN thin-film transistors

Fig. 3.1a shows the photo of the resulting TFT substrate along with the schematic diagrams of the device structure and also chemical structures of the CuSCN semiconducting channel layer and the P(VDF-TrFE-CFE) dielectric layer. The latter was chosen due to its high dielectric constant which can allow low-voltage operation of the transistors. The drain current–gate voltage (or transfer) characteristics of the devices with W = 1000 μ m and L = 30 μ m measured in the saturation regime (V_D = -20 V). are shown in Fig. 3.1b. Clear p-type operation was measured, and good transistor characteristics can be observed from the linear relationship of the square root of drain current vs gate voltage. The latter also allows the extraction of the threshold voltages (V_{th}) which were found to be around -5 V. The on current increases in the order DES/IPA < DES < DES/MeOH < DES/Ace < DES/THF. Correspondingly, the saturation field-effect hole mobility ($\mu_h^{\rm FE}$) also increases following the same order from 0.006 cm² V¹ s¹ of DES/IPA sample to 0.05 cm² V¹ s¹ of DES/THF sample (Fig. 3.1c). Interestingly, the off current remains low, resulting in a large on-to-off current ratio of almost 4 orders of magnitude.

3.3.2. Surface topography of CuSCN treated by anti-solvents

The surface topography was studied by AFM and the results are shown in Fig. 3.2. At the small scale (0.5 x 0.5 μm^2), elongated nanocrystalline grains can still be observed. It appears that THF, Ace, and MeOH reduce the over size of the grains whereas IPA only affects slightly. The treatment with Ace and MeOH also leads to the domains clumping together and less homogeneity at the larger scale (5 x 5 μm^2). On the other hand, THF results in the smoothest film, quantified by the smallest root-mean-square (RMS) roughness of 1.39 nm. We can also observe that the trend in μ_h^{FE} has an inverse relationship with the RMS roughness, i.e., large RMS roughness, smaller μ_h^{FE} .

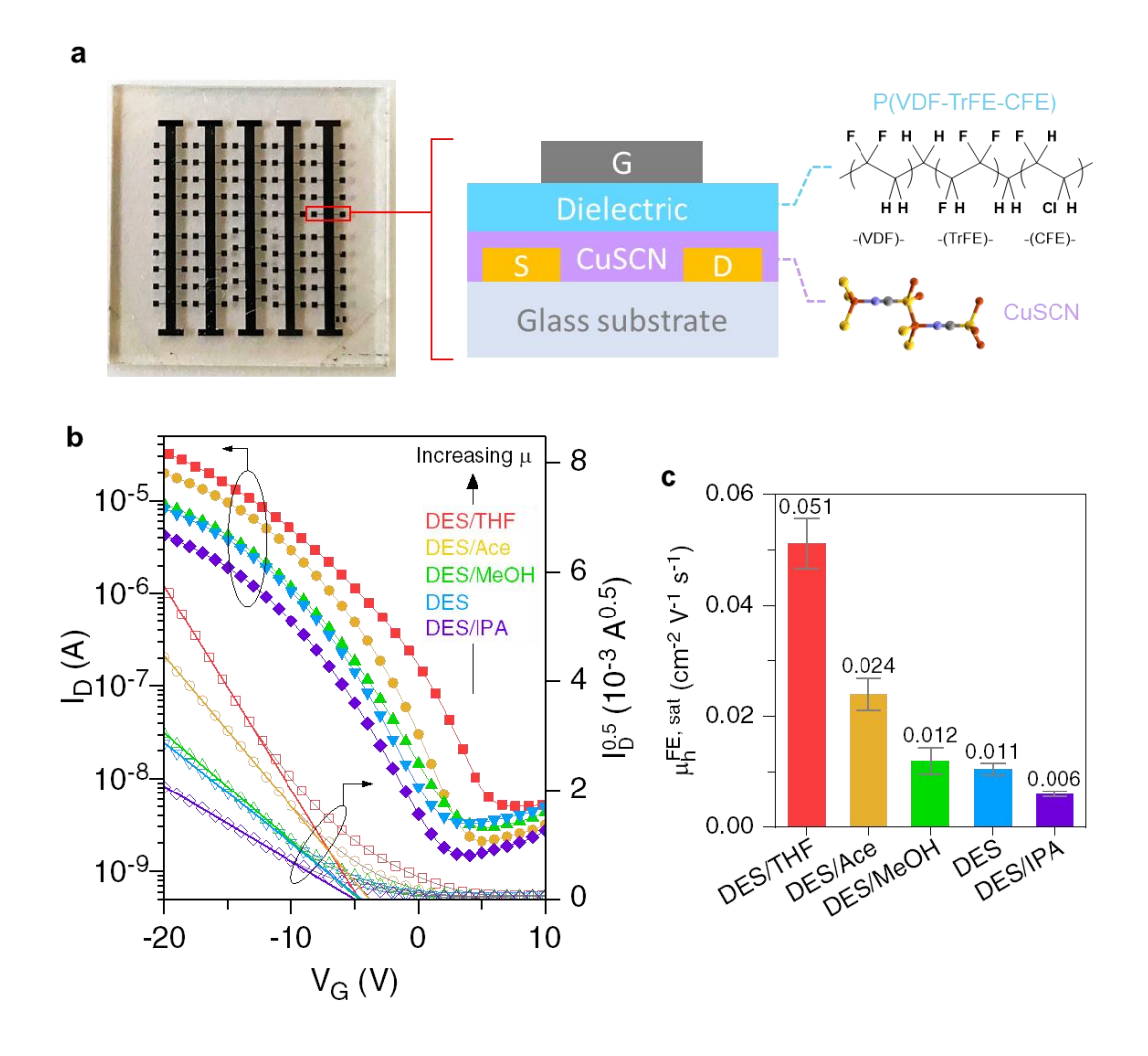


Figure 3.1. (a) Photo of the TG-BC TFT substrate (left), schematic diagram of the device structure cross-section (center), and chemical structures of the CuSCN semiconducting channel and the dielectric layer (right). (b) Transfer characteristics and the plot of square-root of the drain current vs. gate voltage of CuSCN TFTs processed from DES solution without anti-solvent treatment (DES) and those treated with THF (DES/THF), acetone (DES/Ace), methanol (DES/MeOH), and isopropyl alcohol (DES/IPA). The measurements were done at $V_D = -20$ V. The dimensions of the devices were W = 1000 μm and L = 30 μm. (c) Bar chart showing the average and standard-deviation of the field-effect hole mobility calculated from the saturation regime [transfer curves in (b)] of CuSCN TFTs with and without anti-solvent treatment, ranked in descending order from left to right. [Pattanasattayavong *et al.*, Manuscript in Preparation].

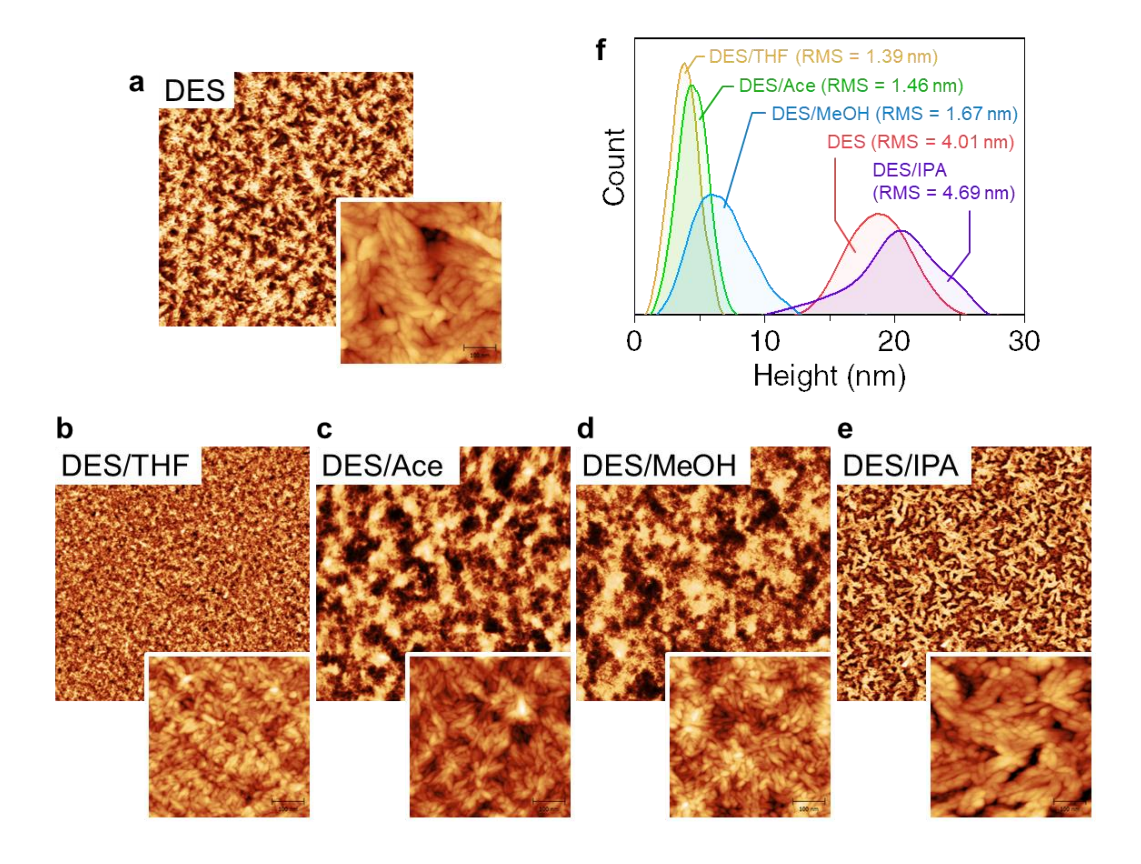


Figure 3.2. Surface topography images of CuSCN films deposited from DES solution without further treatment (a) and those with anti-solvent treatments (b to e). The large images are of scan size 5x5 μm^2 where the insets are 0.5x0.5 μm^2 . (f) Histograms of the surface height information from the large scan size of each image. The root-mean-square (RMS) surface roughness values are given in the brackets. [Pattanasattayavong *et al.*, Manuscript in Preparation].

3.3.3. Microstructure and local atomic environment

We investigated further by considering the microstructure and local atomic environment of the films. We have found that a different form of copper-based thiocyanate compound can be obtained from the slow evaporation of CuSCN in DES solution. The slow crystallization results in needle-shaped crystals that can be identified as $\{Cu(SCN)[(C_2H_5)_2S]\}_n$ or Cu(SCN)(DES), which is a 1D polymer with CuSCN as the backbone and DES molecules as the pendants. It is therefore expected that the films prepared from this solution may contain the mixture of CuSCN (Fig. 3.3a) and Cu(SCN)(DES) (Fig. 3.3b). Using synchrotron-based X-ray absorption measurements, we can indeed observe that the films contain the mixture of both, and the relative fractions of the two are plotted in Fig. 3.3c. The fraction of Cu(SCN)(DES) increases from DES/IPA < DES < DES/MeOH < DES/Ace < DES/THF, which is the same order of the increase in mobility. Also, the thickness of the films increases following the same

order. In short, the treatment of CuSCN film with THF results in a thicker film due to more fraction of Cu(SCN)(DES) that has a more expanded lattice. The smoother film likely contributes to better charge transport.

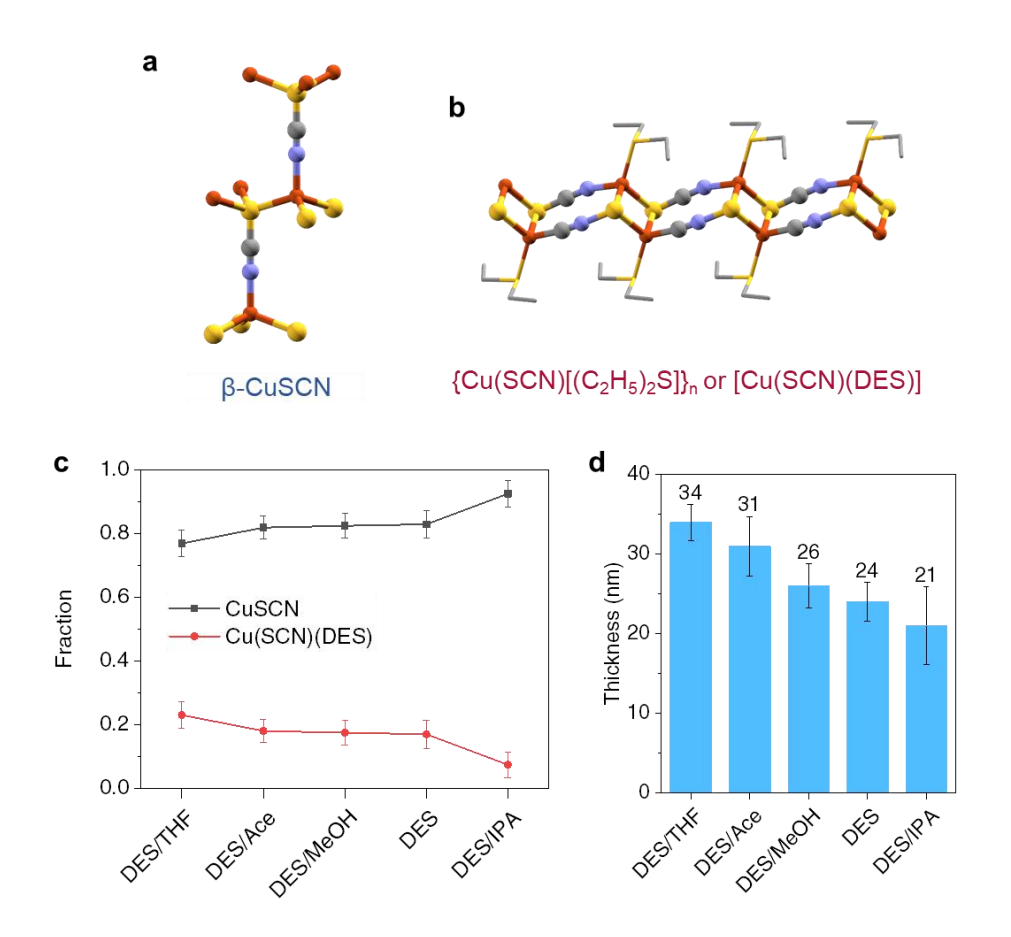


Figure 3.3. (a) Structure of CuSCN in the hexagonal β phase. (b) Structure of 1D coordination polymer based on CuSCN with DES coordination, $\{Cu(SCN)[(C_2H_5)_2S]\}_n$ or [Cu(SCN)(DES)]. (c) The relative fraction of CuSCN and Cu(SCN)(DES) components in the sulfur K-edge X-ray absorption spectra of CuSCN thin films with and without anti-solvent treatment. (d) Thickness of CuSCN thin films with and without anti-solvent treatment. [Pattanasattayavong *et al.*, Manuscript in Preparation].

3.4. Conclusions and outlook

We have successfully shown that treating CuSCN film with anti-solvents can result in the alteration of film morphology and charge transport properties. This is a simple and versatile technique that can be easily applied. In particular, treating the film with THF results in a smooth surface that can increase the saturation field-effect hole mobility by 5 times. This work is in the final stage of collecting supplementary data and will be published.

Chapter 4

High-Efficiency Organic Solar Cells with Anti-Solvent-Treated Copper(I) Thiocyanate (CuSCN) as a Hole Transport Layer

4.1. Introduction

As seen in the previous chapter, the treatment of CuSCN films with anti-solvents can alter the film morphology leading to different hole transport properties. In this work, we apply the similar method on CuSCN films deposited on ITO substrates which are used as the hole transport layer (HTL) in organic solar cells (OSCs).

4.2. Methodology

Solution, film preparation, and anti-solvent treatment

These processes follow the same procedure as described in Section 4.1.

Device fabrication and characterization

In this case, CuSCN films were spin-coated on glass/ITO substrates to be used as the HTL. The active organic bulk-heterojunction (BHJ) layer was PTB7-Th:PC₇₀BM, which is the same system used in Section 2.3.3. The BHJ layer was spin-coated on top of CuSCN layer. The solar cells were then completed by depositing bathocuproine (BCP) as the electron transport layer (ETL) and Al as the cathode by thermal evaporation through a shadow mask. The active cell area was 0.18 cm². The current density-voltage characteristics (*J-V*) of the cells were measured using a DC source/measure unit in air under simulated sunlight (AM1.5 100 mW cm⁻²).

4.3. Results and Discussion

4.3.1. Performance of solar cells with HTL based on CuSCN treated by anti-solvents

The schematic of the OSC structure is shown in Fig. 4.1a, and the energy diagram in Fig. 4.1b. CuSCN is a good candidate for a HTL in OSC due to the appropriate energy levels, i.e., a valence band (VB) near energy levels of ITO and the PTB7-Th polymer donor and a conduction band (CB) high in energy that can effectively block electrons and reduce the leakage current. Regarding the performance of the resulting OSCs, acetone was found to give the best improvement in power conversion efficiency (PCE) of the cells from 8.35% of untreated CuSCN (sample DES) to 8.93% (sample DES/Ace).

Surprisingly, the treatment by THF, which was shown to give the highest μ_h^{FE} in CuSCN TFTs, results in the worse OSC performance with PCE of 7.56% (sample DES/THF). Other solar cell parameters are included in Table 4.1.

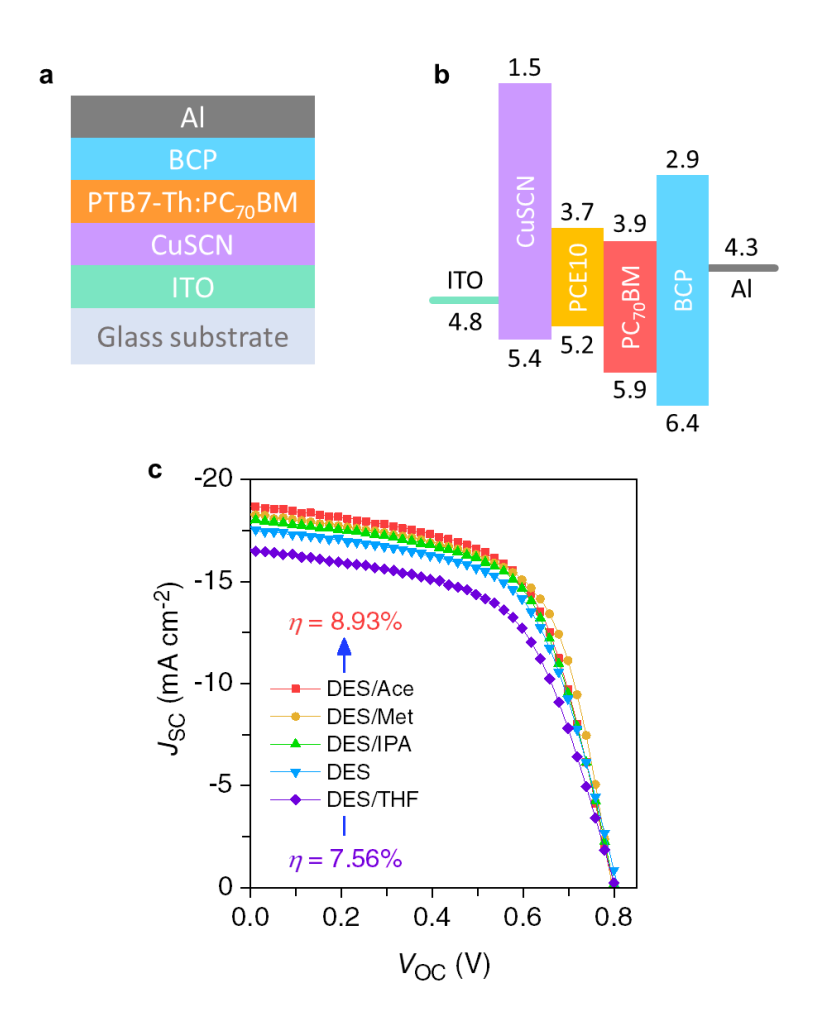


Figure 4.1. (a) Schematic diagram of solar cell structure. (b) Energy diagram of the solar cell components. (c) J-V characteristics of cells based on CuSCN as the HTL showing the effects of antisolvent treatment. [Pattanasattayavong *et al.*, Manuscript in Preparation].

Table 4.1. Solar cell parameter summary of OSCs based on CuSCN with and without anti-solvent treatment as the HTL. [Pattanasattayavong *et al.*, Manuscript in Preparation].

HTL	J _{sc} (mA cm ⁻²)	V _{oc} (V)	FF	PCE (%)
DES	17.5	0.79	0.59	8.35
DES/Ace	18.5	0.79	0.61	8.93
DES/IPA	18.2	0.79	0.61	8.90
DES/MeOH	18.2	0.79	0.60	8.71
DES/THF	16.7	0.79	0.58	7.56

4.3.2. Surface topography of CuSCN films on ITO after anti-solvent treatment

In order to study the effects of anti-solvent treatment on the film morphology, the films were measured with the AFM, and their surface topographical images are shown in Fig. 4.2. All films appear different from those shown in Fig. 3.2, which were CuSCN films deposited onto plain glass substrates. In this case, the films were deposited onto glass/ITO substrates. Since the surface of ITO is not featureless but is rough, containing small grains and also larger plate-like structures, it is likely that the underlying ITO influences the film formation of CuSCN.

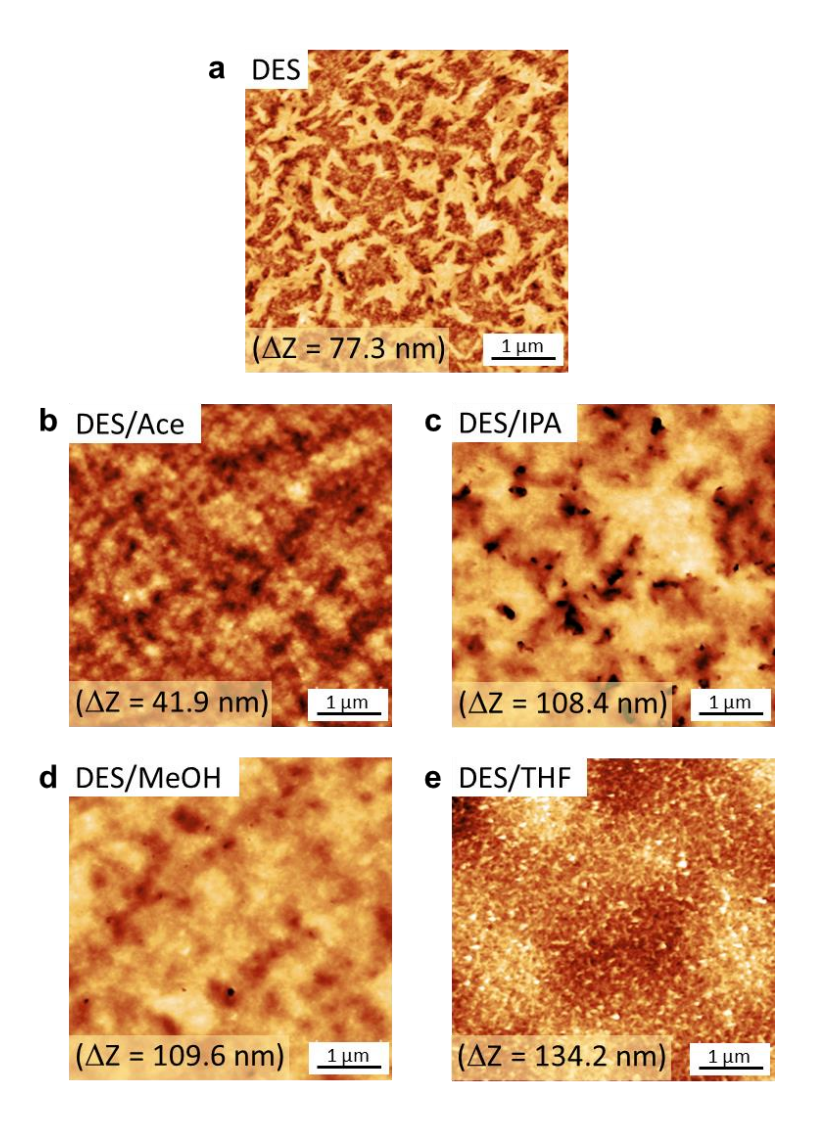


Figure 4.2. Surface topography of CuSCN films deposited onto glass/ITO substrates. (a) Asdeposited film without anti-solvent treatment. (b) Treated with acetone. (c) Treated with isopropyl alcohol. (d) Treated with methanol. (d) Treated with tetrahydrofuran. [Pattanasattayavong *et al.*, Manuscript in Preparation].

4.4. Conclusions and outlook

In addition to improving performance of CuSCN TFTs, anti-solvent treatment can also be used to improve the efficiency of OSCs using CuSCN as the HTL. This work demonstrates further the versatility and simple applicability of the method. We are now investigating more on how the anti-solvents affect the solar cell performance and will also publish the results.

Chapter 5 Summary

We have successfully synthesized and comprehensively characterized a new wide band gap inorganic semiconductor Sn(NCS)₂. This is the first thiocyanate compound based on another metal (other than Cu) that has been identified as a semiconductor. Through density functional theory, we have shown that Sn(NCS)₂ has a promising electronic structure for hole transport due to the Sn 5s electronic states at the top of the valence band. This work opens a new avenue of research towards the development of 'coordination polymer semiconductors'.

Furthermore, we have applied the anti-solvent treatment to the deposition of CuSCN thin films and shown that device performance can be improved both the case of thin-film transistors with CuSCN as the semiconducting channel and organic solar cells employing CuSCN as the hole transport layer. The anti-solvent treatment is simple and versatile and should be easily applicable to the broad research community.

These results have paved the way for our further investigation of 'coordination polymer semiconductors.' Specifically, the work has demonstrated that this family of compounds has the potential beyond CuSCN and that optimization of film deposition and device structure can further improve the charge transport characteristics which result in higher device performance. Coordination polymers have not been widely explored for their electronic properties and applications despite the large library of materials and the broad possibility of chemical modifications of both the metals and ligands. We hope that this research will be a starting point for the fruitful development of coordination polymer semiconductors for electronic applications.

Bibliography

- (1) Thomas, S. R.; Pattanasattayavong, P.; Anthopoulos, T. D. Solution-Processable Metal Oxide Semiconductors for Thin-Film Transistor Applications. *Chem. Soc. Rev.* 2013, 42 (16), 6910.
- (2) Nomura, K.; Ohta, H.; Takagi, A.; Kamiya, T.; Hirano, M.; Hosono, H. Room-Temperature Fabrication of Transparent Flexible Thin-Film Transistors Using Amorphous Oxide Semiconductors. *Nature* **2004**, *432* (7016), 488–492.
- (3) Medvedeva, J. E. Combining Optical Transparency with Electrical Conductivity: Challenges and Prospects. In *Transparent Electronics: From Synthesis to Applications*; Facchetti, A., Marks, T. J., Eds.; John Wiley & Sons: Chichester, UK, 2010; pp 1–29.
- (4) Wang, Z.; Nayak, P. K.; Caraveo-Frescas, J. A.; Alshareef, H. N. Recent Developments in P-Type Oxide Semiconductor Materials and Devices. *Adv. Mater.* 2016, 28, 3831–3892.
- (5) Pattanasattayavong, P.; Yaacobi-Gross, N.; Zhao, K.; Ngonggang Ndjawa, G. O.; Li, J.; Yan, F.; O'Regan, B. C.; Amassian, A.; Anthopoulos, T. D. Hole-Transporting Transistors and Circuits Based on the Transparent Inorganic Semiconductor Copper(I) Thiocyanate (CuSCN) Processed from Solution at Room Temperature. Adv. Mater. 2013, 25 (10), 1504–1509.
- (6) Perumal, A.; Faber, H.; Yaacobi-Gross, N.; Pattanasattayavong, P.; Burgess, C.; Jha, S.; McLachlan, M. A.; Stavrinou, P. N.; Anthopoulos, T. D.; Bradley, D. D. C. High-Efficiency, Solution-Processed, Multilayer Phosphorescent Organic Light-Emitting Diodes with a Copper Thiocyanate Hole-Injection/Hole-Transport Layer. Adv. Mater. 2015, 27 (1), 93–100.
- (7) Yaacobi-Gross, N.; Treat, N. D.; Pattanasattayavong, P.; Faber, H.; Perumal, A. K.; Stingelin, N.; Bradley, D. D. C.; Stavrinou, P. N.; Heeney, M.; Anthopoulos, T. D. High-Efficiency Organic Photovoltaic Cells Based on the Solution-Processable Hole Transporting Interlayer Copper Thiocyanate (CuSCN) as a Replacement for PEDOT:PSS. Adv. Energy Mater. 2015, 5 (3), 1401529.
- (8) Jaffe, J. E.; Kaspar, T. C.; Droubay, T. C.; Varga, T.; Bowden, M. E.; Exarhos, G. J. Electronic and Defect Structures of CuSCN. *J. Phys. Chem. C* **2010**, *114* (19), 9111–9117.
- (9) Li, Y.; Singh, D. J.; Du, M.-H.; Xu, Q.; Zhang, L.; Zheng, W.; Ma, Y. Design of Ternary Alkaline-Earth Metal Sn(II) Oxides with Potential Good p-Type Conductivity. *J. Mater. Chem. C* **2016**, *4* (20), 4592–4599.
- (10) Wahila, M. J.; Butler, K. T.; Lebens-Higgins, Z. W.; Hendon, C. H.; Nandur, A. S.; Treharne, R. E.; Quackenbush, N. F.; Sallis, S.; Mason, K.; Paik, H.; et al. Lone-Pair Stabilization in Transparent Amorphous Tin Oxides: A Potential Route to p-Type Conduction Pathways. Chem. Mater. 2016, 28 (13), 4706–4713.
- (11) Ha, V. A.; Ricci, F.; Rignanese, G. M.; Hautier, G. Structural Design Principles for Low Hole Effective Mass S-Orbital-Based p-Type Oxides. *J. Mater. Chem. C* **2017**, *5* (23), 5772–5779.
- (12) Wijeyasinghe, N.; Regoutz, A.; Eisner, F.; Du, T.; Tsetseris, L.; Lin, Y.-H.; Faber, H.; Pattanasattayavong, P.; Li, J.; Yan, F.; et al. Copper(I) Thiocyanate (CuSCN) Hole-Transport

- Layers Processed from Aqueous Precursor Solutions and Their Application in Thin-Film Transistors and Highly Efficient Organic and Organometal Halide Perovskite Solar Cells. *Adv. Funct. Mater.* **2017**, 27 (35), 1701818.
- (13) Paek, S.; Schouwink, P.; Athanasopoulou, E. N.; Cho, K. T.; Grancini, G.; Lee, Y.; Zhang, Y.; Stellacci, F.; Nazeeruddin, M. K.; Gao, P. From Nano- to Micrometer Scale: The Role of Antisolvent Treatment on High Performance Perovskite Solar Cells. Chem. Mater. 2017, 29 (8), 3490–3498.
- (14) Kresse, G.; Furthmüller, J. Efficient Iterative Schemes for Ab Initio Total-Energy Calculations Using a Plane-Wave Basis Set. Phys. Rev. B 1996, 54 (16), 11169–11186.
- (15) Klimeš, J.; Bowler, D. R.; Michaelides, A. Chemical Accuracy for the van Der Waals Density Functional. *J. Phys. Condens. Matter* **2010**, *22* (2), 022201.
- (16) Klimeš, J.; Bowler, D. R.; Michaelides, A. Van Der Waals Density Functionals Applied to Solids. *Phys. Rev. B* **2011**, *83* (19), 195131.
- (17) Hamada, I. Van Der Waals Density Functional Made Accurate. *Phys. Rev. B* **2014**, 89 (12), 121103.
- (18) Setyawan, W.; Curtarolo, S. High-Throughput Electronic Band Structure Calculations: Challenges and Tools. *Comput. Mater. Sci.* **2010**, *49* (2), 299–312.
- (19) Kolář, M. H.; Hobza, P. Computer Modeling of Halogen Bonds and Other **σ**-Hole Interactions. *Chem. Rev.* **2016**, *116* (9), 5155–5187.
- (20) Ullah, H.; Twamley, B.; Waseem, A.; Khawar Rauf, M.; Tahir, M. N.; Platts, J. A.; Baker, R. J. Tin···Oxygen Tetrel Bonding: A Combined Structural, Spectroscopic, and Computational Study. Cryst. Growth Des. 2017, 17 (7), 4021–4027.
- (21) Wijeyasinghe, N.; Eisner, F.; Tsetseris, L.; Lin, Y.; Seitkhan, A.; Li, J.; Yan, F.; Solomeshch, O.; Tessler, N.; Patsalas, P.; et al. P-Doping of Copper(I) Thiocyanate (CuSCN) Hole-Transport Layers for High-Performance Transistors and Organic Solar Cells. Adv. Funct. Mater. 2018, 1802055 (I), 1802055.

Appendix

Reprints of published articles, conference acceptance letters, and conference abstracts are included in this appendix.





Electronic Properties of Copper(I) Thiocyanate (CuSCN)

Pichaya Pattanasattayavong,* Vinich Promarak, and Thomas D. Anthopoulos

With the emerging applications of copper(I) thiocyanate (CuSCN) as a transparent and solution-processable hole-transporting semiconductor in numerous opto/electronic devices, fundamental studies that cast light on the charge transport physics are essential as they provide insights critical for further materials and devices performance advancement. The aim of this article is to provide a comprehensive and up-to-date report of the electronic properties of CuSCN with key emphasis on the structure-property relationship. The article is divided into four parts. In the first section, recent works on density functional theory calculations of the electronic band structure of hexagonal β-CuSCN are reviewed. Following this, various defects that may contribute to the conductivity of CuSCN are discussed, and newly predicted phases characterized by layered 2-dimensional-like structures are highlighted. Finally, a summary of recent studies on the band-tail states and hole transport mechanisms in solution-deposited, polycrystalline CuSCN layers is presented.

1. Introduction

Copper(I) thiocyanate (CuSCN) has been attracting increasing interest for use as an optically transparent hole-transporting intrinsic semiconductor in various opto/electronic devices including thin-film transistors (TFTs),^[1] organic-light emitting diodes (OLEDs),[2] bulk-heterojunction (BHJ) organic solar cells,^[3,4] extremely thin absorber (ETA) solar cells,^[5] dyesensitized solar cells (DSSCs), [6] and perovskite solar cells (PSCs).[7] Despite the breadth of the high potential technological applications (see also a review by Wijeyasinghe and Anthopoulos^[8] on applications of CuSCN), research into the electronic properties of CuSCN is still in the early stage. Some key aspects that provide the groundwork have recently been investigated both theoretically and experimentally, and it is the aim of this article to summarize these important works.

One important impediment in the development of inorganic semiconductors for plastic/organic electronics and related

Dr. P. Pattanasattayavong, Prof. V. Promarak Department of Materials Science and Engineering School of Molecular Science and Engineering Vidyasirimedhi Institute of Science and Technology (VISTEC)

Rayong 21210, Thailand E-mail: pichaya.p@vistec.ac.th

Prof. T. D. Anthopoulos Department of Physics and Centre for Plastic Electronics Blackett Laboratory Imperial College London London SW7 2AZ, United Kingdom

DOI: 10.1002/aelm.201600378



applications is the scarcity of suitable hole-transporting, wide band gap semiconductors. The arduous pursuit to predict, synthesize, and apply such materials has focused on metal oxide compounds and yielded only limited success, particularly when compared with the rapid advances of the electron-transporting counterparts such as ZnO, In2O3, or indium-galliumzinc oxide (IGZO). Among the range of studied p-type oxides, only Cu₂O, SnO, and NiO have been shown to yield functional opto/electronic devices (see a recent review on p-type oxide semiconductors by Wang et al.^[9]), but their performance is still lacking, especially when high transparency in the visible range is of crucial importance. In addition, their stability and processability are also of concern. On the other hand, CuSCN, a Cu(I) pseudohalide

compound, has been shown to be an intrinsic p-type inorganic semiconductor with a wide band gap ($\geq 3.5 \text{ eV}$)^[10–12] and appropriate electronic levels that allow efficient hole injection/extraction while simultaneously blocking electron transport.[2-4] The latter is a characteristic not shared by Cu2O, SnO, and NiO primarily due to difficulties associated with controlling their stoichiometry. As a result, CuSCN has successfully been employed as a universal, highly transparent hole-injecting/extracting/ transporting layer in a wide range of applications.[8] Additionally, CuSCN is chemically stable [13-15] and can be easily prepared at high purities as well as processed from the solution phase at low temperatures.[16-19] Moreover, owing to its quasimolecular nature, CuSCN can be chemically modified;[20] in fact, the properties and applications of CuSCN derivatives are still awaiting exploration and could potentially open up a new range of possibilities.

With an expanding list of important technological applications, it is now essential that the fundamental electronic properties of CuSCN are understood. Herein, we comprehensively review recent works on the electronic and charge transport properties of CuSCN. The band structure and density of states in hexagonal β -CuSCN are first examined to elucidate the underlying basis for the unique combination of excellent hole transporting characteristics and high optical transparency. Defects that could lead to unintentional doping are then considered. Apart from the known bulk α and β phases, recent works on the prediction of layered 2D-like structures of CuSCN are also presented. These newly predicted phases resemble those of the novel 2D metal dichalcogenides and graphene. In addition, models of different surfaces of hexagonal β -CuSCN are also discussed as the orientation of the structure is expected to



ADVANCED SCIENCE NEWS

www.advancedsciencenews.com

significantly affect the charge transport. Lastly, studies on the tail of localized states in the mobility gap and the resulting hole transport mechanisms in polycrystalline solution-processed layers of CuSCN are summarized.

2. Electronic Properties of CuSCN

Despite the relatively recent history of CuSCN as a promising hole-transporting material for numerous opto/electronic applications, there have been only a handful of published theoretical studies of the electronic properties of CuSCN, in particular by Jaffe et al., [11] Ji et al., [21] Chen et al., [22] and Tsetseris. [23] These works mainly employ the density functional theory (DFT) calculations for elucidating the electronic structure of the most popular form of CuSCN (usually observed in experiments), the hexagonal β -CuSCN (Figure 1a). The results of valence band (VB) and conduction band (CB) structures of different studies are in line with each other, and the two important characteristics near the band edges are: (1) the strong Cu 3d character with some hybridization from the S 3p states near the VB edge, and (2) the antibonding π^* character associated with the cyanide portion near the CB edge. These properties lead to the excellent hole transport and the predicted large indirect band gap, both of which result in the dominant p-type characteristics and the extremely high transparency in the visible range.

2.1. Electronic Band Structure of CuSCN

Different DFT calculations^[11,21,22] have yielded qualitatively consistent results of the band structure of hexagonal β -CuSCN (one set of the results^[22] is displayed in Figure 1b whereas the Brillouin zone of a hexagonal lattice^[24] is shown in Figure 1c). All of them unanimously predict an indirect band gap with a VB maximum (VBM) at the Γ point and a CB minimum (CBM) at the K point (Figure 1b and 1c). The DFT method employing the generalized gradient approximation (GGA), which is well known to underestimate the band gap, showed a relatively small gap of approximately 2 eV. However, by carrying out the DFT calculation with the Heyd-Scuseria-Ernzerhof (HSE) hybrid functional, Chen et al.[22] obtained a value of 3.45 eV which is closer to the experimental values of 3.7-3.9 eV.[11,12,25-27] However, the latter values were mostly obtained via Tauc analysis of the optical absorption spectra assuming a direct band gap (by setting the exponent parameter equal to 2 for the Tauc plot). Pattanasattayavong et al.^[1] carried out a similar analysis but for both indirect and direct types and obtained values of 3.5 and 3.9 eV, respectively. The lower value of the indirect type seems to corroborate the result from the DFT-HSE method while the higher value may indeed point to the existence of a higher energy transition of a direct type which has also been predicted by Jaffe et al.[11] to be at 0.4 eV higher than the lowest transition. On the other hand, Kim et al., [28] employing photoelectron spectroscopy (PES) and inverse photoelectron spectroscopy (IPES) to measure the VBM and the CBM of CuSCN, reported a band gap value of 3.65 eV without specifying whether the type was direct or indirect. Furthermore, the values of the band gap described so far are of CuSCN samples with polycrystalline

Tute's Distinction

Pichaya Pattanasattayavong obtained his BEng in Nano-Engineering (First Class Honors, 2009) from Chulalongkorn University, Thailand. He went on to receive his MSc (2010) and PhD (2014) in Physics from Imperial College London, UK. In 2015, he joined the School of Molecular Science and Engineering, Vidyasirimedhi

Institute of Science and Technology (VISTEC), Thailand, as a lecturer. His current research interests include novel solution-processable materials for opto/electronic applications as well as semiconductor physics and charge transport physics of novel materials and devices.



Vinich Promarak received his D.Phil. degree in Chemistry from University of Oxford, UK, in 2002 and is currently a full Professor of Chemistry at School of Molecular Science and Engineering, Vidyasirimedhi Institute of Science and Technology (VISTEC), Thailand. His research interests revolve around "high-tech" organic

materials that can be used in applications such as organic light-emitting diodes, perovskite/dye-sensitized solar cells, bulk heterojunction solar cells, sensors, optical switches, organic field-effect transistors.



Thomas D. Anthopoulos

received his D.Phil. degree in Physical Electronics from Staffordshire University, UK. In 2005 he was awarded an EPSRC Advanced Fellowship and in 2007 a RCUK Fellowship both hosted in the Department of Physics, Imperial College London, where he is currently a Professor of Experimental

Physics. His research interests are diverse and involve the development and application of novel nano-patterning paradigms, the physics of carbon-based, metal oxides and hybrid organic-inorganic semiconductors & devices and their applications.

or nanocrystalline morphologies which exhibit a significant and rather extensive absorption tail. Such an absorption feature may be due to the indirect band gap, disorder or non-crystallinity, polymorphism, or a combination of these factors.^[11] It





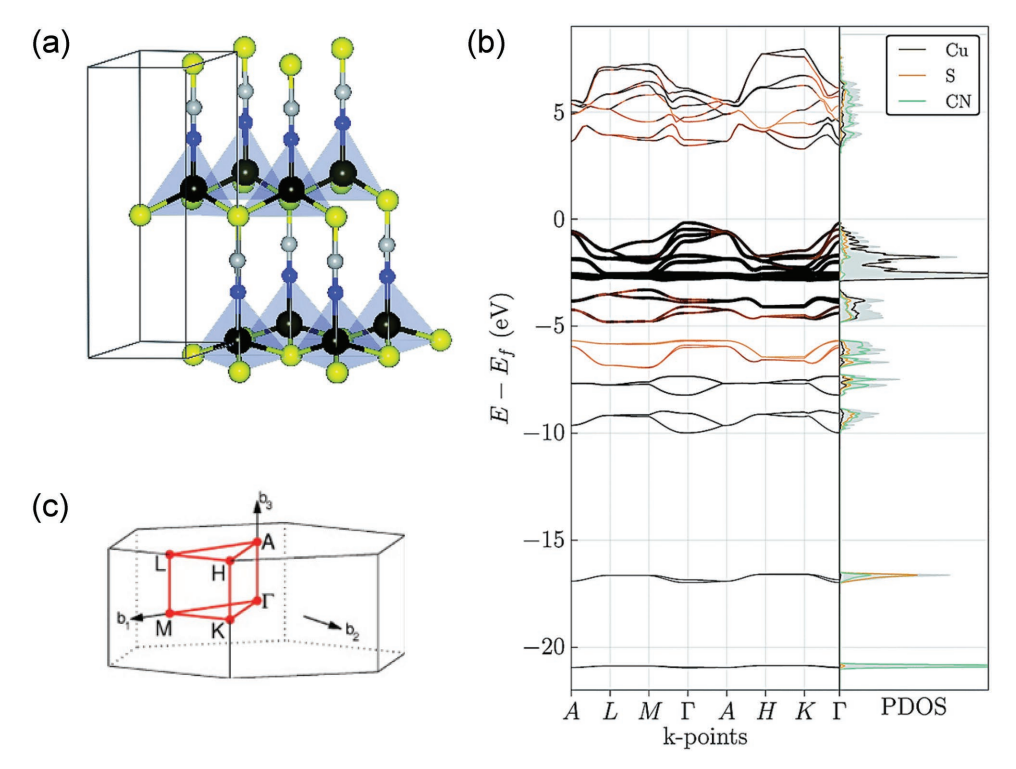


Figure 1. a) Crystal structure of hexagonal β-CuSCN. Atoms are color coded as dark brown for Cu, yellow for S, grey for C, and blue for N. b) Electronic band structure of hexagonal β-CuSCN calculated by DFT with HSE hybrid functional. Reproduced with permission. Copyright 2016, the Royal Society of Chemistry. c) Brillouin zone of a hexagonal lattice showing the high-symmetry path typically used in the electronic band structure calculations. Reproduced with permission. Copyright 2010, Elsevier.

should be noted, therefore, that the analysis of the band gap of CuSCN still requires further experimental verification.

Another important characteristic of the band structure of β -CuSCN is the relatively high dispersion near the top of the VB. Generally, for the common wide band gap semiconductors such as In2O3, SnO2, and ZnO, the CBs are highly dispersive while the VBs are flat near the band edges,^[29] resulting in n-type conductivity and high electron mobility values. On the other hand, calculations have shown that the relative dispersions of the CB and the VB in CuSCN are comparable (see Figure 1b),[11,21,22] suggesting that hole transport is not hindered (and conversely that electron transport is suppressed). The direction of transport is also important due to the alternating planes of Cu and SCN units. Along the c-axis of the crystal (along which the Cu and SCN layers alternate), Jaffe et al.[11] found that the effective masses (m* expressed in terms of multiples of the electron rest mass m_0) were similar, i.e., $m^* \approx m_0$ for electrons and $m^* \approx 0.8m_0$ for both heavy and light holes. On the other hand, the electrons and the heavy holes carried effective masses of $m^* \approx 2m_0$ in the ab plane whereas the light holes showed a smaller value of $m^* \approx 0.5 m_0$. The dispersion characteristics of VB and CB of CuSCN support the dominant hole-transporting properties of this material.

Furthermore, the appropriate level of the VBM (i.e., ionization energy) of CuSCN allows the injection and extraction of holes by common electrodes such as gold or indium tin oxide (ITO)-based conductors. It is crucial that good ohmic contacts can be established; otherwise, the hole-transporting properties

may not be useful if the semiconductor's VBM level is too deep or too shallow such that practical carrier injecting electrodes are not available. The reported values of the VBM of CuSCN are typically in the range of –5 to –6 eV as measured by the PES^[12,28,30] and electrochemical methods.^[31,32] On the other hand, the CBM level of CuSCN determined experimentally via IPES is found to be –2.5 eV.^[28] This characteristically shallow CBM energy makes CuSCN an excellent electron-blocking material as already demonstrated in several studies.^[2–4,33]

2.2. Density of States in CuSCN

Figure 2a shows the total density of states (DOS) and partial density of states (PDOS) of hexagonal β -CuSCN in more detail. The top of the VB from the VB edge (set at E = 0 eV) to approximately -2.5 eV is strongly dominated by the Cu 3d states with some contribution from the S 3p states. From -3.5 to -10 eV, there are four sub-bands altogether. The first three sub-bands, centered around -4, -6, and -7 eV, mainly arise from the p states of S, C, and N, which may be associated with the π bonding within the –SCN unit. The highest of these sub-bands (centered around -4 eV) also has contribution from the Cu 3d in addition to the S 3p and N 2p states, possibly suggesting the character of the bonding between Cu and the coordinating S and N as well. The last of the four sub-bands, located around −9 eV, is dominated by the S 3p and C 2p states, which implies an S-C bond. The photoemission spectrum of CuSCN near the VBM in this energy range is in qualitative agreement with

transport in CuSCN, similar to the case of Cu₂O, also a Cu(I) compound that shows a strong character of Cu 3d states at the VBM.^[34,35] This is in contrast to the dominant O 2p character in the VBM vicinity of important oxide semiconductors such as ZnO, SnO₂, and In₂O₃.^[29]

Interestingly, the CB edge, which is dominated by the C 2p and N 2p states, shows a unique character of the π^* antibonding orbitals of the cyanide part that has no analog in traditional semiconductors. The antibonding characteristics of the CB also results in a CBM located away from the Γ point in the Brillouin zone, [11] leading to the indirect type of the lowest interband transition. The indirect band gap also enhances the optical transparency in the visible range of CuSCN since strong absorption only takes place when the photon energies reach the direct gap which is at a higher energy.

(a) 60 50 40 DOS [states/eV-cell] Total 30 Cu d Ss Sp 20 Sd Cs Cp Ns Np -10 0 5 -20 -15 -5 Energy [eV]

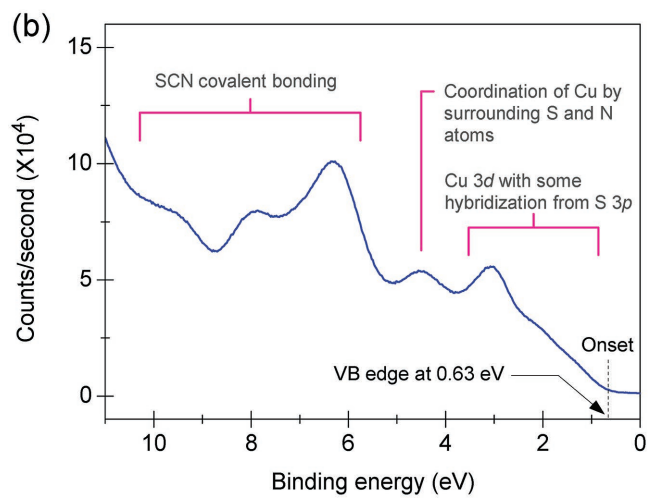


Figure 2. a) Calculated total and partial densities of states of hexagonal β-CuSCN showing the contributions from different states of the constituents of CuSCN. Reproduced with permission. Copyright 2010, American Chemical Society. b) Measured photoemission spectrum near the valence band edge of CuSCN. Features in the spectrum are labelled based on the calculated DOS shown in (a). Reproduced with permission. Copyright 2013, the Royal Society of Chemistry.

the calculated DOS, as displayed in Figure 2b. There are two additional sub-bands deeper in the VB, which predominantly contain the s states of S, C, and N. The sub-band around –16 eV is possibly associated with the S–C bond while the sub-band centered at –19 eV may arise from the σ bonding of the cyanide portion. In summary, with the increasing binding energy, the VB character of hexagonal β -CuSCN consists of: bonding between Cu 3d states with some hybridization from S 3p states, coordination between Cu 3d states and S 3p and N 2p states, and π bonding and σ bonding in the –SCN unit, respectively. The dominating Cu 3d states near the top of VB allows the hole

3. Defects in CuSCN

In an early study, Tennakone et al.[10] showed that the conductivity of CuSCN could be tuned to be either p-type or n-type by adjusting the Cu:SCN ratio. Specifically, the authors employed the chemical bath and electrodeposition methods to obtain both types of CuSCN. Based on their chemical methods and analyses, p-type CuSCN had a Cu:SCN ratio from 0.92 to 0.96 where n-type CuSCN showed a ratio between 1.31 and 1.44. Following, it was also demonstrated that doping CuSCN with SCN could increase its p-type conductivity.[36] Therefore, extrinsic p-doping of CuSCN has generally been associated with the excess SCN or deficient Cu conditions, and naturally the native defect Cu vacancy (V_{Cu}) is proposed to be the major source of excess holes often observed in CuSCN.[11,21,23] In extrinsically p-doped CuSCN, the Fermi level (E_F) has been reported to shift toward the VBM (e.g., 0.63 eV above VBM by Pattanasattayavong et al.[12] and 0.75 eV above VBM by Kim et al.[28]) Reports on n-type conductivity of CuSCN, on the other hand, is not common and, even if attainable, may not be suitable for practical applications because the CBM is shallow (around -2 to -3 eV with respect to the vacuum level) and would require the use of electrodes with extremely low work function and/or the use of doped injection layers. Next, we discuss relevant types of defects that can influence the conductivity of CuSCN.

3.1. Copper Vacancy

Computational results have shown that Cu vacancies should be stable and result in a shallow acceptor level that can contribute to high hole concentrations in hexagonal β -CuSCN. [11,21,23] The removal of a Cu atom from the lattice causes the neighboring atoms to move only slightly. [11,23] For example, Tsetseris [23] calculated that the distance between S atoms would change from 3.85 Å to 3.71 Å. Jaffe et al. [11] reported that the formation energy of a Cu vacancy was around 0.2 eV for a 32-site supercell and estimated that a hole concentration as high as 10^{19} cm⁻³ could be feasible. Interestingly, their calculation result of a larger 72-site supercell (which corresponds to a lower concentration of V_{Cu}) yielded a higher formation energy

of 0.55 eV, possibly further suggesting that high concentrations of V_{Cu} are easily obtainable. Results from Ji et al.^[21] also indicated a similar trend, i.e., a lower V_{Cu} formation energy at a higher concentration; however, their calculated formation energies were rather high (4.45 eV for a 32-site supercell and 5.12 eV for a 72-site supercell). The same authors also reported the effect of a Cu vacancy on the band gap of CuSCN although the results were not straightforward. Specifically, in the case of the 72-site supercell the energy band gap was found to slightly increase while transforming to direct type. On the other hand, in the 32-site supercell the band gap remained indirect but increased significantly. The widening of the bandgap in both cases was caused by a corresponding shift in the CB energy.^[21]

An acceptor level at about 0.1 eV above the VBM has been reported by Jaffe et al.[11] and Ji et al.[21] for the Cu vacancy. The latter study also described another acceptor level at 0.02 eV although they did not specify/elaborate on its possible origin. [21] In contrast, Tsetseris [23] showed that V_{Cu} did not yield an acceptor level but instead caused $E_{\rm F}$ to move into the VB, leading to strongly enhanced p-type conductivity. However, despite the speculation of V_{Cu} being the main contributor of excess holes in CuSCN, its existence and its defect energy level in CuSCN are still awaiting experimental substantiation. To this end, Perera et al. [36] reported that doping CuSCN with SCN resulted in an acceptor level at 1 eV above VBM as experimentally observed from a photoluminescence (PL) emission at 460 nm, yet such a deep level should not contribute to a significant increase in conductivity. Interestingly, significant PL emission at ≈460 nm in CuSCN has been reported previously and was attributed to surface states originating from Cu(SCN)2 impurities.^[37] It is therefore absolutely clear that further work would be required in order to elucidate the origin of these defects.

3.2. Other Native Defects

Another basic vacancy is the removal of the SCN unit (V_{SCN}) , which is predicted to yield a donor level and essentially acting as n-dopant. Tsetseris^[23] reported that V_{SCN} in β -CuSCN lattice would lead to significant changes in the positions of the surrounding atoms, e.g., the Cu-Cu distance would increase from 3.85 Å to 4.33 Å. Jaffe et al.[11] also showed that the formation energy of V_{SCN} would be high (i.e., 3.17 eV for a 32-site supercell) even under favorable Cu-rich conditions and still as high as 2.05 eV under degenerate p-type conditions (when E_F moves into VB) which would highly favor the creation of compensating donors. These values are much higher than those predicted by the authors for V_{Cu} (0.2 to 0.55 eV) as discussed earlier. Jaffe et al. [11] further speculated that V_{SCN} should not exist in significant amount under equilibrium conditions although they may be present in samples which are out of thermodynamic equilibrium, such as those prepared by electrodeposition under certain conditions.[10]

Tsetseris^[23] also considered two other isomers of the SCN unit as substitutional defects on SCN site, i.e., NCS and CNS [which can be represented as (NCS) $_{SCN}$ and (CNS) $_{SCN}$]. The formation energies were calculated to be 0.85 eV and

1.58 eV, respectively, implying that they could still exist in small numbers in β -CuSCN. However, the author only stated the rearrangement of the atoms in the thiocyanate group but did not discuss the details regarding the bonding schemes in these isomers. For example, the NCS may exist as a isothiocyanate (N=C=S) in such circumstance and could lead to extra strain from the different bond angles and distances. Isomerism in CuSCN is not uncommon, [38] and these substitutional defects may be an interesting subject of further study.

On the other hand, Jaffe et al.[11] examined the possibilities of the SCN unit having some parts missing. In particular, removing the cyanide part (a CN vacancy, V_{CN}, or equivalently a substitutional S on SCN site, S_{SCN}) could serve as another acceptor as the divalent sulfide can accept another electron from the lattice. Indeed, its defect energy level was calculated to be sufficiently shallow for p-type doping although its formation energy was not reported. In contrast, removing the sulfide [an S vacancy, V_S, or equivalently a substitutional CN on SCN site, (CN)_{SCN}] would likely lead to an inactive neutral defect due to the same charge on the cyanide and thiocyanate ions. The authors also stated that vacancies of only C or N would unlikely exist due to the strong triple bond and speculated that interstitial and antisite defects would not be likely due to the closepacked hexagonal structure of β -CuSCN and the large asymmetry between the Cu and SCN units.

Although a small number of studies as presented above have considered defects in CuSCN, there is still an apparent lack of intensive and extensive investigation into the topic akin to defect studies in other oxide semiconductors.[39-41] A comprehensive study on the formation energies of various defects in different charge states and under different preparation conditions (Cu-rich or Cu-deficient) as a function of E_F would provide a more complete picture of the defect physics and charge compensation in CuSCN.

3.3. Hydrogen Impurities

Tsetseris^[23] studied the inclusion of hydrogen impurities in the lattice of hexagonal β -CuSCN. The calculation results of a single hydrogen atom showed that the most stable configurations were the formation of S-H or C-H bonds (Figure 3a and 3b) with corresponding formation energies of 0.6 eV and 0.7 eV, respectively. More importantly, two H impurities that resulted in the hydrogenation of the cyanide [H-CN-H defect as depicted in Figure 3c or equivalently substitutional hydrogenated SCN (SCNH₂)_{SCN} were shown to be significantly more stable as the formation was highly exothermic, lowering the energy by approximately 1 eV with respect to the pristine β-CuSCN lattice and a H₂ molecule in vacuum. The author proposed that the H₂ impurities in the form of hydrogenated cyanide defect could likely exist in real β-CuSCN samples. Another report by Pattanasattayavong et al.[12] also showed that some C and N in their CuSCN samples may exist in C=N state instead of the cyanide C≡N state. One of the causes for such observation may be hydrogenation, which would corroborate Tsetseris's findings. However, no final conclusion should be drawn yet until further experiments can confirm the finding. Also,

wileyonlinelibrary.com





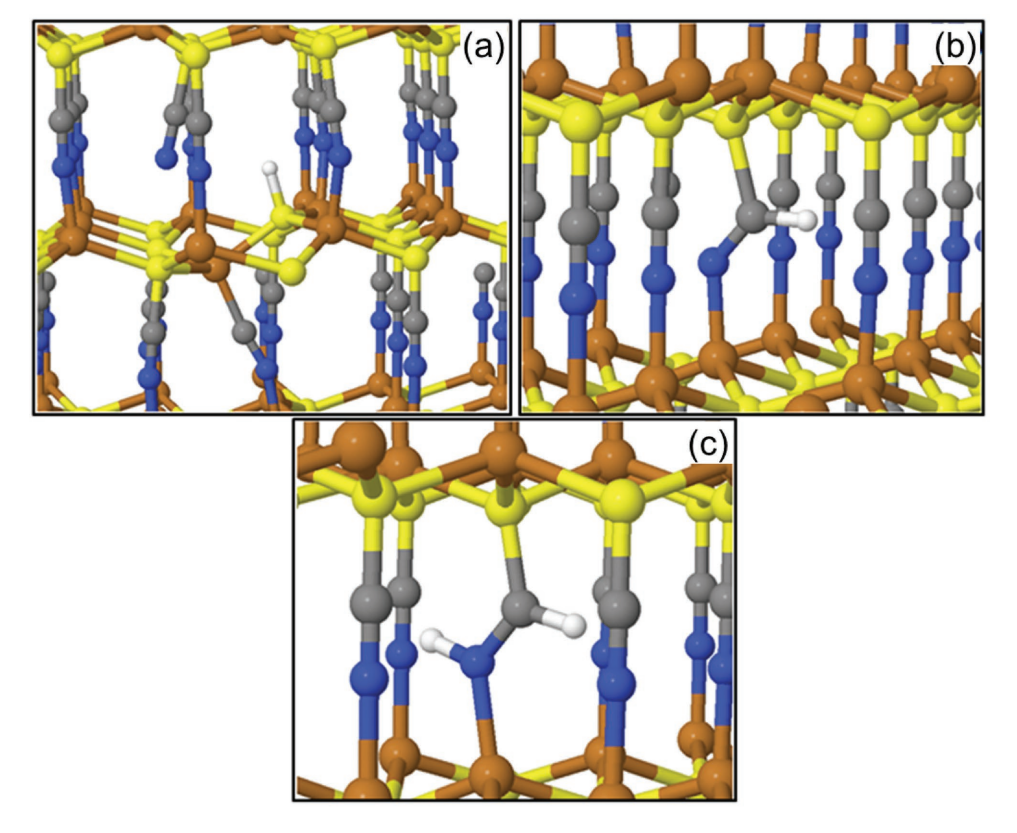


Figure 3. Single H impurity in hexagonal β-CuSCN forming a) S-H bond and b) C-H bond. c) Two H impurities hydrogenating the cyanide portion. Atoms are color coded as brown for Cu, yellow for S, grey for C, and blue for N. Reproduced with permission. Copyright 2016, IOP Publishing.

isomerism of the thiocyanate ion may be another explanation for the C=N state. $^{[38]}$

Regarding the type of defect, the single H impurities (both S–H and C–H) were found to be of acceptor type, and their effects on the electronic structure of $\beta\text{-CuSCN}$ were similar to those of V_{Cu} , i.e., increasing p-type conductivity. [23] Contrastingly, the H–CN–H defect was reported to create a state at 0.2 eV below the CBM that could act as a donor level and may lead to the compensation of acceptors. [23] Again, these computational results still require experimental validation.

4. Polymorphs and Surfaces of CuSCN

Most of the results reported to date, both computational and experimental, were associated with the hexagonal β -CuSCN. [18] Another form, α -CuSCN (**Figure 4**a), has also been reported and its structure characterized although it is less observed in experiments. It should also be noted that the β phase also exhibits polytypism, which results from different stacking sequences along the c-axis of the lattice. The most studied polytype is the hexagonal 2H corresponding to AB type layer stacking also exists. [17] Tsetseris [23] calculated the energies and electronic properties of these two polytypes of β -CuSCN as well as 4H (ABAC-stacked) and 6H (ABCACB-stacked) and found that they could all co-exist and would exhibit similar properties.

4.1. Predicted Layered Structures of CuSCN

Remarkably, in another paper Tsetseris also theoretically predicted layered 2D-like structures of CuSCN, namely the γ , δ , and ε phases (Figure 4c, 4d, and 4e). [42] Interestingly, the structure of \(\gamma \)CuSCN was an analog of that of the 2D metal dichalcogenide while δ-CuSCN resembled the graphene honeycomb structure. These two structures are well known for the 2D materials which currently receive tremendous amount of attention. In fact, a structure similar to that of δ -CuSCN has already been reported for β -CuN₃,^[43] which is also a pseudohalide compound of Cu(I). The ε phase of CuSCN was also honeycomb-like but with high degree of corrugation. Among the different phases of CuSCN, Tsetseris^[42] calculated that the β form was the most stable, followed by the α phase. The layered γ -CuSCN was, however, only slightly higher in energy than α -CuSCN and may possibly be synthesized under the right conditions. The other two phases, δ and ε forms, were significantly higher in energy and thus less stable. The calculated total density of states (DOS) of γ-CuSCN showed that the band gap was widened compared to that of β -CuSCN.^[42] Qualitatively, their plot also suggested that the VB of γ -CuSCN became less dispersive while the CB was more dispersive, which may suggest that the hole transport would be impeded in the layered structure.

Building on the previous study on hydrogen impurities in β -CuSCN, Tsetseris also found that adding hydrogen could significantly improve the stability of the layered forms of

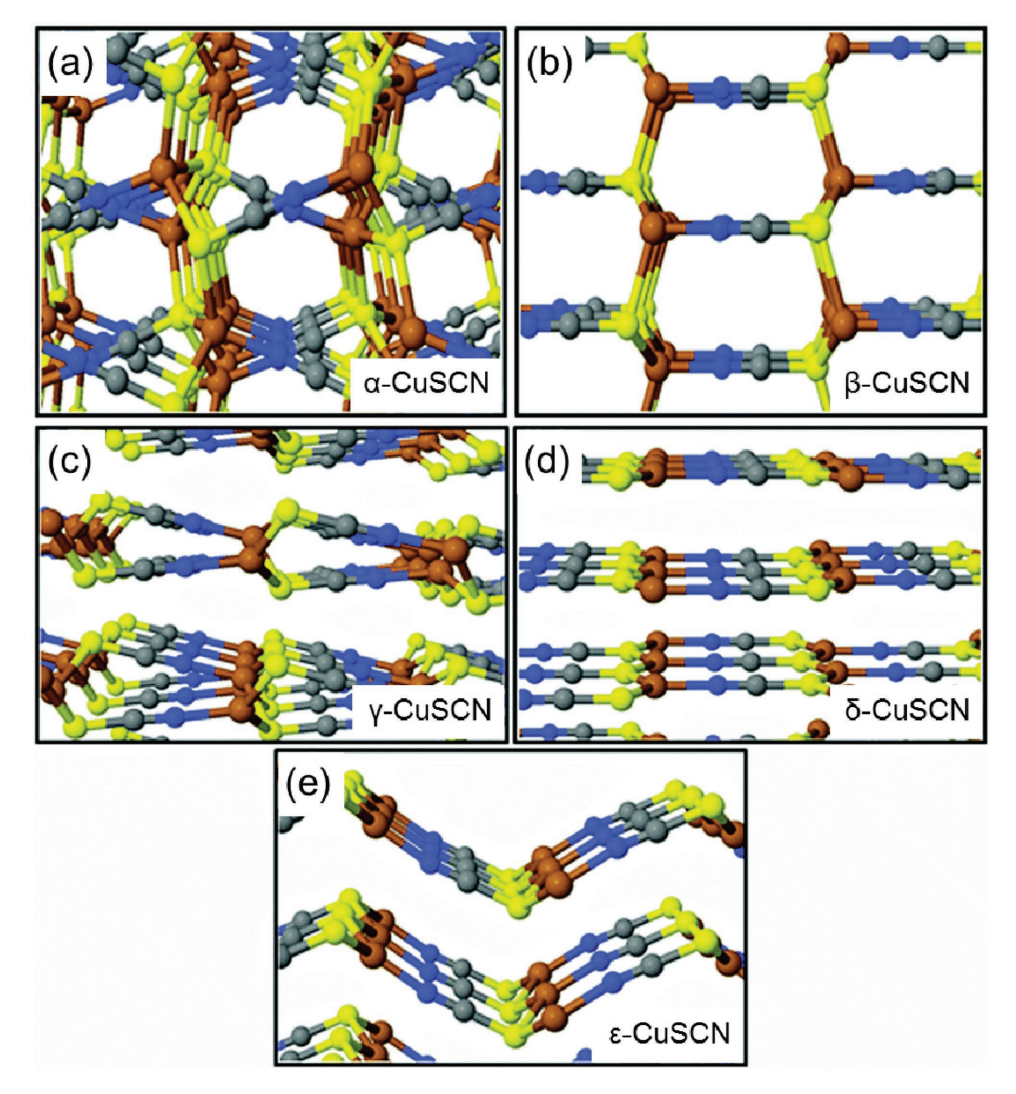


Figure 4. Two phases of bulk CuSCN which have been experimentally observed: a) α and b) β phases (the latter shown in the 2H polytype). Three newly predicted layered 2D-like phases: c) γ , d) δ , and e) ε phases. Atoms are color coded as brown for Cu, yellow for S, grey for C, and blue for N. Reproduced with permission.^[42] Copyright 2016, PCCP Owner Societies.

CuSCN.^[44] In fact, the hydrogenation reactions (specifically adding a hydrogen molecule to the cyanide portion) of α -, β -, γ , and δ -CuSCN were all exothermic. Surprisingly, the fully hydrogenated form of γ -CuSCN (denoted as γ -CuSCNH₂) was the second most stable phase after β -CuSCNH₂. However, the band gap of γ -CuSCNH₂ was significantly reduced, and the DOS also exhibited the adverse trend on the hole transport similar to the case of γ -CuSCN (less dispersive VB and more dispersive CB).

4.2. Surfaces of CuSCN

The orientation of the CuSCN crystal is also of high importance as it could have implications on the charge transport properties due to the highly anisotropic nature of its structure. One example is the difference in the calculated effective masses in the ab plane and along the c-axis of the hexagonal β -CuSCN as discussed previously. Electrodeposition-based methods

have been shown to be able to tune the orientation between the (001)-terminated and (101)-terminated surfaces [(001) or (101) planes parallel to the substrate surface, respectively, (Figure 5)]. [45,46] Although for solution-grown CuSCN films the evidence is not yet clear due to the often small layer thicknesses, results also indicate the presence of (101) or (001) surface-oriented crystals. [111,33] Computational results suggested that the (101)- and (001)-orientations of hexagonal β -CuSCN could be stable especially when terminated with Cu, but the most stable surfaces were (100) and (110). [22] This is mainly because the former pair are characterized by polar surfaces exhibiting a permanent dipole, while the latter are non-polar surfaces.

Interestingly, the results from Chen et al.^[22] showed that the polar surfaces experienced only slight changes in the displacement of the surface atoms and that their partitioned charges were only marginally different from atoms in the bulk, hence supporting the idea of the existence of polar surfaces. Worth noting, however, is the fact that calculations of the electronic





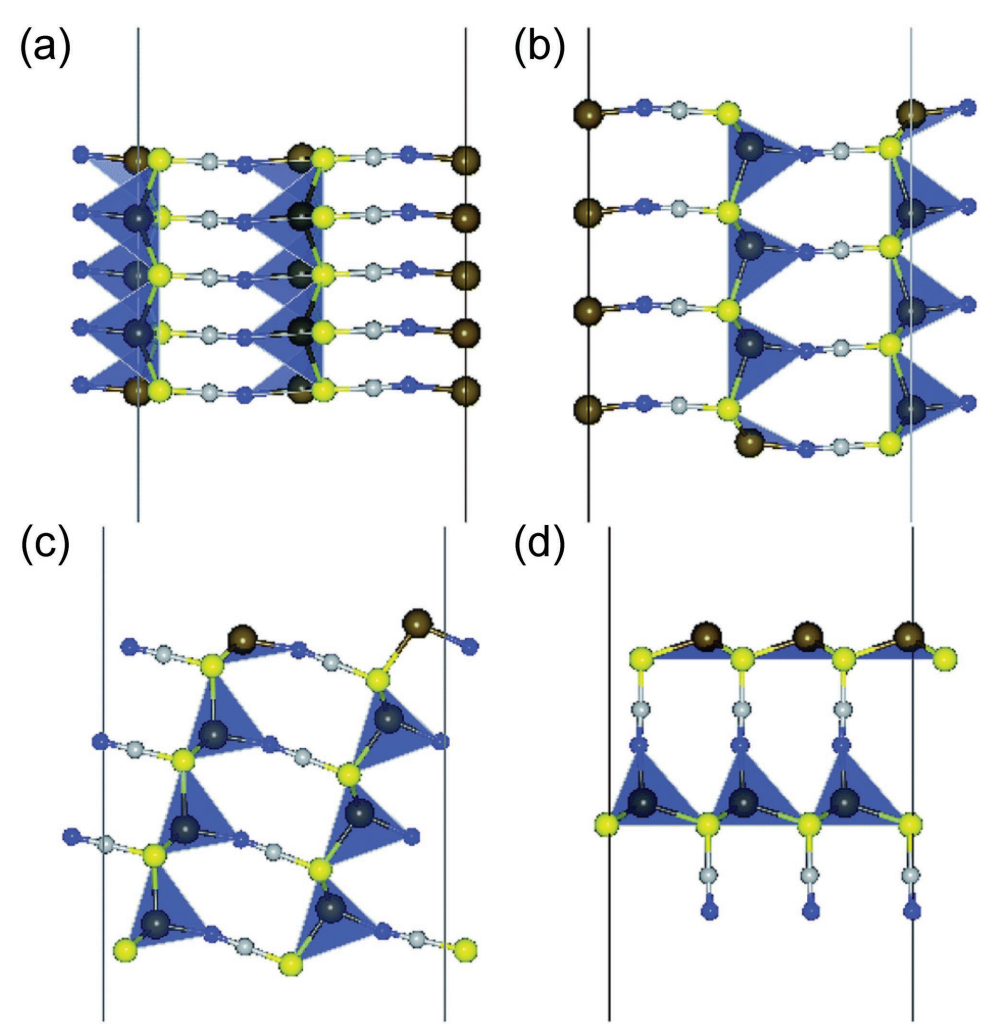


Figure 5. Slabs of hexagonal β-CuSCN displaying the non-polar (110) and (100) surfaces in (a) and (b), respectively, and the polar (101) and (001) surfaces in (c) and (d), respectively. The images are shown as side views with the surfaces orthogonal to the page and the plane normal pointing to the top of the page. Atoms are color coded as dark brown for Cu, yellow for S, grey for C, and blue for N. Reproduced with permission. [22] Copyright 2016, the Royal Society of Chemistry.

properties of polar and non-polar surfaces (modelled as slabs in the computations) of β -CuSCN yielded different results. [22,23] The DOS of the non-polar (110) and (100) surfaces (Figure 5a and 5b) were similar to that of the bulk. On the other hand, those of the polar (101) and (001) surfaces (Figure 5c and 5d) showed a significant number of states within the band gap. Chen et al. [22] proposed that the polar surfaces could be semi-metallic due to the high density of the Cu 4s states near $E_{\rm F}$, which could in turn be a result of under-coordination of Cu atoms at the surface.

5. Hole Transport Properties of CuSCN

As already discussed earlier, CuSCN has been employed as a hole-transporting layer in numerous opto/electronic devices (see the review on the applications of CuSCN by Wijeyasinghe and Anthopoulos^[8]); however, the studies on the hole transport properties of CuSCN are very limited. Pattanasattayavong

et al.,[1] employing field-effect measurements, obtained hole mobilities between 0.01 and 0.1 cm² V⁻¹ s⁻¹ from solution-processed thin film CuSCN layers. These mobility values further corroborated the hole diffusion coefficients (which are related to hole mobilities via the Einstein relation $D = \mu kT/q$, where D is the diffusion coefficient, μ is the mobility, k is the Boltzmann constant, *T* is the temperature, and *q* is the elementary electric charge) which were reported earlier for CuSCN by Mora-Seró et al.[47] to be in the range of 0.001 to 0.01 cm² s⁻¹ based on impedance spectroscopy measurements. More recently, Pattanasattayavong et al.[48] investigated the band-tail states and hole transport processes in CuSCN based on the analyses of field-effect transistors. In addition, Kim et al.[28] used the PES technique with He II source to examine the band-tail states of CuSCN and their effects on the charge extraction in organic photovoltaic devices. It should be noted that the CuSCN samples in both studies were thin films cast from sulfide-based solutions at room temperature followed by thermal annealing in nitrogen environment.

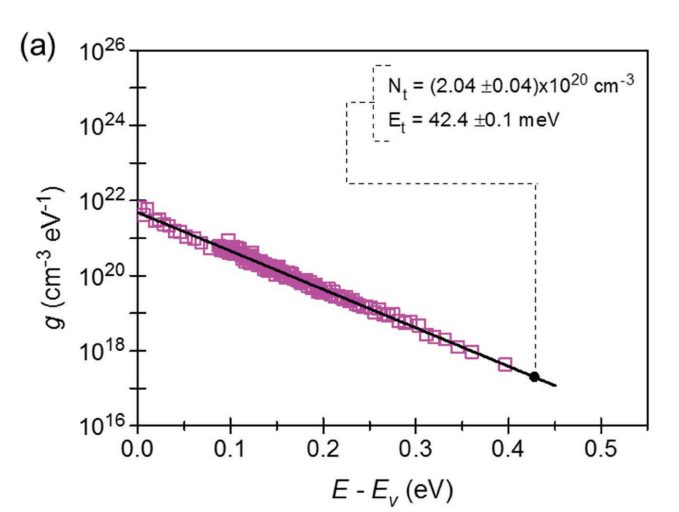
5.1. Band Tail States in CuSCN

www.advancedsciencenews.com

It is well established that charge carrier transport in semiconductors and their devices is strongly influenced by the densities of states near the band edges. In highly crystalline materials (e.g. single crystals), the VB and CB are sharp, and the transport proceeds via band transport mode (extended states-wavefunctions are highly delocalized). In non-crystalline and polycrystalline materials, however, structural disorder as well as chemical impurities and the presence of grain boundaries between crystalline regions/domains (crystallites) create localized states above the VBM or below the CBM within the band gap, disrupting the band transport. In the case where the DOS of these localized states are distributed near the band edges (within the bandgap) and are manifested as an optical absorption tail often called band-tail states. Since these DOS can exist in the supposedly forbidden gap (hence no longer a true energy gap), the notation "mobility gap" is sometimes used to distinguish the region between the VB and CB edges. The gap in this case refers to the separation between the extended states where band transport takes place and the

Pattanasattayavong et al. [48] employed a method developed by Grünewald et al. [49] to analyze the current-voltage characteristics of nanocrystalline CuSCN layer-based field-effect transistors in order to study the band-tail states. Their results showed that the DOS of the tail states followed an exponential distribution with a characteristic energy of around 42 meV (**Figure 6a**), a value which is similar to those of p-type amorphous inorganic semiconductors such as a-Si or a-As₂Se₃. [50–52] It was also shown that the dynamic disorder could play an important role as the DOS became narrower with the decreasing temperature although further investigation is required.

Kim et al.^[28] studied the VB of CuSCN using the PES technique equipped with a He II (40.82 eV) UV source for resolving states near the band edge. The PES spectrum in close proximity of the VBM revealed the existence of exponential tail states extending into the gap (Figure 6b and inset) with a characteristic energy of around 150 meV (calculated from the digitized image). The latter value is significantly larger than that reported by Pattanasattayavong et al., but the results are in qualitative agreement. To this end, it should be noted that the spectra from PES measurements may be broadened by various effects and may add to the characteristic energy of the tail states distribution. The authors also showed that, when CuSCN was used as a hole-transporting interlayer, the bandtail states could assist with the hole transport between the electrode and the active semiconductor layer by providing the transport pathway. Specifically, the hole injection/extraction barrier is effectively reduced by the presence of the band-tail states even when CuSCN is not heavily doped (E_F still lies at a considerable distance from the VBM). Additionally, Aldakov et al.^[53] also analyzed the optical absorption tail (Urbach tail) of their electrodeposited CuSCN samples and reported relatively high values of the characteristic energy in the range of 200–240 meV. The authors cited the possible origins as states within the band gap that may originate from internal strain, composition variations, or surface defects.



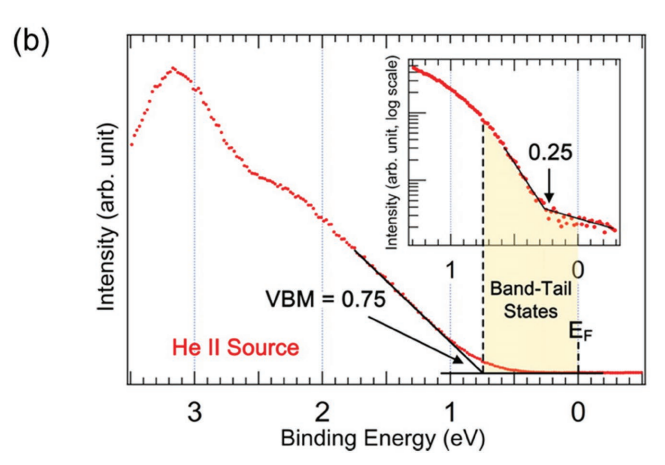


Figure 6. a) Density of states of the tail localized states in the mobility gap of polycrystalline solution-processed CuSCN calculated from the transfer characteristics of CuSCN-based field-effect transistors. Reproduced with permission.^[48] (b) Photoemission spectrum near the valence band edge of CuSCN obtained using the He II UV source and (inset) the close-up showing the band-tail states extending from the valence band edge toward the Fermi level. Reproduced with permission.^[28] Copyright 2016 American Chemical Society.

5.2. Hole Transport in CuSCN

Despite the widespread use of CuSCN as a hole-transporting layer in various optoelectronic devices, the charge carrier transport mechanisms in CuSCN have only been studied recently by Pattanasattayavong et al.^[48] By investigating the temperature dependence of the field-effect hole mobility of CuSCN-based thin-film transistors, three different transport regimes were identified for solution-processed CuSCN layers. At high temperatures (228–303 K), the transport was strongly thermally activated, a signature of the multiple trapping and release (MTR) mode which is an archetype model for transport in noncrystalline inorganic semiconductors.^[54–56] In this case, carriers can still travel as waves (band transport) in the extended states outside the mobility gap but become momentarily trapped by the localized states in the band tail before being released via

thermal activation. At intermediate temperatures (123–228 K), the transport mechanism was also thermally activated but with a smaller energy barrier. Based on similar observations in noncrystalline inorganic semiconductors, the authors proposed that the transport process followed the variable range hopping (VRH) mechanism in this temperature range.^[50,55] The thermal activation persists in this regime due to the hopping process in the tail of localized states.

The transition from MTR to VRH could be understood from the temperature dependence of the transport energy, a representative energy level that the carrier transport takes place. [57,58] For MTR mode, this energy coincides with the band edge, i.e., holes are activated from localized states to the extended states in the VB. When temperature decreases, the transport energy moves away from the VB into the tail states, and the transport mode changes to VRH. Further decrease in temperature causes the transport energy to move deeper into the mobility gap toward the $E_{\rm F}$. At low temperatures (78–123 K), the data was not conclusive, but the authors speculated that the transport mode in this regime may be the field-assisted hopping. In light of these results it can be concluded that hole transport in solution-processed polycrystalline layers of CuSCN appears to follow similar mechanisms already observed in conventional non-crystalline inorganic semiconductors. Although established theories provide an appropriate starting point for the development of a deeper understanding of charge carrier transport in CuSCN, more work is certainly required. Elucidating the fundamental nature of charge transport in CuSCN and the role of the layer microstructure, in particular, will most definitely lead to improved deposition routes as well as assist towards the design of new materials and devices with improved operating characteristics for a wide range of future opto/electronic applications.

6. Related Materials

To the best of our knowledge, CuSCN is so far the only material in the pseudohalide group of compounds that exhibits semiconducting properties suitable for practical electronic applications. Another closely related compound, copper(I) selenocyanate (CuSeCN), has also been studied computationally by Tsetseris^[42,44] and shown to possibly possess electronic properties akin to those of CuSCN. Based on similar DFT calculations with the sulfur atom replaced by a selenium atom, the natural phase of CuSeCN was also predicted to be the β phase while the α and the 2D-like layered γ phases were less stable, [42] analogous to the case of CuSCN. Although the author did not explicitly study the charge carrier transport properties, the plot of the total DOS of β -CuSeCN could imply that holes may be the dominant charge carriers due to the higher dispersion near VBM than CBM. Another prediction was a smaller band gap for CuSeCN compared to that of CuSCN.[44] CuSeCN has been observed in electrochemical systems,[59,60] but more research is required to understand its properties and uses. Also mentioned in Ref. [42] is copper azide CuN₃, which is isoelectronic to CuSCN and exhibits a layered phase similar to those predicted for CuSCN and CuSeCN.[43,61] However, azides are highly explosive and thus unlikely to be suitable for electronic applications.[62]

It is also noteworthy to acknowledge copper iodide (CuI) as it is a well-known p-type metal halide also based on Cu(I) and has been employed in several device applications as a hole-transporting layer. [63–66] Although the conductivity of γ -CuI is electronic, α -CuI and β -CuI also show strong ionic conductivity [67] and may present a challenge in the development of electronic devices. However, a full discussion on CuI is beyond the scope of this work as it is a common metal halide and does not possess the quasi-molecular nature as in the case of pseudohalides. To this end, Grundmann et al. [67] have recently published a comprehensive review of the properties and applications of CuI.

7. Conclusion

We have reviewed key aspects of the electronic and charge transport properties of the quasi-molecular, wide band gap semiconductor CuSCN. Its excellent hole-transporting properties and the high optical transparency can be understood based on the band structure of this rather unique material. Recent DFT calculations of hexagonal β -CuSCN show that the VBM is mainly composed of Cu 3d states with some hybridization from S 3p states whereas the CBM is predominantly the antibonding π^* states of the cyanide portion, resulting in a more dispersive VB as compared with conventional wide band gap inorganic semiconductors.[11,22,23] The antibonding character also leads to an indirect band gap which, coupled with the large band gap of ≥3.5 eV, enhances the optical transparency in the visible range. Calculations of various defects in CuSCN also support the predominant p-type conductivity observed in various CuSCN samples prepared from different methods. The Cu vacancy is the main candidate for the acceptor-type doping as its formation energy is predicted to be sufficiently low and its defect energy level close to the VB.[11,21,23] Other potential candidates include the CN vacancy and H impurities.[11,23]

Polymorphism in CuSCN has also been studied theoretically. [23] The β -CuSCN is shown to be the most stable phase, followed by the already observed α phase. Three new layered structures have been predicted, namely the γ , δ , and ε phases. The stability of γ -CuSCN is reported to be close to that of the α phase, suggesting the possibility of synthesizing this form. Its structure also resembles that of the 2D metal dichalcogenides, which represent an important class of emerging electronic materials. Different orientations of CuSCN could also have an impact on the carrier transport due to its anisotropic structure (and the high asymmetry between the Cu and SCN units). Polar and non-polar surfaces of hexagonal β -CuSCN are shown to have different DOS. [22,23]

The band-tail states in non-crystalline solution-processed samples of CuSCN have also been studied. The distribution of these localized states is reported to be in an exponential form extending from the VBM into the gap.^[28,48,53] Hole transport in this type of CuSCN has been explained based on the theories of multiple trapping and release and variable range hopping.^[48] Theoretical models initially developed for conventional noncrystalline inorganic semiconductors have been shown to offer basic explanation of tail states and hole transport mechanisms in non-crystalline CuSCN.





On the basis of the published literature to date it can be argued that although the general background of semiconductor physics of CuSCN has been laid out, a significant gap in the detailed understanding of the electronic phenomena that govern charge transport in CuSCN still exists. Experimental verifications are also required for many of the properties that have been predicted by theory. As CuSCN becomes more technologically relevant for application as an optically transparent hole-transporting semiconductor in various opto/electronic devices, further studies of its properties are expected to be highly fruitful and critically important.

Acknowledgements

P.P. would like to acknowledge Thailand Research Fund (TRF) for their financial support under the project MRG5980214.

Received: September 14, 2016 Revised: November 14, 2016 Published online:

- P. Pattanasattayavong, N. Yaacobi-Gross, K. Zhao,
 G. O. Ngonggang Ndjawa, J. Li, F. Yan, B. C. O'Regan, A. Amassian,
 T. D. Anthopoulos, Adv. Mater. 2013, 25, 1504.
- [2] A. Perumal, H. Faber, N. Yaacobi-Gross, P. Pattanasattayavong, C. Burgess, S. Jha, M. A. McLachlan, P. N. Stavrinou, T. D. Anthopoulos, D. D. C. Bradley, Adv. Mater. 2015, 27, 93.
- [3] N. Yaacobi-Gross, N. D. Treat, P. Pattanasattayavong, H. Faber, A. K. Perumal, N. Stingelin, D. D. C. Bradley, P. N. Stavrinou, M. Heeney, T. D. Anthopoulos, Adv. Energy Mater. 2015, 5, 1401529.
- [4] N. D. Treat, N. Yaacobi-Gross, H. Faber, A. K. Perumal, D. D. C. Bradley, N. Stingelin, T. D. Anthopoulos, *Appl. Phys. Lett.* 2015, 107, 13301.
- [5] Y. Itzhaik, O. Niitsoo, M. Page, G. Hodes, J. Phys. Chem. C 2009, 113, 4254.
- [6] B. O'Regan, D. T. Schwartz, S. M. Zakeeruddin, M. Grätzel, Adv. Mater. 2000, 12, 1263.
- [7] P. Qin, S. Tanaka, S. Ito, N. Tetreault, K. Manabe, H. Nishino, M. K. Nazeeruddin, M. Grätzel, Nat. Commun. 2014, 5, 1.
- [8] N. Wijeyasinghe, T. D. Anthopoulos, Semicond. Sci. Technol. 2015, 30, 104002
- [9] Z. Wang, P. K. Nayak, J. A. Caraveo-Frescas, H. N. Alshareef, Adv. Mater. 2016, 28, 3831.
- [10] K. Tennakone, A. H. Jayatissa, C. A. N. Fernando, S. Wickramanayake, S. Punchihewa, L. K. Weerasena, W. D. R. Premasiri, *Phys. Status Solidi* 1987, 103, 491.
- [11] J. E. Jaffe, T. C. Kaspar, T. C. Droubay, T. Varga, M. E. Bowden, G. J. Exarhos, J. Phys. Chem. C 2010, 114, 9111.
- [12] P. Pattanasattayavong, G. O. Ngongang Ndjawa, K. Zhao, K. W. Chou, N. Yaacobi-Gross, B. C. O'Regan, A. Amassian, T. D. Anthopoulos, *Chem. Commun.* 2013, 49, 4154.
- [13] B. Ptaszyński, E. Skiba, J. Krystek, Thermochim. Acta 1998, 319, 75.
- [14] K. Tennakone, G. S. Shantha Pushpa, S. Punchihewa, G. Epa, Electrochim. Acta 1986, 31, 315.
- [15] Y. Guo, X. Yu, J. Chen, Corros. Sci. 2009, 51, 1573.
- [16] M. Kabešová, M. Dunaj-jurčo, M. Serator, J. Gažo, J. Garaj, Inorganica Chim. Acta 1976, 17, 161.
- [17] D. L. Smith, V. I. Saunders, Acta Crystallogr. Sect. B Struct. Crystallogr. Cryst. Chem. 1981, 37, 1807.

- [18] D. L. Smith, V. I. Saunders, Acta Crystallogr. Sect. B Struct. Crystallogr. Cryst. Chem. 1982, 38, 907.
- [19] G. R. R. A. Kumara, A. Konno, G. K. R. Senadeera, P. V. V. Jayaweera, D. B. R. A. De Silva, K. Tennakone, Sol. Energy Mater. Sol. Cells 2001, 69, 195.
- [20] K. M. Miller, S. M. McCullough, E. a. Lepekhina, I. J. Thibau, R. D. Pike, X. Li, J. P. Killarney, H. H. Patterson, *Inorg. Chem.* 2011, 50, 7239.
- [21] W. Ji, G.-Q. Yue, F.-S. Ke, S. Wu, H.-B. Zhao, L.-Y. Chen, S.-Y. Wang, Y. Jia, J. Korean Phys. Soc. 2012, 60, 1253.
- [22] K. J. Chen, A. D. Laurent, F. Boucher, F. Odobel, D. Jacquemin, J. Mater. Chem. A 2016, 4, 2217.
- [23] L. Tsetseris, J. Phys. Condens. Matter 2016, 28, 295801.
- [24] W. Setyawan, S. Curtarolo, Comput. Mater. Sci. 2010, 49, 299.
- [25] W. Wu, Z. Jin, Z. Hua, Y. Fu, J. Qiu, Electrochim. Acta 2005, 50, 2343.
- [26] Y. Ni, Z. Jin, Y. Fu, J. Am. Ceram. Soc. 2007, 90, 2966.
- [27] X.-D. Gao, X.-M. Li, W.-D. Yu, J.-J. Qiu, X.-Y. Gan, Thin Solid Films 2008, 517, 554.
- [28] M. Kim, S. Park, J. Jeong, D. Shin, J. Kim, S. H. Ryu, K. S. Kim, H. Lee, Y. Yi, J. Phys. Chem. Lett. 2016, 2856.
- [29] J. E. Medvedeva, in *Transparent Electronics: From Synthesis to Applications* (Eds.: A. Facchetti, T. J. Marks), John Wiley & Sons, Chichester, UK, 2010, pp. 1–29.
- [30] P. P. Boix, G. Larramona, A. Jacob, B. Delatouche, I. Mora-Sero, J. Bisquert, J. Phys. Chem. C 2012, 116, 1579.
- [31] B. O'Regan, D. T. Schwartz, Chem. Mater. 1995, 7, 1349.
- [32] K. Tennakone, G. R. R. A. Kumara, I. R. M. Kottegoda, V. P. S. Perera, G. M. L. P. Aponsu, J. Phys. D. Appl. Phys. 1998, 31, 2326.
- [33] J. W. Jung, C. C. Chueh, A. K. Y. Jen, Adv. Energy Mater. 2015, 5, 1.
- [34] E. Ruiz, S. Alvarez, P. Alemany, R. a. Evarestov, Phys. Rev. B 1997, 56, 7189.
- [35] A. Önsten, M. Månsson, T. Claesson, T. Muro, T. Matsushita, T. Nakamura, T. Kinoshita, U. O. Karlsson, O. Tjernberg, Phys. Rev. B 2007, 76, 115127.
- [36] V. P. S. Perera, M. K. I. Senevirathna, P. K. D. D. P. Pitigala, K. Tennakone, Sol. Energy Mater. Sol. Cells 2005, 86, 443.
- [37] C. A. N. Fernando, I. Kumarawadu, K. Takahashi, A. Kitagawa, M. Suzuki, Sol. Energy Mater. Sol. Cells 1999, 58, 337.
- [38] J. A. Dobado, R. Uggla, M. R. Sundberg, J. Molina, J. Chem. Soc. Dalt. Trans. 1999, 489.
- [39] S. B. Zhang, S.-H. Wei, A. Zunger, Phys. Rev. B 2001, 63, 75205.
- [40] H. Raebiger, S. Lany, A. Zunger, Phys. Rev. B 2007, 76, 45209.
- [41] a. Togo, F. Oba, I. Tanaka, K. Tatsumi, Phys. Rev. B 2006, 74, 195128.
- [42] L. Tsetseris, Phys. Chem. Chem. Phys. 2016, 18, 7837.
- [43] X. Liu, J. George, S. Maintz, R. Dronskowski, Angew. Chemie Int. Ed. 2015, 54, 1954.
- [44] L. Tsetseris, Phys. Chem. Chem. Phys. 2016, 18, 14662.
- [45] C. Liu, W. Wu, K. Liu, M. Li, G. Hu, H. Xu, CrystEngComm 2012, 14, 6750.
- [46] T. Iwamoto, Y. Ogawa, L. Sun, M. S. White, E. D. Glowacki, M. C. Scharber, N. S. Sariciftci, K. Manseki, T. Sugiura, T. Yoshida, J. Phys. Chem. C 2014, 118, 16581.
- [47] I. Mora-Seró, S. Giménez, F. Fabregat-Santiago, E. Azaceta, R. Tena-Zaera, J. Bisquert, Phys. Chem. Chem. Phys. 2011, 13, 7162.
- [48] P. Pattanasattayavong, A. D. Mottram, F. Yan, T. D. Anthopoulos, Adv. Funct. Mater. 2015, 25, 6802.
- [49] M. Grünewald, P. Thomas, D. Würtz, Phys. status solidi 1980, 100, K139.
- [50] D. Monroe, Phys. Rev. Lett. 1985, 54, 146.
- [51] M. H. Cohen, E. N. Economou, C. M. Soukoulis, J. Non. Cryst. Solids 1984, 66, 285.
- [52] J. Orenstein, M. Kastner, Phys. Rev. Lett. 1981, 46, 1421.





- [53] D. Aldakov, C. Chappaz-Gillot, R. Salazar, V. Delaye, K. A. Welsby, V. Ivanova, P. R. Dunstan, J. Phys. Chem. C 2014, 118, 16095.
- [54] M. Shur, M. Hack, J. Appl. Phys. 1984, 55, 3831.
- [55] P. G. Le Comber, W. E. Spear, Phys. Rev. Lett. 1970, 25, 509.
- [56] P. G. Le Comber, A. Madan, W. E. Spear, J. Non. Cryst. Solids 1972, 11, 219.
- [57] F. R. Shapiro, D. Adler, J. Non. Cryst. Solids 1985, 74, 189.
- [58] S. D. Baranovskii, T. Faber, F. Hensel, P. Thomas, *J. Phys. Condens. Matter* **1997**, *9*, 2699.
- [59] A. Manceau, D. L. Gallup, Environ. Sci. Technol. 1997, 31, 968.
- [60] L. K. H. K. Alwis, M. R. Mucalo, B. Ingham, P. Kappen, J. Electrochem. Soc. 2015, 162, H434.

- [61] X. Zhang, X. Zhao, Y. Jing, D. Wu, Z. Zhou, Phys. Chem. Chem. Phys. 2015, 17, 31872.
- [62] B. L. Evans, A. D. Yoffe, P. Gray, Chem. Rev. 1959, 59, 515.
- [63] J. A. Christians, R. C. M. Fung, P. V. Kamat, J. Am. Chem. Soc. 2014, 136, 758.
- [64] Y. Peng, N. Yaacobi-Gross, A. K. Perumal, H. A. Faber, G. Vourlias, P. A. Patsalas, D. D. C. Bradley, Z. He, T. D. Anthopoulos, Appl. Phys. Lett. 2015, 106, 243302.
- [65] W. Sun, S. Ye, H. Rao, Y. Li, Z. Liu, L. Xiao, Z. Chen, Z. Bian, C. Huang, Nanoscale 2016, 8, 15954.
- [66] C. Choi, J. Y. Gorecki, Z. Fang, M. Allen, S. Li, L.-Y. Lin, C.-C. Cheng, C. Chang, J. Mater. Chem. C 2016, 4, 10309.
- [67] M. Grundmann, F.-L. Schein, M. Lorenz, T. Böntgen, J. Lenzner, H. von Wenckstern, Phys. status solidi 2013, 210, 1671.

CORRECTION

Electronic Properties of Copper(I) Thiocyanate (CuSCN)

Pichaya Pattanasattayavong, Vinich Promarak, and Thomas D. Anthopoulos

Adv. Electron. Mater. 2017, 3, 1600378

DOI: 10.1002/aelm.201600378

A funding body was accidentally omitted from the acknowledgements section of this manuscript. The full acknowledgements are as follows:

P.P. would like to acknowledge the funding from the Office of the Higher Education Commission (OHEC) and the Thailand Research Fund (TRF) under grant number MRG5980214.

IOP Publishing Nanotechnology

Nanotechnology 29 (2018) 385603 (9pp)

https://doi.org/10.1088/1361-6528/aacf83

Physico-chemical investigation of ZnS thinfilm deposited from ligand-free nanocrystals synthesized by non-hydrolytic thio-sol-gel

Silvano Del Gobbo^{1,3}, Alexander D Mottram¹, Samy Ould-Chikh², Jidapa Chaopaknam¹, Pichaya Pattanasattayavong¹ and Valerio D'Elia^{1,3}

E-mail: valerio.delia@vistec.ac.th and silvano.d@vistec.ac.th, silvano.delgobbo@gmail.com

Received 11 April 2018, revised 16 June 2018 Accepted for publication 27 June 2018 Published 12 July 2018



Abstract

Ultra-small and monodispersed zinc sulfide nanocrystals (NCs) ($d \le 3$ nm) have been prepared without the use of any surfactants by a synthetic route using benzyl mercaptan as a source of sulfur. The prepared NCs are dispersible in highly polar solvents and display the capability to closely pack-up in a bulky film. The NCs were characterized by TEM, XRD and UV-vis optical absorption as well as by steady-state and time-resolved photoluminescence (PL) spectroscopies. Uniform films of ZnS were spin-coated on glass and ITO-glass substrates using a NCs dispersion in N,N-dimethylformamide. The NCs and the resulting films were characterized by morphological and optoelectronic probing techniques such as AFM, SEM, diffuse reflectance, PL and photoelectron spectroscopy in air. These physical investigations confirmed that the chalcogenide NCs grown by this method have the potential to be utilized directly as photocatalysts and are potentially useful building-blocks/starting materials for the fabrication of semiconductor thin films for optoelectronic applications such as LED, luminescent screens, field effect transistor and solar cells. Insights on the chemistry involved in the NCs growth have been provided revealing that their formation proceeds through a mechanism involving a thioether elimination reaction.

Supplementary material for this article is available online

Keywords: zinc sulfide nanocrystals, non-hydrolytic thio-sol-gel, chalcogenide thin-film, optoelectronic properties, synthesis mechanism

(Some figures may appear in colour only in the online journal)

1. Introduction

ZnS is an important semiconductor for optoelectronic applications. Key applications of ZnS films include the use as layers in electrodes [1], solar cells [1–6], light emitting devices [7–9], photocatalysts [10–14], photodetectors [15, 16] and piezoelectric devices [17–19]. Several efforts have been undertaken to obtain high quality ZnS layers, especially, by the chemical bath

deposition (CBD) [3, 20–22]. Compared to more sophisticated preparative techniques utilized for the synthesis of ZnS films such as ionic layer deposition [23], pulsed laser deposition [9], atomic layer deposition [14], e-beam evaporation [16], techniques such as CBD and spin-coating present clear advantages as they are inexpensive, easy to operate and readily available [24, 25]. However, CBD may suffer some limitations such as low material yields compared to the starting reagents and the production of large amounts of waste solutions [26]. Spincoating is a key technology in optoelectronics [6] and

¹ Department of Materials Science and Engineering, School of Molecular Science and Engineering, Vidyasirimedhi Institute of Science and Technology (VISTEC), Rayong, 21210, Thailand ² KAUST Catalysis Center (KCC), King Abdullah University of Science and Technology (KAUST), 23955-6900 Thuwal, Saudi Arabia

³ Authors to whom any correspondence should be addressed.

nanoparticles represent excellent starting material for the preparation of films for optoelectronic devices and other applications by this technique [15, 27–29]. From this perspective, the access to semiconducting nanoparticles through convenient synthetic methods is a fundamental leap in materials science. Previous reports employing standard precipitation techniques to obtain large ZnS nanoparticles (10–150 nm) were indeed not suitable for use in spin-coating and led to inhomogeneous and/or porous films [30, 31]. It is clear that nanoparticles with very small size, a narrow size distribution and high dispersibility are required to produce uniform films. A significant breakthrough in the synthesis of nanoparticles was achieved when group II (Zn, Cd, Hg) chalcogenide quantum dots were first prepared by colloidal growth [32, 33]. This technique was then refined and extended to other materials such as group IV and V chalcogenides [34, 35], transition metal pnictides (e.g. Cd₃P₂, Zn₃P₂, Fe₃P₂, Ta_3N_5) [36, 37] and to a wide spectrum of metal oxides [38, 39]. Although a precise control of size and shape can be achieved through this method, the synthetic process requires the assistance of long-chain fatty acids or amines as well as of the ubiquitously used trioctylphosphine oxide for stabilizing the nanoparticles and controlling their growth. Nevertheless, for some applications, the presence of the organic shell coating the nanoparticle is definitely undesirable [35]. Indeed, a major advantage in having uncoated nanocrystals (NCs) is that it is possible to use them as starting material to cast homogeneous semiconductor films without employing time-consuming and not always effective ligand exchange procedures [34, 40]. Furthermore, upon removal of the long-chain organic ligand from the NPs surface, the dispersibility in organic solvents might be dramatically reduced [32]. An approach to synthesize semiconducting nanoparticles, that does not account for the use of surfactants, is represented by the non-hydrolytic sol-gel route (NHSG) [41–44]. This method has been successfully utilized for the preparation of several single- and bi-metallic metal oxides of different sizes and morphologies using metal-organic precursors such as acetates, halides, acetylacetonates and alkoxides that react with benzyl alcohol and benzylamine. This kind of reaction usually proceeds via ester or ether elimination pathways [43, 45, 46].

Some methods for the preparation of metal sulfides nanoparticles inspired by the NHSG methodology were explored in the past [47]. Niederberger *et al* employed benzyl mercaptan (BM) as a source of sulfur and as the reaction solvent, yet in absence of surfactants to control the growth. The particles obtained in this early report were rather large in size (9–18 nm according to the zinc precursor employed) [47]. Based on a different method, La Porta *et al* [48] prepared smaller ZnS nanoparticles (although no TEM analysis was performed to confirm the morphological nature of the nanoparticles) using thiourea as a source of sulfur and ethylene glycol as the solvent. In both cases, the dispersibility and the possibility to cast a film with the thus-prepared material were not considered. Furthermore, the mechanism of the process of NCs formation was never investigated in detail.

In this work, a surfactant-free protocol using either dibenzyl ether or anisole as the solvent and BM as a source of sulfur was applied to synthesize ZnS NCs that could be regarded as quantum dots given the reduced size approaching the Bohr's radius ($r_{\rm B}=2.5\,{\rm nm}$) [49]. With respect to application, the ZnS-NCs prepared according to this method can be considered as virtually bare NCs since they are coated only by a monolayer of BM molecules that are chemically bound to ZnS surface [50–52]. However, if necessary, BM could be removed by a thermal treatment in inert environment [35]. The resulting NCs can be easily dispersed in dry N_iN_i -dimethylformamide (DMF) by ultrasonication, and then cast into film on ITO and glass substrates by spin-coating. NCs grown by this method are thus largely preferable to colloidal NCs for the fabrication of films [53–55], mainly because no trace of bulky organic molecules, that would be detrimental for the electronic properties of the film, are left [35].

In order to evidence the suitable morphological, optical and electronic properties of the NCs and of the resulting film, a physical investigation was carried out and discussed throughout the manuscript. Furthermore, a mechanistic investigation on the formation of ZnS-NCs was conducted suggesting that the formation of the NCs proceeds via a thioether elimination mechanism.

2. Experimental methods

2.1. Synthesis of ZnS-NCs

The synthesis of the ZnS-NCs was carried out by the surfactants-free reaction between the zinc acetate (Zn(OAc)₂) precursor and BM as a source of sulfur in dibenzyl ether at 190 °C or in anisole at 125 °C. Briefly, 1.853 g (0.01 mol) of zinc acetate anhydrous 99.9+% metal basis Alfa Aesar was loaded in a Schlenk type flask and added with 30 ml of dibenzyl ether Merck and 2.34 ml (0.02 mmol) of BM 99% (Alfa Aesar), preheated at 100 °C to allow the dissolution of zinc acetate, and then the temperature was increased up to the desired value. An off-white dense precipitate started forming within 1 h. The reaction was carried out for 24 h and then allowed to cool to room temperature. The pale-yellow precipitate was separated from the supernatant by vacuum filtration using PVDF Durapore membrane filters with 0.22 μ m pore size (MILLIPORE). It was washed three times with absolute ethanol and one time with diethyl ether and dried under vacuum overnight. The ZnS-NCs powder was finely crushed by an agate mortar for characterization and to prepare the dispersion. A small aliquot of the solvent containing the reaction sub-products were analyzed by gas chromatography coupled with mass spectroscopy (GC-MS). Using anisole as medium, the reaction was carried out and worked up as in DBE but at 125 °C, a temperature compatible with the boiling point of anisole (153.8 °C). Purified ZnS-NCs result in large yellow chunks with crystalline appearance (see figure S1(a), which is available online at stacks.iop.org/NANO/29/ 385603/mmedia) that can be reduced in powder by crushing in agate mortar. The blank reactions were carried out as follows: 0.80 ml of BM in 10 ml of dibenzyl ether or 10 ml of anisole were loaded in a Schlenk flask, degassed, flushed with N₂ 99.999% and kept under a nitrogen atmosphere at 125 °C

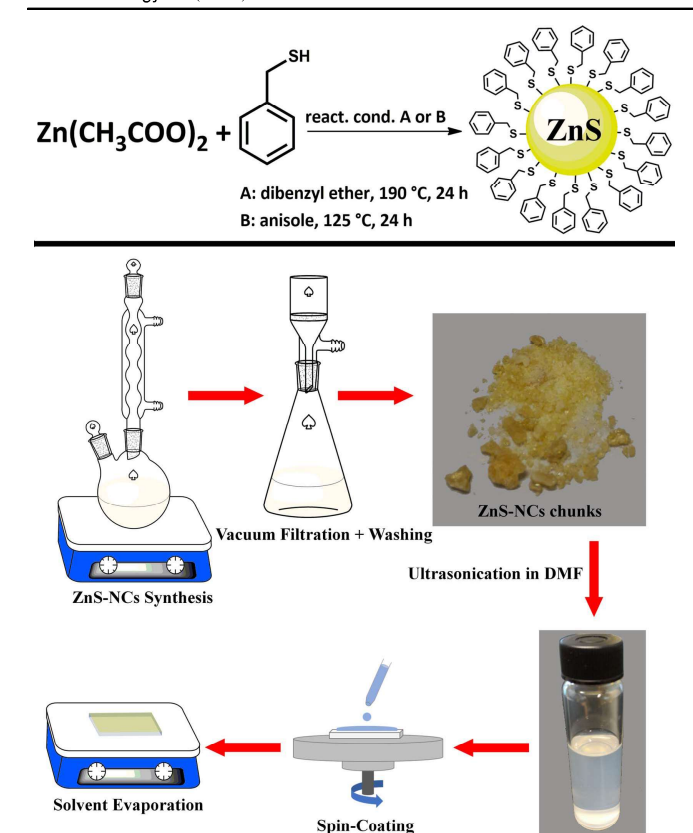


Figure 1. Schematic description of the reaction leading to the formation of ZnS-NCs (upper scheme) and of the steps involved in the ZnS-NCs synthesis and thin-film fabrication (bottom scheme).

for one day. After filtration by $0.22 \mu m$ PTFE syringe filter, the reaction products were analyzed by NMR and GC-MS. A scheme of the chemical reaction leading to the formation of ZnS-NCs is portrayed in figure 1 (upper scheme).

2.2. Thin-film deposition

The dispersion was prepared by ultrasonicating in a glass vial, for 1 h, 50 mg of the purified ZnS-NCs powder in 5 ml *N*,*N*-dimethylformamide RE grade from QRëC dried on molecular sieves. The dispersion was allowed to settle down overnight and the supernatant, containing highly dispersed NCs, was separated from the precipitate and used for the morphological and optical characterizations and for the deposition of the ZnS film.

ZnS films were deposited by spin-coating 70–100 μ l of the dispersion at 2000 rpm on borosilicate glass and on ITO coated glass substrates and dried on a hot plate at 60 °C for 30 min. The substrates were previously cleaned by subsequent sonication in deionized water, acetone and isopropyl alcohol for a minimum of 10 min each before being exposed to UV-ozone for 10 min immediately prior to film deposition. Drop casting of ZnS film was carried out by dropping the DMF dispersion on the cleaned borosilicate substrate and heating at 60 °C to accelerate the evaporation of the solvent. A scheme of the steps involved in the preparation of the ZnS film is depicted in figure 1 (bottom scheme).

2.3. Morphological study

Powder x-ray diffraction (PXRD) patterns were acquired on purified ZnS-NCs powder by using a Bruker Discovery D8 diffractometer in powder configuration using the rotating sample with anti-air scatterer options without slit. The powders were finely ground in an agate mortar prior the measurement to avoid preferential orientation features in the diffraction pattern.

Aberration-corrected high-angle annular dark-field scanning transmission electron microscopy (HAADF-STEM) was performed on a Titan G 60–300 CT electron microscope at an accelerating voltage of 300 kV. The electron gun was used in the unfiltered mode, and the probe size during STEM analysis was estimated to be approximately 0.5 nm with a beam current of 0.08 nA. A camera length of 360 mm and a condenser aperture size of 50 mm were used for imaging. Additional high resolution transmission electron microscopy (HRTEM) images were acquired by a JEOL ACCELARM JEM-ARM200F transmission electron microscope. TEM samples were prepared by dropping the NCs dispersion in DMF on 200 nm mesh CF200-CU copper coated carbon grids by Electron Microscopy Sciences and drying by a N₂ flow followed by overnight vacuum treatment.

SEM images of ZnS film were acquired on the film prepared by spin-coating the ZnS-NCs dispersion in DMF on ITO glass by using a JEOL JSM-7610F field emission scanning electron microscope. AFM images of the ZnS-NCs film were acquired by using a Park Systems NX10 atomic force microscope. The film was obtained by spin-coating on borosilicate glass slide the NCs dispersion in DMF.

2.4. Optoelectronic investigation

Optical absorption and steady-state/time-resolved photoluminescence (PL) measurements were performed on the ZnS-NCs dispersion and film respectively. However, due to a larger thickness of the film, better results in terms of intensity were obtained when PL and diffuse reflectance measurements were taken on a drop-cast film. UV-vis spectra of ZnS-NCs were acquired by a Perkin Elmer Lambda 1050 spectrometer equipped with an integrating sphere for total reflectance measurements. The ZnS-NCs dispersion in DMF was measured in transmission mode using a quartz cuvette. Similarly, absorption measurements of ZnS thin films were acquired in transmission mode by placing the film deposited on glass substrate in the optical path. Diffuse reflectance spectra of the ZnS thin-film deposited on glass were acquired using the same instrument though by placing the substrate in the port of the integrating sphere (diffuse reflectance mode).

Steady-state and time-resolved PL measurements were performed by an Edinburgh Instruments FLS 980 Spectrometer. Steady-state PL spectra of the ZnS-NCs dispersion and of the film were acquired using monochromatic excitation light at 300 nm and a photomultiplier detector for emitted light. The PL-decay was measured at 440 nm (maximum of intensity) using a pulsed laser source emitting at 370.8 nm, with a signal which was deconvoluted from the signal of the

source by measuring the decay of a colloidal silica dispersion (LUDOX HS-40 Sigma Aldrich) 10% in water. The lifetime of the electronic state was estimated by a double exponential fit of the experimental data (equation (S1)) and evaluating the time constant τ in terms of averaged time constant $\tau_{\rm avg}$ as in equation (S2).

Photoelectron spectroscopy in air (PESA) were performed by a RKI AC-2 photoelectron spectrometer on ZnS-NCs film deposited on ITO glass by spin-coating. The edge of valence band was evaluated from the onset of the electron emission yield (square root of electron counts) obtained through linear fitting.

2.5. Mechanistic studies

The mechanistic studies were carried out by analyzing the GC-MS of the reaction products separated from the NCs by filtration with a membrane filter. Briefly, $100\,\mu l$ of the resulting reaction products were filtered by $0.46\,\mu m$ pore membrane syringe filter and diluted in 3 ml of dichloromethane (Honeywell HPLC grade) and analyzed by a gas chromatography equipment Perkin-Elmer Clarus 680 GC coupled with Clarus SQ 8 T mass spectrometer (GC-MS). The injection temperature was set at 60 °C for identifying also the lightest compounds, while the oven temperature was set to $100\,^{\circ}$ C.

Further experimental details are reported in the supplementary material.

3. Results and discussion

The NCs were prepared according to the procedure reported in the experimental section and depicted in figure 1 (upper scheme). When purified and dry, they tend to agglomerate in large yellow crystals (bottom-up assembly) [56] (figure S1(a)) resembling bulk ZnS. This behavior is due to the extremely reduced size and the absence of a bulky organic coordinating shell. However, with the assistance of ultrasonication, ZnS-NCs could be dispersed in highly polar aprotic solvents such as N-methyl pyrrolidinone and N,N-dimethylformamide. These solvents are well known for their ability to disperse various nanostructures, including carbon nanotubes bundles and other carbon nanostructures, thanks to their tendency to form coordination shells [57, 58]. Combining these two properties, it was possible to prepare NCs dispersions and to spin-coat a thin-film suitable for morphological and optoelectronic characterization, as well as, in perspective, for future technological applications. It is important to use dry DMF to avoid the degradation of the as-prepared ZnS-NCs that are not protected by long-chain stabilizing molecules. An image of ZnS-NCs dispersion is reported in figures 1 and S1(b). It was observed that the suspension remains stable for months with no precipitation.

ZnS-NCs were characterized by HRTEM using the aberration-corrected scanning TEM mode (HAADF-STEM). A HAADF-STEM image of the NCs assembly is shown in figure 2(a) and a normal HRTEM image is shown in figure

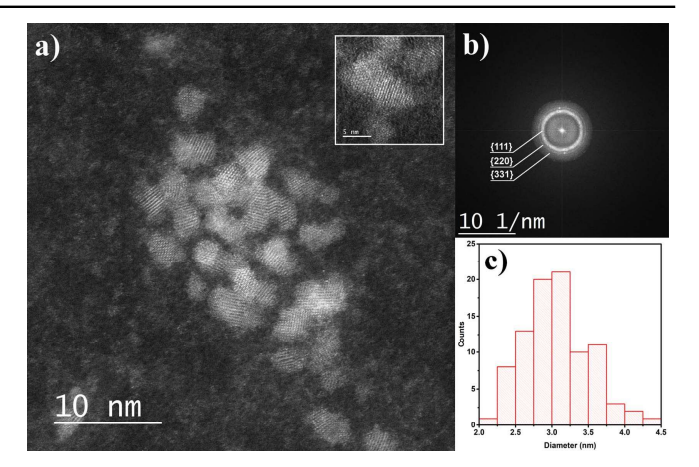


Figure 2. (a) Aberration-corrected high-angle annular dark-field scanning transmission electron microscopy (HAADF-STEM) image and, in the inset, high magnification HAADF-STEM images of a few NCs with different orientation of the *z* axis. (b) SAED pattern of a single ZnS-NC. The three main reflections have been labeled with their relative Miller indexes; with crystallographic *c*-axis lying parallel to the image plane; (c) histogram of the statistical size analysis of NCs done on several HRTEM images.

S2. Here NCs appear partially agglomerated after the solvent evaporation. A better outline of the NCs can be observed in the inset of figures 2(a) and of figure S2 where a single NC is magnified allowing us to see the atomic planes of the Würtzite crystal with the c-axis parallel to the plane of the image. The results of a statistical size analysis over a large number of NCs is reported as a histogram in figure 2(c). The NCs diameter distribution is centered at 3 nm and does not exceed 4.5 nm. This result is confirmed by PXRD patterns (figure 3(b)) that evidence very broad diffraction peaks corresponding to small-sized ZnS-NCs. By using the Debye-Scherrer formula $D = k\lambda/B\cos\theta$, where B is the full width at half maximum of the Miller indexes, $\lambda = 1.54060 \,\text{Å}$ (Cu K α) is the x-ray wavelength, k = 0.94 is the shape factor for cubic crystals and θ is the Bragg angle. A diameter of D = 2.7 nm was estimated. This value is slightly smaller than the D value obtained from TEM analysis due to the fact that it estimates the coherent domain which is always smaller than the actual particle size. Application of the Debye–Scherrer formula to the PXRD pattern of ZnS-NCs synthesized in anisole provides a substantially lower diameter D = 2.1 nm (figure 3(b)), probably, as an effect of the lower reaction temperature (vide infra). The characteristic position and intensity of the {111}⁵, {220} and {331} reflections are observed by PXRD and selected area electron diffraction (SAED) (figure 2(b)) which shows that the ZnS-NCs have the Würtzite crystalline structure [56].

The optical absorption spectra of ZnS-NCs shown in figures 4(a) and (b) for dispersion in DMF and drop-cast film, respectively, reveal the typical absorption edge of semiconducting NCs with the excitonic peak blue-shifted with respect to bulk ZnS. In this case, the excitonic peak is not well defined as in the case of ligand-coated NCs [32, 33], probably due to a higher surface exciton recombination rate that quenches the excited state caused by the absence of the ligand

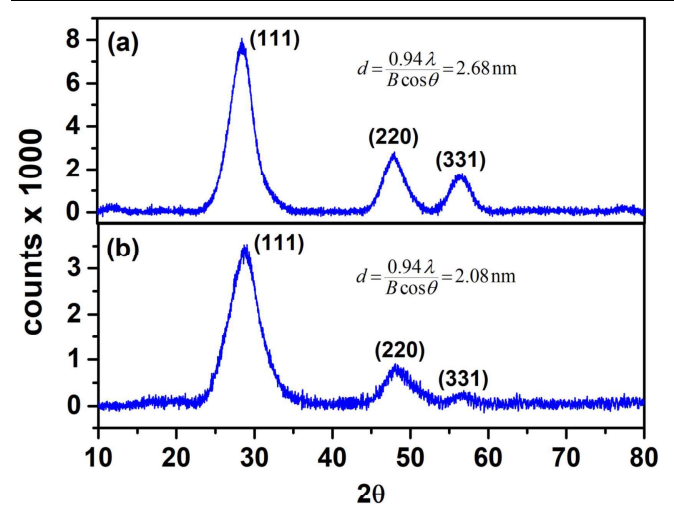


Figure 3. Powder XRD pattern of ZnS-NCs synthesized in (a) dibenzyl ether and (b) anisole media.

and by a partial agglomeration [52]. The energy of the $1S_h \rightarrow 1S_e$ electronic transition between the molecular-like discrete electronic levels was estimated to be, from the onset of the Tauc plot, $E_g(R) = 3.71$ eV (figure 4(c)). Tauc plot was traced by measuring the diffuse reflectance (Kubelka–Munk function) of the NCs drop-cast film performed by an integrating sphere. $E_g(R)$ is, as expected, slightly blue-shifted due to quantum confinement effect from the bulk band-gap energy of $E_g = 3.68$ eV. This value is also in a good agreement with the E(r) predicted by the theory (Brus' equation [59] (equation (1))). Using $r_{NC} = 1.5$ nm ($d_{NC} = 3$ nm) obtained from TEM images statistical analysis, see histogram in the inset of figure 2(c), a $1S_h \rightarrow 1S_e$ optical transition energy $E_g(r) = 3.74$ eV was obtained

$$E(r) = E_{\rm g} + \frac{\hbar^2 \pi^2}{2\mu_e r^2} - \frac{1.8e^2}{\varepsilon r},$$
 (1)

where $E_{\rm g}$ is the bulk ZnS band-gap, \hbar is the reduced Planck's constant, e is the electron charge, ε is the dielectric constant of bulk ZnS and μ_e , expressed as follows

$$\mu_e = 0.21m_e + 2.39 \exp\left(-\frac{R}{5.59}\right) \tag{2}$$

is the semi-empirical expression for the size-dependent effective mass of the electron [60], where m_e is the mass of the electron. This value is very close to the experimental 3.71 eV obtained by the Tauc plot.

PL measurements of solution and powder shown in figures 4(a) and (b) highlight the good emissive properties of the material. For ZnS-NCs dispersion in DMF, the PL peak is centered at 440 nm while for the powder is slightly red-shifted to 446 nm. This small shift can be caused by the close packing of the NCs resulting in an electronic coupling between the NCs and thus in an overlap of the wavefunctions [56]. Based on PL-decay measurements shown in figures S3 and S4, the electronic state lifetime was estimated. Through fitting the experimental data with a double exponential function, the average time constants $\tau_{\rm disp}=3.04\,\rm ns$ and $\tau_{\rm film}=1.49\,\rm ns$ were found, respectively, for NCs dispersion and film. These

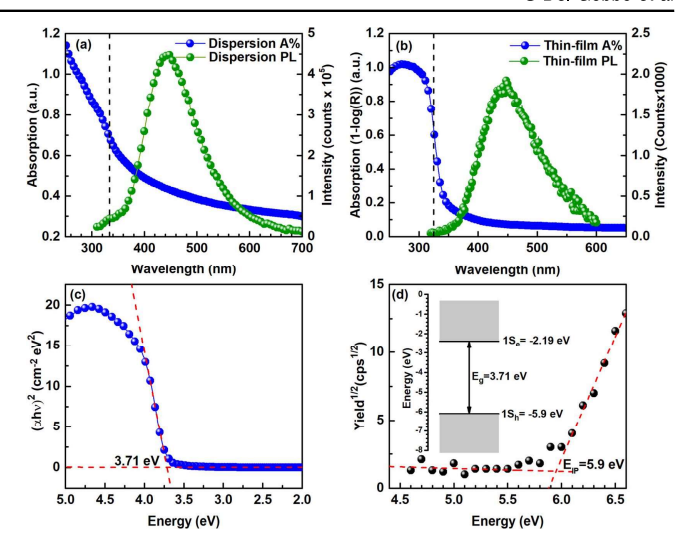


Figure 4. (a) UV–vis absorption (blue dots) and steady-state PL (green dots) spectra of ZnS-NCs dispersion in DMF. (b) UV–vis absorption (blue dots) and steady-state PL (green dots) spectra of ZnS-NCs drop-cast on a fused silica substrate. (c) Tauc plot of the drop-cast ZnS-NCs on fused silica substrate. (d) PESA spectrum of a ZnS-NCs powder. The inset shows the energy level diagram based on the ionization potential obtained from PESA (for 1S_h level) and optical gap from UV–vis measurements.

values of τ are the weighted average values of the two-time constants occurring in the biexponential formula used to fit the experimental data (equation (S1) in supplementary data). Although these time constants are of the same order of magnitude, the lifetime for NPs in solution is slightly longer than for the NPs in the thin-film. The small difference between the two PL-decay curves lies mostly in the difference between the fast components which are originated from the surface defects-related non-radiative decay [61, 62], which effectively leads to a more pronounced quenching due to stronger NC-NC interactions in the film [52]. On the contrary, there is no significant difference between the slow components assignable to the non-radiative decay occurring in NC core which are originated from material non-stoichiometries and vacancies [61] and, to a lesser extent, from phonon-electron scattering, not particularly significant in direct gap semiconductors such as ZnS [63]. It is worth to notice that the lifetime of the electronic state is in the one nanosecond scale, thus in the order of magnitude of PLenhanced Mn²⁺:ZnS-NCs [64]. On the other hand, as expected, PL-lifetime is one order of magnitude lower (i.e., faster decay) than NCs coated with organic molecules or by a layer of inorganic material (core-shell structure), both acting as surface defects passivators [65-68]. If desired, a PL-lifetime extension can be eventually obtained by carrying out a suitable post-synthetic ligand exchange with long-chain molecules [69] or by coating NCs with a passivating inorganic layer (core-shell) [70].

From the onset of the photoelectron yield spectrum measured with PESA, the $1S_h$ electronic level of the film was found to be $-5.70\,\mathrm{eV}$ respective of the vacuum level. Nevertheless, ZnS-NCs in powder form measured by PESA show a $1S_h$ level of $-5.90\,\mathrm{eV}$, hence closer to literature

values. We consider this value more reliable since the measurement on thin-film might have been affected by the influence of the underlying ITO substrate, given the extremely thin nature of the film. PESA curve of ZnS-NCs powder with relative linear fit are presented in figure 4(d). By adding the optical gap energy obtained from diffuse reflectance measurements (Tauc plot in figure 4(c)), the energy of the 1S_e level has been calculated to be $-2.19 \,\mathrm{eV}$ respective to the vacuum level. For clarity, a scheme of the band-gap related electronic levels of ZnS-NCs is shown in the inset of figure 4(d). Both 1S_h and 1S_e molecular-like states (originated from bulk valence and conduction bands respectively) are, when compared to literature values of bulk ZnS [71] and ZnS-NCs [72], shifted toward the vacuum level, i.e., toward less negative energies. However, considering that photoelectron spectroscopy performed in air may provide results that differ from measurements done in ultrahigh vacuum (using ultraviolet photoelectron spectroscopy, UPS), a reference workfunction measurement of a gold standard by PESA is also performed, providing $E_{WF(Au)} = 4.72 \text{ eV}$ (4.78 eV for PESA literature value [73]), versus $E_{WF(Au)} = 5.1 \text{ eV}$ obtained from UPS measurements [74].

Morphological analysis of ZnS films deposited by spincoating from NCs dispersions was carried out by scanning electron microscopy (SEM) and by atomic force microscopy (AFM). SEM images of the ZnS film deposited on ITO glass are shown in figure S5 of the supporting information. Figure S5(a) is relative to films deposited from ZnS-NCs synthesized at 190 °C in DBE whereas figures S5(b) and (c) are relative to a film fabricated from ZnS-NCs synthesized at 125 °C in anisole. In the first case, the film has a quite elevated roughness, and the presence of large NCs agglomerates lying on the film surface is evident. In the second case, when a dispersion of smaller NCs synthesized at 125 °C in anisole is used, the film appears much more uniform and composed of 20-30 nm NCs island-like grains (see figure S5(c)) and without NCs agglomerates on the surface. This is confirmed by AFM topography shown in figures S6(c) and (d) of supporting data. Agglomerations confer to the film a roughness of $R_a = 6.8$ nm comparable to, if not better than, ZnS films obtained by CBD [22, 75, 76] and oxides films cast from NCs dispersion [53-55]. On the other hand, when larger NCs are used, namely NCs synthesized at 190 °C in DBE, the film has a roughness of $R_a = 15$ nm (figures S6(a) and (b)). It is thus clear the NCs size plays a fundamental role on their dispersibility and consequently on the quality of the resulting film. Therefore, these measurements highlight the suitability of this method for casting ZnS films starting from a ligandfree NCs dispersion. We anticipate that this method can be applied to chalcogenides in general and it appears particularly suitable for the fabrication of optoelectronic devices such as luminescent screens, LED, transistors and solar cells.

The mechanism of the reaction leading to the formation of the ZnS-NCs was investigated by the analysis of the reaction products formed in solution by GC-MS (from figures S7 to S10). The fact that similar ZnS-NCs could be prepared in both DBE and anisole with a yield close to 100% suggest

Scheme 1. Plausible ZnS-NCs formation pathways: (top) via reaction of benzyl mercaptan with $Zn(OAc)_2$ followed by the elimination of dibenzyl sulfide (bottom) (b) as an effect of the *in situ* formation of H_2S by the condensation of two molecules of benzyl mercaptan.

the absence of a specific role of the solvent on the reaction pathway.

It is well known that the formation of metal oxides in the NHSG can proceed via halide, ether, ester or aldol elimination [45, 46]. Yet, concerning the synthesis of ZnS-NCs by the thio-sol-gel route, as previously suggested by Niederberger *et al* [47], the formation of a thioacetic ester in the reaction of Zn(OAc)₂ and BM would lead to ZnO rather than ZnS. The replacement of the acetate ligands by molecules of BM, the formation of zinc benzyl thiolate as intermediate and the subsequent elimination of dibenzyl sulfide would initiate the formation of the growing ZnS chain according to the thioether elimination mechanism depicted in scheme 1(a).

Indeed, GC-MS analysis of the reaction mixture following the synthesis of ZnS-NCs in anisole at 125 °C (figure S7) shows the formation of dibenzyl thioether as the main reaction product along with minor amounts of dibenzyl disulfide. The latter product is likely to arise from the coupling of two molecules of dibenzyl thioether. No traces of thioacetic ester were found. Furthermore, when a blank reaction was carried out by dissolving BM in anisole under identical conditions as per the synthesis of ZnS-NCs but in the absence of Zn(OAc)2, no formation of dibenzyl thioether was observed (figure S8). This observation demonstrates that the latter compound is generated as an effect of the reaction of BM with Zn(OAc)₂ leading to the formation of ZnS. The GC-MS chromatogram of the reaction mixture from the synthesis of ZnS-NCs in dibenzyl ether (figure S9) is more complex and less clean than for the corresponding reaction in anisole. Dibenzyl thioether is, however, the main product. Dibenzyl disulfide, trisulfide and several oxidation products of the various thio- compounds are also found in the reaction mixture. The formation of the latter series of compounds is likely to arise from the higher reaction temperatures employed when compared to the analogous synthesis in anisole. Interestingly, the chromatogram of the blank reaction carried out in dibenzyl ether under identical reaction conditions as per the synthesis of the ZnS-NCs, but in the absence of Zn(OAc)₂ (figure \$10), shows the formation of small amounts of dibenzyl thioether, disulfide and trisulfide even in the absence of $Zn(OAc)_2$. The formation of dibenzyl disulfide and trisulfide in dibenzyl ether at 190 °C is supposed to take place due to the presence of H_2S originated from the condensation of two BM molecules as in scheme 1(b). The presence of free H_2S in the reaction environment probably leads to a less controlled formation of ZnS. Indeed, it is well known that the addition of H_2S to solutions of $Zn(OAc)_2$ leads to the precipitation of ZnS due to the low K_{ps} of this compound in water as well as in organic solvents (scheme 1(b)) [77]. Therefore, the side formation of H_2S could partly affect the controlled formation of the ZnS-NCs in dibenzyl ether and be at the origin of the slightly larger particle size found when DBE at 190 °C is used instead of anisole at 125 °C.

4. Conclusions

In conclusion, ZnS-NCs have been synthesized by a ligandfree thiol-based synthesis obtaining surface uncoated ZnS-NCs. This method allowed us to obtain very small NCs $(d \le 3 \text{ nm})$ that show quantum confinement effects given the reduced size. The reduced size also allowed the preparation of stable dispersion of the NCs in polar organic solvents that can be deposited on suitable substrates by spin-coating. A morphological and optoelectronic characterization of the NCs and of the resulting film was carried out demonstrating that NCs prepared by this method can be effectively utilized as building-blocks for the deposition of semiconducting material thinfilms for optoelectronic applications circumventing the problem of organic ligand exchange or removal. Furthermore, this method has the potential to be extended to other more relevant optoelectronic materials in the future. Finally, the mechanism of ZnS-NCs growth was also elucidated by analyzing the reaction sub-products through NMR and GC-MS techniques. A main reaction mechanism involving the initial formation of a zinc benzyl thiolate with thioether elimination was identified.

Acknowledgments

The authors would like to thank the Frontier Research Center (FRC) of VISTEC for support of characterization instruments and, in particular, Somlak Ittisanronnachai for TEM measurements and technical support for SEM. S D G and V D E would like to thank the Thailand Research Fund (Grant No. RSA6080059) for funding this research. P P would like to acknowledge the funding from the Office of the Higher Education Commission (OHEC) and the Thailand Research Fund (TRF) under Grant No. MRG5980214.

ORCID iDs

Silvano Del Gobbo https://orcid.org/0000-0003-4110-2700 Valerio D'Elia https://orcid.org/0000-0002-5881-2496

References

- [1] Lee W J, Yu H J, Wi J H, Cho D H, Han W S, Yoo J, Yi Y, Song J H and Chung Y D 2016 Behavior of photocarriers in the light-induced metastable state in the p—n heterojunction of a Cu(In,Ga)Se₂ solar cell with CBD-ZnS buffer layer *ACS Appl. Mater. Interfaces* 8 22151–8
- [2] Ummartyotin S and Infahsaeng Y 2016 A comprehensive review on ZnS: from synthesis to an approach on solar cell *Renew. Sustain. Energy Rev.* 55 17–24
- [3] Nakada T, Hongo M and Hayashi E 2003 Band offset of high efficiency CBD-ZnS/CIGS thin film solar cells *Thin Solid* Films 431-432 242-8
- [4] Shin D H, Kim J H, Shin Y M, Yoon K H, Al-Ammar E A and Ahn B T 2013 Improvement of the cell performance in the ZnS/Cu(In,Ga)Se₂ solar cells by the sputter deposition of a bilayer ZnO:Al film *Prog. Photovolt.*, Res. Appl. 21 217–25
- [5] Cerdán-Pasarán A, Esparza D, Zarazúa I, Reséndiz M, López-Luke T, De la Rosa E, Fuentes-Ramírez R, Alatorre-Ordaz A and Martínez-Benítez A 2016 Photovoltaic study of quantum dot-sensitized TiO₂/CdS/ZnS solar cell with P₃HT or P₃OT added *J. Appl. Electrochem.* 46 975–85
- [6] Krebs F C 2009 Fabrication and processing of polymer solar cells: a review of printing and coating techniques Sol. Energy Mater. Sol. Cells 93 394–412
- [7] Qi L, Lee B I, Kim J M, Jang J E and Choe J Y 2003 Synthesis and characterization of ZnS:Cu,Al phosphor prepared by a chemical solution method J. Lumin. 104 261-6
- [8] Tanaka M, Sawai S, Sengoku M, Kato M and Masumoto Y 2000 Luminescence properties of ZnS phosphor nanocrystals prepared by the laser-induced gas-evaporation method J. Appl. Phys. 87 8535–40
- [9] Katiyar A K, Sinha A K, Manna S and Ray S K 2014 Fabrication of Si/ZnS radial nanowire heterojunction arrays for white light emitting devices on Si substrates ACS Appl. Mater. Interfaces 6 15007–14
- [10] Wu X, Jiang P, Ding Y, Cai W, Xie S and Wang Z L 2007 Mismatch strain induced formation of ZnO/ZnS heterostructured rings Adv. Mater. 19 2319–23
- [11] Zamiri R, Tobaldi D M, Ahangar H A, Rebelo A, Seabra M P, Belsley M S and Ferreira J M F 2014 Study of far infrared optical properties and, photocatalytic activity of ZnO/ZnS heteronanocomposite structure RSC Adv. 4 35383–9
- [12] Sanchez-Tovar R, Fernandez-Domene R M, Montanes M T, Sanz-Marco A and Garcia-Anton J 2016 ZnO/ZnS heterostructures for hydrogen production by photoelectrochemical water splitting RSC Adv. 6 30425–35
- [13] Kushwaha A and Aslam M 2014 ZnS shielded ZnO nanowire photoanodes for efficient water splitting *Electrochim. Acta* 130 222–31
- [14] Kim W J, Jang E and Park T J 2017 Enhanced visible-light photocatalytic activity of ZnS/g-C₃N₄ type-II heterojunction nanocomposites synthesized with atomic layer deposition *Appl. Surf. Sci.* 419 159–64
- [15] Zhang C, Xie Y, Deng H, Tumlin T, Zhang C, Su J-W, Yu P and Lin J 2017 Monolithic and flexible ZnS/SnO₂ ultraviolet photodetectors with lateral graphene electrodes Small 13 1604197
- [16] Jia F, Huang F, Ouyang S, Cai C, Xu Z, Wu C, Ma Y and Wang M 2016 Design of photoactive hybrid based intelligent photodetectors for identifying the detected wavelength J. Mater. Chem. C 4 10797–803
- [17] Alam M M, Sultana A, Sarkar D and Mandal D 2017
 Electroactive β-crystalline phase inclusion and photoluminescence response of a heat-controlled spin-coated PVDF/TiO₂ free-standing nanocomposite film for a

- nanogenerator and an active nanosensor *Nanotechnology* **28** 365401
- [18] Sultana A, Alam M M, Garain S, Sinha T K, Middya T R and Mandal D 2015 An effective electrical throughput from PANI supplement ZnS nanorods and PDMS-based flexible piezoelectric nanogenerator for power up portable electronic devices: an alternative of MWCNT filler ACS Appl. Mater. Interfaces 7 19091–7
- [19] Sultana A, Alam M M, Biswas A, Middya T R and Mandal D 2016 Fabrication of wearable semiconducting piezoelectric nanogenerator made with electrospun-derived zinc sulfide nanorods and poly(vinyl alcohol) nanofibers *Trans. Mater.* Res. 3 45001
- [20] Hong J, Lim D, Eo Y-J and Choi C 2018 Chemical bath deposited ZnS buffer layer for Cu(In,Ga)Se₂ thin film solar cell Appl. Surf. Sci. 432 250–4
- [21] Zhang Y, Dang X Y, Jin J, Yu T, Li B Z, He Q, Li F Y and Sun Y 2010 ZnS thin film deposited with chemical bath deposition process directed by different stirring speeds *Appl.* Surf. Sci. 256 6871–5
- [22] Deepa K, Preetha K C, Murali K V, Dhanya A C, Ragina A J and Remadevi T L 2014 The effect of various complexing agents on the morphology and optoelectronic properties of chemically deposited ZnS thin films: a comparative study *Optik* 125 5727–32
- [23] Takayama K, Fujiwara K, Kume T, Naya S I and Tada H 2017 Electron filtering by an intervening ZnS thin film in the gold nanoparticle-loaded CdS plasmonic photocatalyst *J. Phys. Chem. Lett.* 8 86–90
- [24] Sahu N, Parija B and Panigrahi S 2009 Fundamental understanding and modeling of spin coating process: a review *Indian J. Phys.* 83 493–502
- [25] Cho D-H, Lee W-J, Park S-W, Wi J-H, Han W S, Kim J, Cho M-H, Kim D and Chung Y-D 2014 Non-toxically enhanced sulfur reaction for formation of chalcogenide thin films using a thermal cracker J. Mater. Chem. A 2 14593–9
- [26] Hariskos D, Powalla M, Chevaldonnet N, Lincot D, Schindler A and Dimmler B 2001 Chemical bath deposition of CdS buffer layer: prospects of increasing materials yield and reducing waste *Thin Solid Films* 387 179–81
- [27] Jiang C, Ng S M, Leung C W and Pong P W T 2017 Magnetically assembled iron oxide nanoparticle coatings and their integration with pseudo-spin-valve thin films J. Mater. Chem. C 5 252-63
- [28] Iskandar F 2009 Nanoparticle processing for optical applications—a review Adv. Powder Technol. 20 283–92
- [29] Xu L, Karunakaran R G, Guo J and Yang S 2012 Transparent, superhydrophobic surfaces from one-step spin coating of hydrophobic nanoparticles ACS Appl. Mater. Interfaces 4 1118–25
- [30] Bhattacharjee B and Lu C H 2006 Multicolor luminescence of undoped zinc sulfide nanocrystalline thin films at room temperature *Thin Solid Films* 514 132–7
- [31] Akhtar M S, Riaz S, Mehmood R F, Ahmad K S, Alghamdi Y, Malik M A and Naseem S 2017 Surfactant and template free synthesis of porous ZnS nanoparticles *Mater. Chem. Phys.* 189 28–34
- [32] Murray C B, Kagan C R and Bawendi M G 2000 Synthesis and characterization of monodispersed nanocrystals and closepacked nanocrystals assemblies *Annu. Rev. Mater. Sci.* 30 545–610
- [33] Herron N, Wang Y and Eckert H 1990 Synthesis and characterization of surface-capped, size-quantized cadmium sulfide clusters. Chemical control of cluster size *J. Am. Chem. Soc.* 112 1322–6
- [34] Abulikemu M, Del Gobbo S, Anjum D H, Malik M A and Bakr O M 2016 Colloidal Sb₂S₃ nanocrystals: synthesis, characterization and fabrication of solid-state semiconductor

- sensitized solar cells J. Mater. Chem. A 4 6809–14
- [35] Barbé J, Eid J, Ahlswede E, Spiering S, Powalla M, Agrawal R and Del Gobbo S 2016 Inkjet printed Cu(In,Ga)S₂ nanoparticles for low-cost solar cells J. Nanoparticle Res. 18 379
- [36] Luber E J, Mobarok M H and Buriak J M 2013 Solutionprocessed zinc phosphide (α-Zn₃P₂) colloidal semiconducting nanocrystals for thin film photovoltaic applications ACS Nano 7 8136–46
- [37] Ho C T, Low K B, Klie R F, Maeda K, Domen K, Meyer R J and Snee P T 2011 Synthesis and characterization of semiconductor tantalum nitride nanoparticles *J. Phys. Chem.* C 115 647–52
- [38] Liu Y, Ai K, Yuan Q and Lu L 2011 Fluorescence-enhanced gadolinium-doped zinc oxide quantum dots for magnetic resonance and fluorescence imaging *Biomaterials* 32 1185–92
- [39] Jana N R, Yu H, Ali E M, Zheng Y and Ying J Y 2007 Controlled photostability of luminescent nanocrystalline ZnO solution for selective detection of aldehydes *Chem. Commun.* 0 1406–8
- [40] Masala S, Adinolfi V, Sun J-P, Del Gobbo S, Voznyy O, Kramer I J, Hill I G and Sargent E H 2015 The silicon: colloidal quantum dot heterojunction Adv. Mater. 27 7445–50
- [41] Bourget L, Corriu R J P, Leclercq D, Mutin P H and Vioux A 1998 Non-hydrolytic sol-gel routes to silica J. Non-Cryst. Solids 242 81-91
- [42] Niederberger M, Bartl M H and Stucky G D 2002 Benzyl alcohol and titanium tetrachloride—a versatile reaction system for the nonaqueous and low-temperature preparation of crystalline and luminescent titania nanoparticles *Chem. Mater.* 14 4364–70
- [43] Niederberger M, Bartl M H and Stucky G D 2002 Benzyl alcohol and transition metal chlorides as a versatile reaction system for the nonaqueous and low-temperature synthesis of crystalline nano-objects with controlled dimensionality *J. Am. Chem. Soc.* **124** 13642–3
- [44] Acosta S, Corriu R J P, Leclercq D, Lefevre P, Mutin P H and Vioux A 1994 Preparation of alumina gels by a nonhydrolytic sol–gel processing method J. Non-Cryst. Solids 170 234–42
- [45] Niederberger M 2007 Nonaqueous sol—gel routes to metal oxide nanoparticles *Acc. Chem. Res.* **40** 793–800
- [46] Niederberger M and Garnweitner G 2006 Organic reaction pathways in the nonaqueous synthesis of metal oxide nanoparticles Chem. Eur. J. 12 7282–302
- [47] Ludi B, Olliges-Stadler I, Rossell M D and Niederberger M 2011 Extension of the benzyl alcohol route to metal sulfides: 'nonhydrolytic' thio sol-gel synthesis of ZnS and SnS₂ Chem. Commun. 47 5280–2
- [48] La Porta F A, Andrés J, Li M S, Sambrano J R, Varela J A and Longo E 2014 Zinc blende versus wurtzite ZnS nanoparticles: control of the phase and optical properties by tetrabutylammonium hydroxide *Phys. Chem. Chem. Phys.* 16 20127–37
- [49] Chukwuocha E O, Onyeaju M C and Harry T S T 2012 Theoretical studies on the effect of confinement on quantum dots using the brus equation World J. Condens. Matter Phys. 2 96–100
- [50] Pong B-K, Trout B L and Lee J-Y 2008 Modified ligandexchange for efficient solubilization of CdSe/ZnS quantum dots in water: a procedure guided by computational studies *Langmuir* 24 5270–6
- [51] Jeong S, Achermann M, Nanda J, Ivanov S, Klimov A V I and Hollingsworth J A 2005 Effect of the thiol—thiolate equilibrium on the photophysical properties of aqueous CdSe/ZnS nanocrystal quantum dots J. Am. Chem. Soc. 127 10126–7

- [52] Zillner E, Fengler S, Niyamakom P, Rauscher F, Köhler K and Dittrich T 2012 Role of ligand exchange at CdSe quantum dot layers for charge separation J. Phys. Chem. C 116 16747–54
- [53] Wojciechowski K, Saliba M, Leijtens T, Abate A and Snaith H J 2014 Sub-150 °C processed mesosuperstructured perovskite solar cells with enhanced efficiency *Energy Environ. Sci.* 7 1142–7
- [54] Zhou H, Chen Q, Li G, Luo S, Song T-B, Duan H-S, Hong Z, You J, Liu Y and Yang Y 2014 Interface engineering of highly efficient perovskite solar cells Science 345 542–6
- [55] Abulikemu M, Neophytou M, Barbé J M, Tietze M L, El Labban A, Anjum D H, Amassian A, McCulloch I and Del Gobbo S 2017 Microwave-synthesized tin oxide nanocrystals for low-temperature solution-processed planar junction organo-halide perovskite solar cells *J. Mater.* Chem. A 5 7759–63
- [56] AbdulHalim L G, Bootharaju M S, Tang Q, Del Gobbo S, AbdulHalim R G, Eddaoudi M, Jiang D E and Bakr O M 2015 Ag29(BDT)12(TPP)4: a tetravalent nanocluster *J. Am. Chem. Soc.* 137 11970–5
- [57] Giordani S, Bergin S D, Nicolosi V, Lebedkin S, Kappes M M, Blau W J and Coleman J N 2006 Debundling of singlewalled nanotubes by dilution: observation of large populations of individual nanotubes in amide solvent dispersions J. Phys. Chem. B 110 15708–18
- [58] Bergin S D, Sun Z, Rickard D, Streich P V, Hamilton J P and Coleman J N 2009 Multicomponent solubility parameters for single-walled carbon nanotube-solvent mixtures ACS Nano 3 2340–50
- [59] Brus L E 1984 Electron electron and electron-hole interactions in small semiconductor crystallites—the size dependence of the lowest excited electronic state *J. Chem. Phys.* 80 4403–9
- [60] Vatankhah C and Ebadi A 2013 Quantum size effects on effective mass and band gap of semiconductor quantum dots Res. J. Recent Sci. 2 21–4
- [61] Li L, Pandey A, Werder D J, Khanal B P, Pietryga J M and Klimov V I 2011 Efficient synthesis of highly luminescent copper indium sulfide-based core/shell nanocrystals with surprisingly long-lived emission J. Am. Chem. Soc. 133 1176–9
- [62] Underwood D F, Kippeny T and Rosenthal S J 2001 Ultrafast carrier dynamics in CdSe nanocrystals determined by femtosecond fluorescence upconversion spectroscopy *J. Phys. Chem.* B 105 436–43
- [63] Delerue C, Allan G, Reynaud C, Guillois O, Ledoux G and Huisken F 2006 Multiexponential photoluminescence decay

- in indirect-gap semiconductor nanocrystals *Phys. Rev.* B **73** 235318
- [64] Bhargava R N, Gallagher D, Hong X and Nurmikko A 1994 Optical properties of manganese-doped nanocrystals of ZnS Phys. Rev. Lett. 72 416–9
- [65] Hanrath T, Veldman D, Choi J J, Christova C G, Wienk M M and Janssen R A J 2009 PbSe nanocrystal network formation during pyridine ligand displacement ACS Appl. Mater. Interfaces 1 244–50
- [66] Lefrançois A, Couderc E, Faure-Vincent J, Sadki S, Pron A and Reiss P 2011 Effect of the treatment with (di-) amines and dithiols on the spectroscopic, electrochemical and electrical properties of CdSe nanocrystals' thin films J. Mater. Chem. 21 11524–31
- [67] Ji X, Copenhaver D, Sichmeller C and Peng X 2008 Ligand bonding and dynamics on colloidal nanocrystals at room temperature: the case of alkylamines on CdSe nanocrystals J. Am. Chem. Soc. 130 5726–35
- [68] Bullen C and Mulvaney P 2006 The effects of chemisorption on the luminescence of CdSe quantum dots *Langmuir* 22 3007–13
- [69] Knauf R R, Lennox J C and Dempsey J L 2016 Quantifying ligand exchange reactions at CdSe nanocrystal surfaces Chem. Mater. 28 4762–70
- [70] Xiao Q and Xiao C 2008 Synthesis and photoluminescence of water-soluble Mn:ZnS/ZnS core/shell quantum dots using nucleation-doping strategy Opt. Mater. 31 455–60
- [71] de Mello Donegá C 2011 Synthesis and properties of colloidal heteronanocrystals *Chem. Soc. Rev.* 40 1512–46
- [72] Stevanović V, Lany S, Ginley D S, Tumas W and Zunger A 2014 Assessing capability of semiconductors to split water using ionization potentials and electron affinities only *Phys. Chem. Chem. Phys.* 16 3706–14
- [73] Uda M 1985 Open counter for low energy electron detection Japan. J. Appl. Phys. 24 284–8
- [74] Eastman D E 1970 Photoelectric work functions of transition, rare-earth, and noble metals *Phys. Rev.* B 2 1–2
- [75] Roy P, Ota J R and Srivastava S K 2006 Crystalline ZnS thin films by chemical bath deposition method and its characterization *Thin Solid Films* 515 1912–7
- [76] Qi L, Mao G and Ao J 2008 Chemical bath-deposited ZnS thin films: preparation and characterization Appl. Surf. Sci. 254 5711–4
- [77] Fogo J K and Popowsky M 1948 Spectrophotometric determination of hydrogen sulfide Anal. Chem. 21 732–4



The 6th Thailand International Nanotechnology Conference (NanoThailand 2018)

December 12-14, 2018

The Thailand Science Park Convention Center (TSP-CC)

Pathum Thani, Thailand

Dear Ms. Jidapa Chaopaknam,

Chulalongkorn University, Nanotechnology Association of Thailand and National Nanotechnology Center (NANOTEC) are jointly organizing the 6th Thailand International Nanotechnology Conference (NanoThailand 2018) which will be held during December 12-14, 2018 under the theme of "From frontier research to innovation and Commercialization" at The Thailand Science Park Convention Center (TSP-CC), Pathum Thani, Thailand. This conference will apply nanotechnology in various fields for a better life, to create a platform for knowledge exchange to further advance technological areas.

Regarding your submitted abstract entitled "New Wide Band Gap Inorganic Semiconductor tin(II) Thiocyanate [Sn(NCS)2] as Its Application in Organic Solar Cell" to present in this conference, the scientific committee would like to notify that your abstract has been accepted for poster presentation. For more information regarding registration, please visit our website (http://www.nano-thailand.com/2018/Annual/).

Yours sincerely,

Rul T

Assoc. Prof. Dr. Patchanita Thamyongkit

Scientific Committee Chairperson

NanoThailand 2018

Department of Chemistry

Faculty of Science, Chulalongkorn University, Thailand

Email: nanothailand2018@gmail.com Website: http://www.nano-thailand.com

New wide band gap inorganic semiconductor tin(II) thiocyanate [Sn(NCS)₂] as its application in organic solar cell

Jidapa Chaopaknama, Chayanit Wechwithayakhlunga, Pichaya Pattanasattayavonga.*

^aDepartment of Materials Science and Engineering School of Molecular Science and Engineering Vidyasirimedhi Institute of Science and Technology (VISTEC) Rayong 21210, Thailand

*e-mail: pichaya.p@vistec.ac.th

Polymeric metal thiocyanates are introduced as a new class of semiconductors with unique electronic properties of the metal centers combined with wide band gaps from bonding with the thiocyanate ligand. One example is copper(I) thiocyanate (CuSCN) which is an excellent transparent p-type semiconductor and has already shown a great potential in electronic application particularly thin film transistors (TFTs), perovskite solar cells (PSCs), organic solar cells (OSCs), and organic light emitting diodes (OLEDs).^{1,2,3} Herein, we introduce tin(II) thiocyanate [Sn(NCS)₂] as another inorganic coordination polymer semiconductor. Sn(II) compounds show promising applications in opto/electronic devices due to its electronic structure, for example, SnO is an excellent p-type oxide with high hole mobility.⁴ It is of great interest to study the properties of Sn(NCS)₂ and its applications in electronic devices.

 $Sn(NCS)_2$ was synthesized and solution-processed into thin films by spin coating. Film annealing can be carried out at temperatures below $80^{\circ}C$, showing compatibility with organic layer processing and plastic substrates. As part of this study, optical, chemical, and morphological characterization was performed. Absorption spectrum of $SnSCN_2$ also demonstrated absorption in UV region which related to high transparency of $SnSCN_2$ thin film in visible and NIR region. The chemical composition of $Sn(NCS)_2$ thin film was confirmed by X-ray photoelectron spectroscopy (XPS). Atomic force microscopy (AFM) presented morphology and roughness of $Sn(NCS)_2$ film. The result shows that the film had high smoothness (RMS = 7.5 nm.) and excellent film quality. In addition, organic solar cells were fabricated using either P3HT:PC70BM or PBDTTT-EFT:PC70BM as the active light-absorbing layer and employing $Sn(NCS)_2$ as the hole transport layer. Device fabrication currently investigates the deposition parameters to optimize the device efficiency.

In conclusion, Tin thiocyanate was demonstrated as one of the new p-type material based on thiocyanate ligand which exhibits remarkable properties and a potential to use in OPVs. Further studies are required to understand charge transport mechanism and investigate new electronic applications.

Keywords : Tin(II) Thiocyanate [Sn(NCS)₂], P-type Semiconductor, Hole Transport Layer, Organic Solar Cells

REFERENCES

- 1. P. Pattanasattayavong, V. Promarak, T. D. Anthopoulos, Adv. Electron. Mater. 2017, 3, 1.
- 2. N. Yaacobi-Gross, N. D. Treat, P. Pattanasattayavong, H. Faber, A. K. Perumal, N. Stingelin, D. D. C. Bradley, P. N. Stavrinou, M. Heeney, T. D. Anthopoulos, *Adv. Energy Mater.* **2015**, *5*, 1.
- 3. N. Wijeyasinghe, A. Regoutz, F. Eisner, T. Du, L. Tsetseris, Y. H. Lin, H. Faber, P. Pattanasattayavong, J. Li, F. Yan, M. A. McLachlan, D. J. Payne, M. Heeney, T. D. Anthopoulos, *Adv. Funct. Mater.* **2017**, *27*, 1.
- 4. Z. Wang, P. K. Nayak, J. A. Caraveo-Frescas, H. N. Alshareef, *Adv. Mater.* **2016**, *28*, 3831.



The 6th Thailand International Nanotechnology Conference (NanoThailand 2018)

December 12-14, 2018

The Thailand Science Park Convention Center (TSP-CC)

Pathum Thani, Thailand

Dear Ms. Pimpisut Worakajit,

Chulalongkorn University, Nanotechnology Association of Thailand and National Nanotechnology Center (NANOTEC) are jointly organizing the 6th Thailand International Nanotechnology Conference (NanoThailand 2018) which will be held during December 12-14, 2018 under the theme of "From frontier research to innovation and Commercialization" at The Thailand Science Park Convention Center (TSP-CC), Pathum Thani, Thailand. This conference will apply nanotechnology in various fields for a better life, to create a platform for knowledge exchange to further advance technological areas.

Regarding your submitted abstract entitled "Improving Charge Transport in CuSCN Hole Transport Later by Anti-Solvent Treatment and Application in High-Efficiency Organic Solar Cells" to present in this conference, the scientific committee would like to notify that your abstract has been accepted for poster presentation. For more information regarding registration, please visit our website (http://www.nano-thailand.com/2018/Annual/).

Yours sincerely,

Rul T

Assoc. Prof. Dr. Patchanita Thamyongkit

Scientific Committee Chairperson

NanoThailand 2018

Department of Chemistry

Faculty of Science, Chulalongkorn University, Thailand

Email: nanothailand2018@gmail.com Website: http://www.nano-thailand.com

Improving charge transport in CuSCN hole transport layer by anti-solvent treatment and application in high-efficiency organic solar cells

Pimpisut Worakajita, Pichaya Pattanasattayavonga,*

^aDepartment of Materials Science and Engineering School of Molecular Science and Engineering Vidyasirimedhi Institute of Science and Technology (VISTEC) Rayong 21210, Thailand *e-mail: pichaya.p@vistec.ac.th

Copper(I) thiocyanate (CuSCN) is a wide bang gap transparent p-type semiconductor with remarkable potential as a hole transporting material. Low-temperature, solution processability is another advantage of applying CuSCN in large-area electronic applications. CuSCN was recently reported to use as a hole transport layer in organic photovoltaic (OPVs) and organic light emitting diodes (OLEDs) in order to replace the conventional materials such as PEDOT:PSS. Interestingly, CuSCN devices exhibit higher efficiency than PEDOT:PSS. However, the development of CuSCN as hole transport layer is still in the early stage and further optimization is expected to improve performance, especially by improving the charge transport properties within CuSCN film which is the fundamental factor to control device efficiency.

Here, we report on adjusting film morphology by anti solvent treatment that leads to improved hole transport in the films. The common solvents were applied in a second spin coating step, using as an antisolvent including Acetone (Ace), Methanol (MeOH), Isopropanol (IPA) and Tetrahydrofuran (THF). The resultant films were highly transparent in visible and NIR region similar to an untreated film. In addition, film morphology was observed using atomic force microscopy (AFM). The results show that CuSCN film treated by Ace, IPA and THF exhibit better film quality than the other bacause of smaller grain size and reducing root mean square roughness (RMS). These smoother films enhance the transport of charge carriers as proved by five times increasing of CuSCN thin-film transistor mobility. Thus, anti-solvent method appear to be a remarkable approach to enhance OPVs devices efficiency.

Keywords: Copper(I) thiocyanate, CuSCN, Solution-processed, Charge Transport, Organic Photovoltaic

REFERENCES

- 1. P. Pattanasattayavong, V. Promarak, T. D. Anthopoulos, Adv. Electron. Mater. 2017, 3, 1.
- 2. N. Yaacobi-Gross, N. D. Treat, P. Pattanasattayavong, H. Faber, A. K. Perumal, N. Stingelin, D. D. C. Bradley, P. N. Stavrinou, M. Heeney, T. D. Anthopoulos, *Adv. Energy Mater.* **2015**, *5*, 1.
- 3. N. Wijeyasinghe, A. Regoutz, F. Eisner, T. Du, L. Tsetseris, Y. H. Lin, H. Faber, P. Pattanasattayavong, J. Li, F. Yan, M. A. McLachlan, D. J. Payne, M. Heeney, T. D. Anthopoulos, *Adv. Funct. Mater.* 2017, *27*, 1.



INVITATION LETTER

To:

Pichaya Pattanasattayavong

Affiliation:

Vidyasirimedhi Institute of Science and Technology VISTEC,

555 Moo 1 Payupnai, Wangchan, Rayong, 21210, Thailand

Date:

03/05/2018

Dear Dr. Pichaya Pattanasattayavong,

We are glad to invite you to participate at the 11th International Symposium on Flexible Organic Electronics – ISFOE18 that will take place at 2–5 July 2018 in Thessaloniki, Greece, which is part of the NANOTEXNOLOGY 2018 multi-event, in order to provide an Oral Presentation with title:

Improving Hole Transport in CuSCN Thin-Film Transistors by Solvent Treatment

P. Pattanasattayavong, P. Worakajit

We are looking forward to meet you in Thessaloniki, Greece in July.

Prof. S. Logothetidis

NANOTEXNOLOGY 2018 Chairman

11th International Symposium on Flexible Organic Electronics (ISFOE18) 2-5 July 2018, Thessaloniki, Greece

Improving Hole Transport in CuSCN Thin-Film Transistors by Solvent Treatment

P. Pattanasattayavong¹, P. Worakajit¹

¹Department of Materials Science and Engineering, School of Molecular Science and Engineering, Vidyasirimedhi Institute of Science and Technology (VISTEC)

Rayong, 21210, Thailand

Abstract: Copper(I) thiocyanate (CuSCN) has been presented as a promising wide band gap semiconductor with novel characteristics that feature high optical transparency in the UV, visible, and near-infrared range as well as the ability to transport holes. Moreover, CuSCN can be deposited from solution and only requires mild annealing condition around 80 to 120 °C, making it compatible with large-area plastic substrates. The unique properties of CuSCN have led to the demonstrations of p-type thin-film transistors (TFTs) based on solutionprocessed, transparent, inorganic semiconductor using CuSCN as the active channel layer on both rigid and flexible substrates (Adv. Mater. 2013, 25, 1504; Appl Phys. Lett. 2017, 110, 113504.). In this work, we investigate the solution-processing of CuSCN thin film further by employing solvent treatment after the deposition of CuSCN thin films. The base CuSCN films were deposited by spin-coating CuSCN solution in diethyl sulfide (DES) on glass substrates and were subsequently treated by spin-coating neat solvent on top. Four solvents that do not dissolve CuSCN (i.e., antisolvents) were tested, namely acetone, methanol, isopropanol, and tetrahydrofuran. Photoelectron spectroscopy (PES) was used to study the changes in the chemical and electronic properties whereas scanning electron microscopy (SEM) and atomic force microscopy (AFM) were employed for the characterization of surface morphology. Top-gate bottom-contact (TGBC) TFTs using CuSCN treated with various solvents as the active channel layer and poly(methyl methacrylate) (PMMA) as the dielectric were fabricated. Significant increase between 2-fold up to 5-fold of maximum drain current and hole mobility was observed. This work shows that the simple technique of solvent treatment can be used to improve hole transport in CuSCN film and that further optimization of CuSCN solution-processing is possible.



Dear Colleague,

Thank you for submitting an abstract for a presentation at the

14th International Conference on Organic Electronics

to be held on June 18-22 2018, in Bordeaux, France.

We are delighted to inform you that your abstract has been selected as oral communication.

Presenting authors must be registered participants at ICOE2018. Early bird fees will be available until March 11^{th} . Regular registration deadline is June 1^{st} , no on-site registration will be offered.

We advise you to book a hotel room as soon as possible : accommodation in Bordeaux can often be fully booked at this time of the year.

We also like to highlight that the gala dinner will be held at Château Soutard, a Saint-Emilion wine producing chateau, on Wednesday $20^{\rm th}$ June. More information can be found on the conference website.

Please do not hesitate to contact us at icoe2018@u-bordeaux.fr should you need any assistance in organizing your stay.

We are looking forward to welcoming you in Bordeaux,

Guillaume WANTZ, Chair Natalie STINGELIN, Co-chair Georges HADZIIOANNOU, Honorary Chair

14th International Conference on Organic Electronics Bordeaux, France — June 18-22, 2018 icoe2018.u-bordeaux.fr

Improving solution-processing of copper(I) thiocyanate hole transport material

Pichaya Pattanasattayavong

Department of Materials Science and Engineering, School of Molecular Science and Engineering, Vidyasirimedhi Institute of Science and Technology (VISTEC), Rayong, 21210, Thailand

pichaya.p@vistec.ac.th

Copper(I) thiocyanate (CuSCN) has recently been shown as a high-potential wide band gap, hole-transporting semiconductor with promising applications demonstrated in a variety of applications from a p-type active channel layer in thin-film transistors (TFTs) [1] and a transparent hole transport layer (HTL) in organic light-emitting diodes (OLEDs) [2], organic photovoltaics (OPVs) [3], and perovskite solar cells [4]. In particular, CuSCN as HTL can improve the efficiencies of devices when compared to the incumbent PEDOT:PSS, owing to its large band gap (> 3.5 eV), moderate hole mobility (0.01 to 0.1 cm² V⁻¹ s⁻¹), and appropriate energy level for hole injection/extraction (valence band around 5-5.5 eV) [5]. However, solution processing of CuSCN has remained a key issue that limits its optimization and wider utilization. Specifically, two key aspects will be highlighted in this talk: the choice of solvents and the complexation of solvent molecules with CuSCN. Firstly, in addition to diethyl sulfide (DES), dipropyl sulfide (DPS), and aqueous ammonia [NH₃(aq)] which have been previously employed to process CuSCN, we report here that pyridine, diethyl amine, dipropyl amine, and dibutyl amine can also dissolve CuSCN. Various thinfilm characterization techniques such as photoelectron spectroscopy (PES), X-ray diffraction (XRD), atomic force microscopy (AFM), and UV-visible spectroscopy (UV-Vis) have been used to study the chemical, structural, morphological, and optical properties of the resulting CuSCN thin films deposited from these alternative solvents. Although, the optical band gaps (Eg,opt) and valence band edge (VBE) structures are mostly similar to CuSCN processed from DES or DPS, i.e., Egopt in the range of 3.8 to 3.9 eV and VBE lying approximately 1 eV below the Fermi level, we have observed varying chemical and structural/morphological properties, such as different Cu(I)/Cu(II) ratios and extent of preferred crystallographic orientations. Secondly, we have found that CuSCN and solvent molecules can form stable complexes. Solids obtained from slow evaporation of CuSCN dissolved in sulfidebased solvents have been characterized by single-crystal X-ray diffraction (SCXRD) and shown to be solvates containing CuSCN and solvent molecules as ligands. Based on thermogravimetric analysis (TGA), CuSCN-DPS solvates show a 50% mass loss at 110°C. Immersing these solvates in alcohols shows that the mass loss is reduced to 2%, suggesting an alternative method to remove solvents from CuSCN thin films. The two points discussed here can provide direction for further modification and optimization of CuSCN thin film and improved device performance.

- [1] P. Pattanasattayavong et al, *Adv. Mater.* **25**, 1504 (2013)
- [2] A. Perumal et al, *Adv. Mater.* **27**, 93 (2015)
- [3] N. Yaacobi-Gross et al, Adv. Energy. Mater. 5, 1401529 (2015)
- [4] N. Wijeyasinghe et al, Adv. Funct. Mater. 27, 1701818 (2017)
- [5] P. Pattanasattayavong et al, Adv. Electron. Mater. 3, 1600378 (2017)



October 31 – November 3, 2017 at Convention Center, The Empress Hotel, Chiang Mai, THAILAND http://www.mrs-thailand2017.science.cmu.ac.th

August 18, 2017

Dear Dr. Pichaya Pattanasattayavong,

On behalf of the Materials Research Society of Thailand, we are pleased to cordially invite you as **our Invited Speaker** at The First Materials Research Society of Thailand International Conference (MRS-Thailand 2017), which will be held during October 31 - November 3, 2017 at Convention Center, The Empress Hotel, Chiang Mai, THAILAND. We are expecting that there will be about 800 participates including about 300 participates from overseas. The details of MRS-Thailand 2017 can be found from the conference website: http://www.mrs-thailand2017.science.cmu.ac.th.

Regarding your trip, we would like to provide:

- 1. Hotel accommodation (maximum 3 nights from October 31 November 3, 2017 at the conference hotel).
- 2. Conference registration fee waiver

We do hope that you will consider our invitation. In order to help us coordinating, please kindly return the attached form to us via email: 1mrsthailand2017@gmail.com.

Best regards,

Prof. Dr. Santi Maensiri

President, Materials Research Society of Thailand

& Chairman for MRS-Thailand 2017 Organizing Committee

Copper(I) Thiocyanate (CuSCN) as a Transparent P-type Semiconductor for Novel Organic Electronic Applications

Pichaya Pattanasattayayong

Department of Materials Science and Engineering, School of Molecular Science and Engineering, Vidyasirimedhi Institute of Science and Technology (VISTEC), Rayong 21210 Thailand

Oxide semiconductors, particularly ZnO, SnO₂, and In₂O₃ have shown great potential in plastic and organic opto/electronic applications due to their high charge carrier mobility, stability, and manufacturing versatility. However, there has always been one hurdle that prevents their full utilization – the lack of p-type or hole-transporting counterparts. The electronic structures of the prevalent oxide semiconductors do not favor holes as charge carriers, and attempts at pdoping have not been fruitful. Copper(I) thiocyanate (CuSCN), a pseudo-halide compound, is one of a handful of inorganic compounds that have been successfully shown functional applications based on its hole-transporting characteristics. Coupled with its wide band gap of larger than 3.5 eV, CuSCN yields the unique combination of hole transport and high optical transparency.^{1,2} Recent demonstrations have shown its enormous potential as a transparent ptype channel layer in thin-film transistors^{3,4} as well as a hole-extracting/injecting layer in organic photovoltaics^{5,6} and organic light-emitting diodes.⁷ The latter two applications also exhibited improved efficiencies when compared with devices based on the incumbent poly(3,4ethylenedioxythiophene:polystyrenesulphonate) (PEDOT:PSS) as the hole-transporting layer. In this talk, I will present an up-to-date summary of the development of CuSCN for plastic and organic opto/electronics and as well as our recent investigations on the processing of CuSCN thin films.

References

- (1) Pattanasattayavong, P.; Ngongang Ndjawa, G. O.; Zhao, K.; Chou, K. W.; Yaacobi-Gross, N.; O'Regan, B. C.; Amassian, A.; Anthopoulos, T. D. Electric Field-Induced Hole Transport in copper(I) Thiocyanate (CuSCN) Thin-Films Processed from Solution at Room Temperature. *Chem. Commun.* **2013**, *49* (39), 4154–4156.
- (2) Pattanasattayavong, P.; Promarak, V.; Anthopoulos, T. D. Electronic Properties of Copper(I) Thiocyanate (CuSCN). *Adv. Electron. Mater.* **2017**, *3* (3), 1600378.
- (3) Pattanasattayavong, P.; Yaacobi-Gross, N.; Zhao, K.; Ngonggang Ndjawa, G. O.; Li, J.; Yan, F.; O'Regan, B. C.; Amassian, A.; Anthopoulos, T. D. Hole-Transporting Transistors and Circuits Based on the Transparent Inorganic Semiconductor Copper(I) Thiocyanate (CuSCN) Processed from Solution at Room Temperature. *Adv. Mater.* **2013**, *25* (10), 1504–1509.
- (4) Petti, L.; Pattanasattayavong, P.; Lin, Y.-H.; Münzenrieder, N.; Cantarella, G.; Yaacobi-Gross, N.; Yan, F.; Tröster, G.; Anthopoulos, T. D. Solution-Processed P-Type copper(I) Thiocyanate (CuSCN) for Low-Voltage Flexible Thin-Film Transistors and Integrated Inverter Circuits. *Appl. Phys. Lett.* **2017**, *110* (11), 113504.
- Yaacobi-Gross, N.; Treat, N. D.; Pattanasattayavong, P.; Faber, H.; Perumal, A. K.; Stingelin, N.; Bradley, D. D. C.; Stavrinou, P. N.; Heeney, M.; Anthopoulos, T. D. High-Efficiency Organic Photovoltaic Cells Based on the Solution-Processable Hole Transporting Interlayer Copper Thiocyanate (CuSCN) as a Replacement for PEDOT:PSS. *Adv. Energy Mater.* **2015**, *5* (3), 1401529.
- (6) Wijeyasinghe, N.; Regoutz, A.; Eisner, F.; Du, T.; Tsetseris, L.; Lin, Y.-H.; Faber, H.; Pattanasattayavong, P.; Li, J.; Yan, F.; McLachlan, M. A.; Payne, D. J.; Heeney, M.; Anthopoulos, T. D. Copper(I) Thiocyanate (CuSCN) Hole-Transport Layers Processed from Aqueous Precursor Solutions and Their Application in Thin-Film Transistors and Highly Efficient Organic and Organometal Halide Perovskite Solar Cells. Adv. Funct. Mater. 2017, In press, 1701818.
- (7) Perumal, A.; Faber, H.; Yaacobi-Gross, N.; Pattanasattayavong, P.; Burgess, C.; Jha, S.; McLachlan, M. A.; Stavrinou, P. N.; Anthopoulos, T. D.; Bradley, D. D. C. High-Efficiency, Solution-Processed, Multilayer Phosphorescent Organic Light-Emitting Diodes with a Copper Thiocyanate Hole-Injection/Hole-Transport Layer. *Adv. Mater.* 2015, 27 (1), 93–100.



3 September 2017

Dear Miss PIMPISUT WORAKAJIT

On behalf of the MRS Thailand 2017 organizing committee, I am pleased to inform that your abstract has been accepted for the presentation at The First Materials Research Society of Thailand International Conference (1st MRS Thailand International Conference), which will be held at Convention Center, The Empress Hotel, Chiang Mai, Thailand during October 31st - November 3rd 2017. We take this opportunity to invite you to give the presentation of your research, as detailed below, at this 1st MRS Thailand International Conference,

Paper title: Finding New Solvents for Processing Copper(I) Thiocyanate

Type of presentation: Poster

Paper ID: S11-P8

Symposium 11: Sensors, Organic Electronics and Printed Electronics

Please kindly be reminded that full papers need to be submitted on-site at the Registration Desk (Submission Deadline is 1 November 2017, by 12.00 PM) by the authors. The manuscript submission form, 3 hard copies and 1 CD (MS word and pdf files) are required for a complete submission. For more information, please visit our website at

http://www.mrs-thailand2017.science.cmu.ac.th

If you have further inquiries, please contact us at email: 1mrsthailand2017@gmail.com

We are looking forward to meeting you in Chiang Mai, Thailand.

Sincerely yours,

(Prof. Dr. Santi Maensiri, Ph.D.)

President

Materials Research Society of Thailand

The First Materials Research Society of Thailand International Conference (1st MRS Thailand International Conference)
October 31 – November 3, 2017
The Empress Convention Center, Chiang Mai, Thailand

Finding New Solvents for Processing Copper(I) Thiocyanate

Pimpisut Worakajit^a, Pichaya Pattanasattayavong^{a,*}

^aDepartment of Materials Science and Engineering School of Molecular Science and Engineering Vidyasirimedhi Institute of Science and Technology (VISTEC) Rayong 21210, Thailand

*Corresponding Author's E-mail: pichaya.p@vistec.ac.th

Abstract

Copper(I) thiocyanate (CuSCN) is a p-type semiconductor with great potential as the active layer in thin film transistors (TFT), or as a hole transporting material in other electronic devices such as solar cells and light emitting diode. A major obstacle limiting the use of CuSCN in large area applications is its solubility. Current literature reports only a few solvents that dissolve CuSCN such as diethyl sulfide (DES) and dipropyl sulfide (DPS). However, these solvents are irritants and expensive. Here we present a study of alternative solvents along with their electronic and morphological effects on thin films of CuSCN.

This report introduces multiple organic solvents including Pyridine, Diethylamine and Dibutylamine to dissolve CuSCN for thin film processing. Fourier-transform infrared spectroscopy (FT-IR) was used to observe atomic bonding between the chosen solvents and CuSCN molecules. Next, films of CuSCN were deposited via spin-casting at low temperatures (≤100°C). The resultant films were highly transparent in visible and NIR region (≤1% absorption) as demonstrated from UV-vis-NIR spectroscopy results. The optical band gaps of the films produced from these new solvents showed values of approximately 3.9 eV, comparable to the optical band gap of CuSCN films produced from solutions of DES and DPS. Scanning electron microscopy (SEM) and atomic force microscopy (AFM) were used to examine the ensuing film morphology. From these measurements a solvent dependent morphology was observed. Finally, X-ray photoelectron spectroscopy (XPS) was used to further study and determine the oxidation state of Copper element in the CuSCN films.

In conclusion, this study characterizes safer and less expensive alternative solvents for CuSCN solutions, crucial in the development of large area electronic processing. These solvents produced new morphologies of CuSCN films while maintaining comparable optical and electronic properties.

Keywords: Copper(I) thiocyanate, CuSCN, Thin film, Optical property, Solution-processed, Dissolution, Solubility



The 3rd International Congress on Advanced Materials (AM 2016)

November 27-30, 2016 . Centara Grand at Central Plaza Ladprao Bangkok, Thailand

August 22, 2016

Dear Dr. Pichaya Pattanasattayawong,

The Department of Chemistry, Faculty of Science Chulalongkorn University, the Science Society of Thailand under the Patronage of His Majesty the King, the International Union of Advanced Materials and the Chinese Advanced Materials Society are jointly organizing the 3rd International Congress on Advanced Materials (AM2016) which will be held during November 27-30, 2016 at Centara Grand at Central Plaza Ladprao, Bangkok, Thailand.

On behalf of the Organizing Committee, I would like to invite you to be a **Keynote Speaker** (30 min talk-time).

We will confirm date and time of your presentation soon.

You will be provided free registration and all social function.

<u>Please kindly send us your CV and the abstract(s) of your presentation(s) no later than September 15, 2016.</u>

Brief CV form and instruction for abstract submission are attached. The requested items should be submitted to the secretariat at advanced.materials2016@gmail.com

We trust that your knowledge and experiences contributed during the congress would be very valuable and fruitful to all participants. We are looking forward to hearing from you soon.

Yours sincerely,

Professor Vudhichai Parasuk

Congress Chairman,

Associate Professor and Head of Department of Chemistry

Faculty of Science, Chulalongkorn University, Thailand

COPPER(I) THIOCYANATE FOR PLASTIC AND ORGANIC ELECTRONICS: A UNIQUE COMBINATION OF HOLE-TRANSPORTING PROPERTIES AND OPTICAL TRANSPARENCY

Pichaya Pattanasattayavong

Department of Materials Science and Engineering School of Molecular Science and Engineering Vidyasirimedhi Institute of Science and Technology (VISTEC)

Oxide semiconductors, particularly ZnO, SnO₂, and In₂O₃ have shown great potential in plastic and organic opto/electronic applications due to their high charge carrier mobility, stability, and manufacturing versatility. However, there has always been one hurdle that prevents their full utilization – the lack of p-type or hole-transporting counterparts. The electronic structures of the prevalent oxide semiconductors do not favor holes as charge carriers, and attempts at pdoping have not been fruitful. Copper(I) thiocyanate (CuSCN), a pseudo-halide compound, is one of a handful of inorganic compounds that have been successfully shown functional applications based on its hole-transporting characteristics. Coupled with its wide band gap of larger than 3.5 eV, CuSCN yields the unique combination of hole transport and high optical transparency. Recent demonstrations have shown its enormous potential as a transparent p-type channel layer in thin-film transistors (Adv. Mater. 2013, 25, 1504) as well as a holeextracting/injecting layer in organic photovoltaics (Adv. Energy Mater. 2015, 5, 1401529) and organic light-emitting diodes (Adv. Mater. 2015, 27, 93). The latter two applications also exhibited improved efficiencies when compared with devices based on the incumbent poly(3,4ethylenedioxythiophene:polystyrenesulphonate) (PEDOT:PSS) as the hole-transporting layer. In this talk, I will present a summary of the development of CuSCN for plastic and organic opto/electronics and as well as a review on the recent studies on fundamental properties of CuSCN.





March 10, 2016, Guangzhou

Prof. Yuguang Ma Chairman of ICSM 2016 South China University of Technology State Key Laboratory of Luminescent Materials and Devices Guangzhou, 510640, China

Phone: +86-20-22237005 Email: office@icsm2016.com

Dear Dr. Pichaya Pattanasattayavong

On behalf of the Organizing Committee, I cordially invite you to attend the International Conference of Synthetic Metal 2016 (ICSM 2016). The ICSM is the longest-running conference series in the field of conducting and semiconducting organic materials started in 1976 in Siofok (Hungary) which has now become the premiere venue for discussion of the latest developments in the areas of organic electronics and photonics, from synthesis to characterization, computational modeling, device fabrication, and real-world applications. ICSM 2016 will be held in Guangzhou, China, from Sunday June 26, 2016, to Friday, July 1, 2016.

This invitation letter is destined to:

Name: Pichaya Pattanasattayavong

Date of birth: 1986-11-23

Gender: male

Passport number: AA6420096

Institution/Company: Vidyasirimedhi Institute of Science and Technology

City: Rayong

Country/Region: Thailand

Expected Arrival date: 25/06/2016 Expected departure date: 02/07/2016

Further information on the conference is at the website: http://www.icsm2016.com

Yours sincerely,

Yuguang Ma

Director of State Key Labo addy of Lumescent Materials and Devices

Professor of South China University of Technology

Chairman of the ICSM 2016

Study of Hole Localized States and Transport Mechanisms of Copper(I) Thiocyanate Based on Field-Effect Measurements

<u>Pichaya Pattanasattayavong</u> ^{a)*}, Alexander D. Mottram ^{b)}, Feng Yan ^{c)} and Thomas D. Anthopoulos ^{b)}

- a) Department of Materials Science and Engineering, School of Molecular Science and Engineering, Vidyasirimedhi Institute of Science and Technology, Rayong 21210, Thailand b) Centre for Plastic Electronics and Department of Physics, Blackett Laboratory, Imperial College London, London SW7 2AZ, United Kingdom
- c) Department of Applied Physics and Materials Research Centre, The Hong Kong Polytechnic University, Hong Kong, China

E-mail: pichaya.p@vistec.ac.th

Copper(I) thiocyanate (CuSCN) is a solution-processable inorganic semiconductor that combines two sought-after characteristics of good hole-transporting properties and high optical transparency. As recently reviewed [1], its use in thin-film electronic devices is gaining more attention due to its versatility, favorable energetics, and p-type characteristics. Albeit having been utilized in various types of solar cells such as the bulk-heterojunction (BHJ) cells, dye-sensitized solar cells (DSSCs), and perovskite solar cells (PSCs) as well as in organic light-emitting diodes (OLEDs) and thin-film transistors (TFTs), there is still a crucial lack of understanding of electrical and electronic properties of CuSCN.

In this work, we fabricated metal-insulator-semiconductor (MIS) capacitors and topgate bottom-contact TFTs based on CuSCN as the semiconductor layer and two different polymeric insulators and analyzed field-effect measurements to obtain several important parameters: dielectric constant (5.1 \pm 1.0), flat-band voltage ($-0.7 \pm 0.1 \text{ V}$), and unintentional doping concentration $(7.2 \pm 1.4 \times 1017 \text{ cm}^{-3})$. The subthreshold characteristics of CuSCN-based TFTs also reveal the presence of localized hole states that can be characterized by an exponential distribution with a characteristic energy of 42.4 ±0.1 meV. Investigating the temperature dependence of the transistor transfer characteristics also allows the study of the hole transport processes in CuSCN which are found to exhibit three transport regimes. The first regime observed at high temperatures (228 to 330 K) appears to follow the multiple trapping and release mechanism while the second regime seen at intermediate temperatures (123 to 228 K) can be described with the variable range hopping mechanism. The third regime at low temperatures (78 to 123) K) displays weak temperature dependence and is speculated to arise from a fieldassisted hopping process. The transitions from one transport mechanism to another are explained by the temperature dependence of the transport energy. Devices based on two different polymeric insulators showed similar behaviors, asserting that the observed results are characteristics of CuSCN.

Due to the recent increasing interest in CuSCN, this work timely discusses the electrical and electronic properties of this material which are important for further development as a high potential hole-transporting wide band gap semiconductor to replace the incumbent PEDOT:PSS as well as to match with the transparent n-type oxides in order to realize transparent electronics.

[1] N. Wijeyasinghe and T. D. Anthopoulos, "Copper(I) thiocyanate (CuSCN) as a hole-transport material for large-area opto/electronics", *Semiconductor Science and Technology*, Vol. 30, No. 10, (2015), p 104002.